SEDIMENT TRANSPORT BY RIVER AND SEDIMENT INTERACTION WITH RIPARIAN VEGETATION GROWTH

（河川中の土砂輸送と河岸植生の生長との関わりについて）

2020 年9月

埼玉大学大学院理工学研究科（博士後期課程）
環境制御工学専攻（ 主指導教員　藤野　毅）

BANIYA MAHENDRA BAHADUR

SEDIMENT TRANSPORT BY RIVER AND SEDIMENT INTERACTION WITH RIPARIAN VEGETATION GROWTH

BANIYA MAHENDRA BAHADUR

17DE051

A dissertation submitted in partial fulfillment of the requirements for the degree of **DOCTOR OF ENGINEERING** in Environmental Science and Infrastructure Engineering

Supervisor: Professor Takeshi Fujino

Saitama University

Graduate School of Science and Engineering

September 2020

"This work is dedicated to my loving parents, brother and his family, and my wife, son and daughters"

Acknowledgements

I am very much grateful to my supervisor Prof. Takeshi Fujino for his valuable comments and supervision during my research in Saitama University. I would like to express my deep gratitude to Emeritus Prof. Takashi Asaeda for supervising, advising and helping in academic activities. Besides my supervisor, I would like to thank my thesis committee members: Prof. Maki Kawai-Yamada, Prof. Yasuko Kaneko and Assoc. Prof. Kiyotaka Fukahori for their valuable comments and suggestions during linking up the studies. I also take this opportunity to thank Assistant Prof. Dr. Senavirathna M.D.H. Jayasanka and my brother Mr. Arjun Baniya, lab mate Miss Guligena Muhetaer, sister Sandhya Nepal, friend Deepak Shrestha and lab secretary Mrs. Endo and Mrs. Takakura for their kind cooperation and suggestions. I would like to thank JASSO and Kubota fund, Japan for providing private funding scholarship and Saitama University for providing TA, RA, partial and full tuition exemption during my study period. I would also to thank Government of Nepal, Ministry of Federal Affairs and General Administration, Department of Local Infrastructure Development and Agricultural Road (DoLIDAR) for arranging study leave in my job. I would also like to give thanks to Er. Shivaram K.C., Nepal Electricity Authority and Er. Rocky Talchabhadel, Ministry of Energy, Water Resources and irrigation, Department of Hydrology and Meteorology, Nepal for historical sediment, discharge and climate data.

Finally, I would like to thank my parents, wife Mrs Tika Karki and especially my son Aakrist and daughters Aaradhya and Aarunya Baniya for their energetic inspiration from Nepal during my study period.

Preview

This thesis is organized in four different parts namely: Part I, Part II, Part III and Part IV consisting of different chapters (Figure 1). Part I deals about the hydraulic parameters for sediment transport and prediction of suspended sediment for Kali Gandaki River basin, Himalaya, Nepal. Part II analyses effects of rainfall on fluvial discharge and suspended sediment transport in same river basin. Rainfall trend analysis of the same basin are described in the Part III. These three parts are related for sediment transport by river in Nepal.

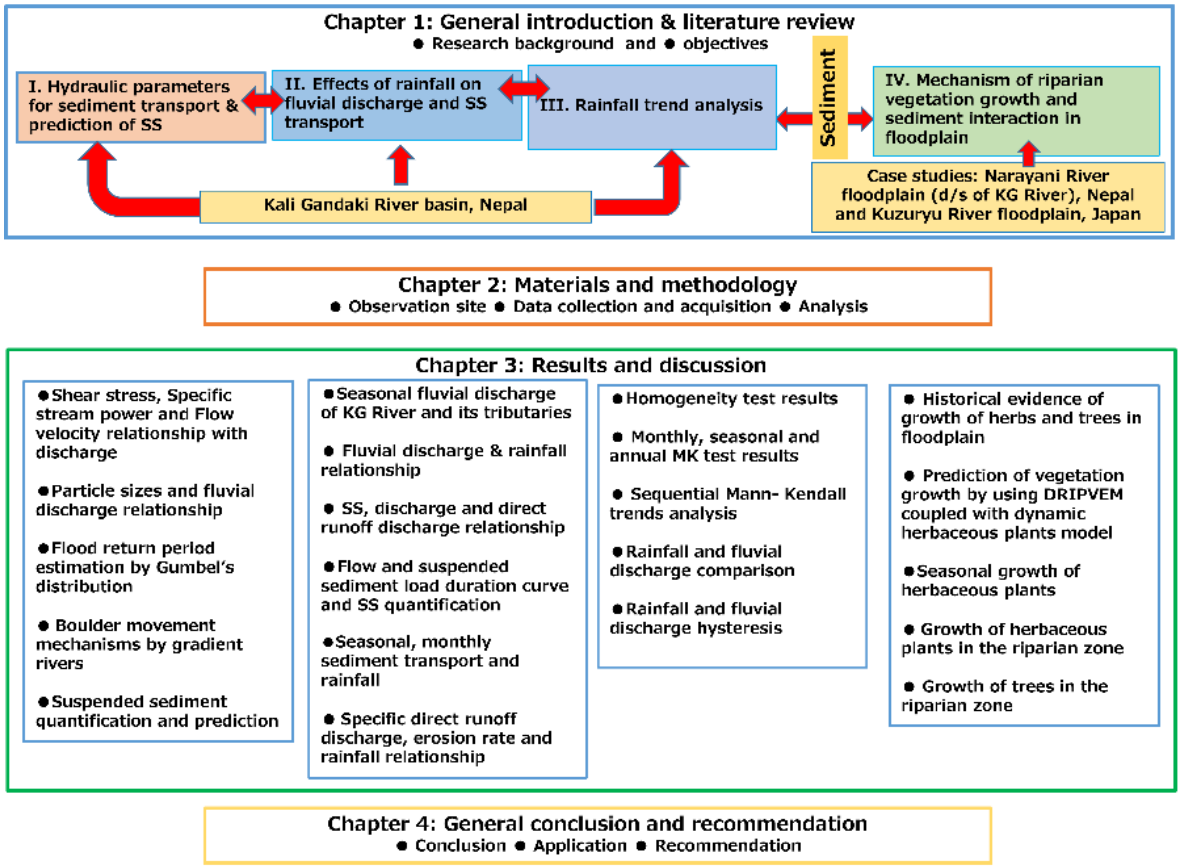

Figure 1. Structure of thesis

The mechanism of riparian vegetation growth and sediment interaction in floodplain are presented in Part IV which consists of two different case studies: Narayani River flood plain, Nepal and Kuzuryu River reach, Japan. The effects of sediment sizes (D_{50}) on riparian

vegetation coverage are analyzed and verified in historical data available in Japan using the Dynamic Riparian Vegetation Model (DRIPVEM) coupled with a Dynamic Herbaceous Model. Observation of biomass of herbs and trees in Narayani River floodplain in Nepal should be conducted for calibration of coupled DRIPVEM. Each part consists of Chapter 1 to Chapter 4 except Part IV. A discussion part is added as extra in Part IV.

Summary

Sediment yield from a catchment is a complex phenomenon of weathering, land sliding, glacial and fluvial erosion which depends on geological as well as fluvial characteristics. The bed shear stress (τ_b), specific stream power (ω), and flow velocity (v) associated with maximum boulder size transport were determined throughout years 2003 to 2011 by using derived lower boundary equation from the available data for Kali Gandaki (KG) River at Setibeni, Syangja located about 5 kms upstream from a hydropower dam. The river transported an average of 40.904±12.453 Mega ton (Mt) of suspended sediment (SS) during the period 2006-2011 and the artificial neural networks (ANNs) predicted the daily SS rate and annual sediment load as 35.190±7.018 Mega tons (Mt) satisfactorily compared to multiple linear regression, nonlinear multiple regression, general power model, log transform models including sediment rating curve (SRC).

Fluvial discharge is a principal driver of SS transport in Himalaya mountain. The study basin has three hydrometric stations in main river, four hydrometric stations in its tributaries, and a hydropower reservoir site where suspended sediment transport is measured. This study also analysed relationship of specific discharge of main and tributaries rivers with rainfalls of the main basin and its sub basins together with SS transport. Annual anticlockwise hysteresis loops were developed between specific discharge and rainfall at three hydrometric stations of main KG River, whereas its tributaries namely Aandhi Khola, Seti Khola and Modi Khola followed anticlockwise, and Myagdi Khola showed an eight-shaped hysteresis loop. The clockwise hysteresis loop developed between SS concentration and fluvial discharge was eliminated and changed to linear relationship with the direct runoff discharge. The result showed that about

97% of SS was transported during monsoon season (June-September), comprising an annual weathering rate of KG basin estimated to be 4390 tons/km^2/yr which is equivalent to 1.66 mm/yr between the period 2006-2017. Particularly, specific direct runoff discharge and monsoonal daily erosion rate of major rainfall events (>30 mm/day) showed linear increasing trend with rainfall in KG basin.

Stream flow alteration is one of the most noticeable effects of rainfall change patterns in this catchment. The study also depicted fluvial flow changing patterns of three hydrometric stations of KG River, four hydrometric stations of tributaries due to changing seasonal and annual rainfall trends in twenty-seven rain gauge stations located between the elevation ranges of 700 to 2744 m MSL of this basin over the period of 1957-2018. Monthly rainfall data were used to examine the rainfall and discharge trends. Mann- Kendall trend test (MKT) test along with Sen's slope and sequential Mann- Kendall trend (SQMKT) analysis on homogenized time series data were used to evaluate the existence of monotonic trends, magnitude of trend and identify shifting of rainfall trend.

Finally, the ecological dynamics of riparian area interact with sediment transport in river system, which plays an active role in riparian vegetation growth in the floodplain. Frequently flood disturbance, extreme floods, sediment transport with nutrients and seeds by fluvial discharge, sediment deposition and erosion phenomena which frequently occurred in the floodplain, changed without vegetation land area to vegetative area and vice versa. The sediment grain size (D_{50}) plays important role in riparian vegetation area coverage in the floodplain. Mathematical models describing vegetation growth in flood plain during short period of time available in literature. However, long-term prediction by modelling and

validations of riparian vegetation are still lacking. The long-term prediction of riparian vegetation is important in perspective of floodplain management. In order to cover long-term vegetation growth modelling, a Dynamic Riparian Vegetation Model (DRIPVEM) was coupled with Dynamic Herbaceous Model used to establish the interactive relationship of sediment grain sizes (D_{50}) and riparian vegetation in the two rivers: Narayani River floodplain, Nepal and Kuzuryu River floodplain, Japan. In context of Nepal, the calibration of coupled DRIPVEM, observation of species wise herbs and tree biomass, sediment particle sizes with nutrients availability in the floodplain should be conducted. The riparian vegetation observation and calibration of coupled DRIPVEM and prediction of spatial distribution of riparian vegetation in Narayani floodplain, Nepal would be future perspective of this study.

Publications

International peer reviewed journals

Baniya, M.B., Asaeda, T., Fujino, T., Jayasanka, S.M.D.H., Muhetaer, G., Li, J., 2020. Mechanism of Riparian Vegetation Growth and Sediment Transport Interaction in Floodplain: A Dynamic Riparian Vegetation Model (DRIPVEM) Approach. Water 12, 77.

Baniya, M.B., Asaeda, T., KC, S., Jayashanka, S.M.D.H., 2019. Hydraulic Parameters for Sediment Transport and Prediction of Suspended Sediment for Kali Gandaki River Basin, Himalaya, Nepal. Water 11, 1229.

Muhetaer G., Asaeda T., Jayasanka S.M.D.H., **Baniya M.B.**, Abeynayaka H.D.L., Rashid M.H., Yan H.Y., 2020. Effects of Light Intensity and Exposure period on the Growth and Stress Responses of Two Cyanobacteria species: *Pseudanabaena galeata* and *Microcystis aeruginosa* Water 12, 407.

Conference proceedings

Baniya, M.B., Asaeda, T., Jayashanka, S.M.D.H., KC, S., 2018 Palaeohydraulic Parameters for Initiation Sediment Transport in Kaligandaki River, Nepal (12th International Symposium on Ecohydraulics, Aug 19-24, 2018 Tokyo, Japan)

Asaeda, T., Nallaperuma, B., **Baniya, M.B.**, Mdh, S., 2019. Riparian vegetation Classification Using the Dynamic Riparian Vegetation Model. E-proceedings 38th IAHR World Congr. Sept. 1-6, 2019, Panama City, Panama. https://doi.org/10.3850/38WC092019-0989

Baniya, M. B., Asaeda, T., Fujino, T., Talchabhadel, R. KC, S., Muhetaer, G. Effects of Raindall Changing Patterns on Fluvial and Suspended Sediment Discharge in Kali Gandaki Hydropower Reservoir, Nepal (Full paper accepted in 22nd IAHR-APD Congress 2020 in Sapporo)

List of Figures

Figure 1. Structure of thesis v

Figure 2. (a) Shear stress and particle size relationship (b) Specific power and particle size relationship 5

Figure 3. Flow velocity and particle size relationship..... 7

Figure 4. (a) Map of KG River catchment area (b) Longitudinal profile of KG River 9

Figure 5. Elevation wise catchment area and snow contribution 10

Figure 6.(a) Flow height and discharge relationship (b) Cross section area (calculated from height) and discharge relationship 11

Figure 7.Yearly (a) discharge (NEA 2003- 2012) (b) Cross profiles (2002-2011) of KG River 15

Figure 8. Relationship of fluvial discharge and (a) Shear stress (b) Specific power..... 16

Figure 9. Relationship of fluvial discharge and (a) Flow velocity (b) Particle size (D_{50}) 17

Figure 10. Relationship of shear stress and particle size (D_{50}) and comparison with different researchers..... 18

Figure 11. Relationship of specific power and particle size (D_{50}) and comparison with different researchers..... 19

Figure 12. Relationship of flow velocity and particle size (D_{50}) and comparison with different researchers 20

Figure 13. (a) Gumbel flood return period, (b) Extreme fluvial discharge 21

Figure 14. (a) Natural landslide dam formation on May 24, 2015 (~ 56 km upstream of dam) (b) Lake formation after blockage of river (c) Downstream fluvial discharge after blockage of river (d) Flash flood after breaching of landslide dam May 25, 2015..... 22

Figure 15. (a) Seasonal hysteresis loop of sediment load (b) Suspended sediment – discharge rating curve. 24

Figure 16. Hysteresis index derivational demonstration 24

Figure 17. (a) Seasonal SS yield (b) Yearly SS transport and hysteresis index (HI_{mid})..... 26

Figure 18. Observed and predicted daily suspended sediment rate (a) SRC (Q_w and Q_s) model (b) Power model (Q_w) (c) Log transform linear model (Q_w and R_t) (d) ANN model 28

Figure 19. Comparison of annual observed and different model predicted SS 29

Figure 20. (a) Map of Kali Gandaki River catchment area (b) L- profile of Kali Gandaki River (c) L- profile of Aandhi Khola (d) L- profile of Seti Khola (e) L- profile of Modi Khola (f) L- profile of Myagdi Khola.... 36

Figure 21. Seasonal discharge of KG River and its tributaries during (a) Winter and Pre-monsoon (b) Monsoon and Post-monsoon..... 40

Figure 22. Discharge and rainfall of KG River and its tributaries. 41

Figure 23. Specific discharge and rainfall relationship for KG River at (a) Setibeni (2002-2017) (b) Modibeni (1992-2013) (c) Tatopani (2004-2014)..... 42

Figure 24. Specific discharge and rainfall relationship (a) Aandhikhola (2000-2015) (b) Setikhola (1989-2009) (c) Modikhola (1975-2015) (d) Myagdikhola (1976-2015)..... 43

Figure 25. Suspended sediment concentration and fluvial discharge relationship with clockwise hysteresis loop (b) Suspended sediment concentration and direct discharge relationship without hysteresis loop for KG River (2006-2017). 45
Figure 26. (a-k) Typical hysteresis during SSC_{max} extreme events 47
Figure 27. (a-k) Typical hysteresis during discharge, Q_{wmax} extreme events 48
Figure 28. (a)Time lag of discharge and suspended sediment (b) Particle size distribution of SS 49
Figure 29. (a-b) Seasonal flow duration curve (c-d) Seasonal suspended sediment load duration curve 50
Figure 30. (a) Monthly flow duration curves and (b) Monthly suspended sediment load duration curve 51
Figure 31. (a) Sources of sediment (b) Sediment transport by fluvial discharge (c) Deposited sediment in KG hydropower reservoir (d) Flushing of deposited sediment in KG hydropower reservoir. 52
Figure 32. (a-d) Seasonal SSL and discharge relationship 53
Figure 33. (a-d) Monthly SSL and discharge relationship for monsoon 54
Figure 34. Suspended sediment transport and average total rainfall of KG basin 55
Figure 35. (a) Specific direct discharge and rainfall relationship (b) Erosion rate and major rainfall events (daily rainfall >30 mm) relationship 56
Figure 36. (a) Map of Kali Gandaki River catchment area (b) Longitudinal profile of Kali Gandaki River. 62
Figure 37. (a) Comparison of homogeneous and change in data stations (b) Classification of stations 71
Figure 38. Change year in annual rainfall series for different stations 73
Figure 39. Change year in annual rainfall series for different stations 73
Figure 40. Change year in annual rainfall series for different stations 74
Figure 41. Sample autocorrelation of meteorological station (a) Jhomsom[601] and (b) Lumle[814]. 74
Figure 42. (a) Overall trends of rainfall stations (b) Significant and Non-significant number of rainfall stations 75
Figure 43. Sen's slope magnitude (a) for winter (b) for pre-monsoon 78
Figure 44. Sen's slope magnitude (a) for monsoon (b) for post-monsoon 78
Figure 45. (a) Average annual rainfall (b) Annual Sen's slope magnitude 79
Figure 46. SQMKT z- values against time (a) for winter and (b) pre-monsoon for Bhaudare[813], Ghandruk[821], Lumle[814], Pamdur[830], Salyan[829], Dandaswarna[832], Syangja[805], Waling[826]. 80
Figure 47. SQMKT z- values against time (a) for monsoon and (b) post-monsoon for Bhaudare[813], Ghandruk[821], Lumle[814], Pamdur[830], Salyan[829], Dandaswarna[832], Syangja[805], Waling[826]. 81
Figure 48. SQMKT z- values against time for annual total monsoon for Bhaudare[813], Ghandruk[821], Lumle[814], Pamdur[830], Salyan[829], Dandaswarna[832], Syangja[805], Waling[826] 81
Figure 49. SQMKT z- values against time for (a) winter and (b) pre-monsoon for Baglung[605], Benibazar[609], Bhagara[629], Ghorepani[619], Gurjakhani[616], Muna[628], Karkineta[613], Bhobang[615]. 82
Figure 50. SQMKT z- values against time for (a) monsoon and (b) post-monsoon for Baglung[605], Benibazar[609],

Bhagara[629], Ghorepani[619], Gurjakhani[616], Muna[628], Karkineta[613], Bhobang[615]. 83
Figure 51. SQMKT z- values against time for annual total monsoon for Baglung605, Benibazar[609], Bhagara[629], Ghorepani[619], Gurjakhani[616], Muna[628], Karkineta[613], Bhobang[615]. 83
Figure 52. SQMKT z- values against time for (a) winter and (b) pre-monsoon for Jhomsom[601], Thakmarpha[604], Tatopaani[606], Bega[626]. 84
Figure 53. SQMKT z- values against time for (a) monsoon and (b) post-monsoon for Jhomsom[601], Thakmarpha[604], Tatopaani[606], Bega[626]. 84
Figure 54. SQMKT z- values against time for annual total monsoon for Jhomsom[601], Thakmarpha[604], Tatopaani[606], Bega[626]. 84
Figure 55. Average (a) daily rainfall and fluvial discharge (b) monthly rainfall and fluvial discharge in KG basin. 85
Figure 56. (a) Rainfall and fluvial discharge hysteresis. (b) Number of rainy days during different months. 87
Figure 57. Interactive parameters for riparian vegetation growth in a floodplain 93
Figure 58. Location map of floodplain located downstream of confluence of KG and Trisuli Rivers 95
Figure 59. Location map of Kuzuryu River (a) Study reach (b) Magnified view of study reach 96
Figure 60. Schematic structure of Dynamic Herbaceous Model 98
Figure 61. Schematic structure of Dynamic Riparian Vegetation Model (DRIPVEM) coupled with Dynamic Herbaceous Model. 104
Figure 62. Historical aerial images in chronological sequence illustrating vegetation growth in Narayani River, Nepal (a) 2004 (b) 2010 (c) 2014 (d) 2020 106
Figure 63. Riparian area calculation from historical aerial images in chronological sequence in Narayani River, Nepal (a) 2004 (b) 2010 (c) 2014 (d) 2020 107
Figure 64. (a) Relationship between riparian area and floodplain area (b) Tree and herb coverage area 108
Figure 65. Kuzuryu River (a) Historical flood level (b) Floodplain elevation 109
Figure 66. Observed and simulated biomass *P. japonica* at different habitants (a) Above ground biomass (AGB) (b) Below ground biomass (BGB). 110
Figure 67. Historical aerial images in chronological sequence illustrating vegetation growth in Kuzuryu River, Japan (a) 1982 (b) 1994 (c) 2004 (d) 2018 111
Figure 68. Simulated spatial distribution of herbs in floodplain (a) D_{50}= 1 mm size (b) D_{50}= 50 mm size. 112
Figure 69. Simulated spatial distribution of trees in sandy floodplain (a) Density wise distribution (b) Age wise distribution. 112

Lists of Tables

Table 1. Literature review for bed shear stress 4
Table 2. Literature review for specific power 5
Table 3. Literature review for flow velocity 6
Table 4. Main characteristics of river basin 8
Table 5. MLR models 27
Table 6. NLMR models 27
Table 7. General power model 27
Table 8. Log transform models 27
Table 9. ANN models 27
Table 10. Details of hydrometric stations 37
Table 11. Details of meteorological stations 38
Table 12. Main characteristics of river basin and sub basins. 39
Table 13. Typical features during extreme events 49
Table 14. Seasonal sediment rating curves and average suspended sediment load 54
Table 15. Homogeneity tests of meteorological stations in Kali Gandaki catchment. 72
Table 16. Mann-Kendall trend test results for different months of meteorological stations of KG catchment 77
Table 17. Mann-Kendall trend test results for different seasons of meteorological stations of KG catchment 77
Table 18. Main physiographic characteristics of study river reach. 96
Table 19. Some important equations employed in the herb biomass calculation 103
Table 20. Allometric relationships and conditions employed for trees 103

List of contents

Acknowledgements iv
Preview v
Summary vii
Publications x
List of Figures xi
Lists of Tables xiv

PART I- HYDRAULIC PARAMETERS FOR SEDIMENT TRANSPORT AND SUSPENDED SEDIMENT PREDECTION FOR KALI GANDAKI RIVER BASIN, HIMALAYA, NEPAL 1

ABSTRACT 1

CHAPTER 1. GENERAL INTRODUCTION AND LITERATURE REVIEW 2
1.1 Research background 2
1.2 Research objectives 7

CHAPTER 2.0 MATERIALS AND METHODS 8
2.1 Observation site 8
2.2 Data collection and acquisition 10
2.3 Analysis of hydraulic parameters for sediment transport 11
2.4 Model development for suspended sediment predictions 12
2.5 Model performance indicators 13

CHAPTER 3.0 RESULTS AND DISCUSSION 15
3.2 Shear stress, Specific stream power and Flow velocity relationship with discharge 15
3.3 Particle sizes and fluvial discharge relationship 16
3.4 Flood return period estimation by Gumbel's distribution 20
3.5 Boulder movement mechanisms by high gradient river 21
3.6 Suspended sediment quantification and prediction 23

CHAPTER4.0 GENERAL CONCLUSIONS AND RECOMMENDATIONS 30
4.1 Conclusion 30
4.2 Application of study 30
4.3 Recommendations 30

PART II- EFFECTS OF RAINFALL ON FLUVIAL DISCHARGE AND SUSPENDED SEDIMENT TRANSPORT IN KALI GANDAKI RIVER BASIN, HIMALAYA, NEPAL 31

ABSTRACT 31

CHAPTER 1. GENERAL INTRODUCTION AND LITERATURE REVIEW 32

1.1 Research background 32
1.2 Research objectives 34

CHAPTER 2.0 MATERIALS AND METHODS 35
2.1 Observation site 35
2.2 Data collection and acquisition 36
2.3 Analysis of direct runoff discharge and quantification of monthly sediment transport 39

CHAPTER 3.0 RESULTS AND DISCUSSION 40
3.1 Seasonal fluvial discharge of KG River and its tributaries 40
3.2 Fluvial discharge and rainfall relationship 41
3.3 Suspended sediment, fluvial discharge and direct runoff discharge relationship 44
3.4 Flow and suspended sediment load duration curve and SS quantification 50
3.5 Seasonal, monthly sediment transport and rainfall 51
3.6 Specific direct runoff discharge, erosion rate and rainfall relationship 55

CHAPTER4.0 GENERAL CONCLUSIONS AND RECOMMENDATIONS 57
4.1 Conclusion 57
4.2 Application of study 57

PART III- RAINFALL TREND ANALYSIS IN KALI GANDAKI RIVER BASIN, HIMALAYA, NEPAL 58
ABSTRACT 58

CHAPTER 1. GENERAL INTRODUCTION AND LITERATURE REVIEW 59
1.1 Research background 59
1.2 Research objectives 60

CHAPTER 2.0 MATERIALS AND METHODS 61
2.1 Observation site 61
2.2 Data collection and acquisition 62

CHAPTER 3.0 RESULTS AND DISCUSSION 71
3.1 Homogeneity tests results 71
3.2 Monthly, seasonal and annual MKT test results 74
3.3 Sequential Mann- Kendall trends analysis 79
3.4 Rainfall and fluvial discharge comparison 84
3.5 Rainfall and fluvial discharge hysteresis 86

CHAPTER4.0 GENERAL CONCLUSIONS AND RECOMMENDATIONS 88
4.1 Conclusion 88
4.2 Application of study 88

PART IV- MECHANISM OF RIPARIAN VEGETATION GROWTH AND SEDIMENT TRANSPORT INTERACTION IN FLOODPLAIN..... 90
ABSTRACT 90
CHAPTER 1. GENERAL INTRODUCTION AND LITERATURE REVIEW 91
1.1 Research background 91
1.2 Research objectives 94
CHAPTER 2.0 MATERIALS AND METHODS 95
2.1 Study Site Description 95
2.2 Model development 97
CHAPTER 3.0 RESULTS 106
3.1 Case study (Nepal) 106
3.2 Case study (Japan) 109
CHAPTER 4.0 DISCUSSION 113
4.1 Growth of herbaceous plants in the riparian zone 113
4.2 Growth of trees in the riparian zone 114
CHAPTER 5 GENERAL CONCLUSIONS AND RECOMMENDATIONS 115
5.1 Conclusion 115
5.2 Application of the model 115
5.3 Recommendations 115
Overall conclusion and recommendation 116
References 118

PART I- HYDRAULIC PARAMETERS FOR SEDIMENT TRANSPORT AND SUSPENDED SEDIMENT PREDECTION FOR KALI GANDAKI RIVER BASIN, HIMALAYA, NEPAL

ABSTRACT

Sediment yield from a basin is a complex phenomenon of weathering, land sliding, glacial and fluvial erosion. The quantity of sediment yield is highly dependent on catchment area, topography, the slope of the catchment terrain, intensity of rainfall, temperature, amount of snow fall and melt and soil characteristics within the catchment. This study evaluated key hydraulic parameters for sediment transport in Kali Gandaki (KG) River at Setibeni, Syangja. The outlet point is located about 5 kms upstream from a hydropower dam. Key parameters, bed shear stress (τ_b), specific stream power (ω) and flow velocity (v) associated with maximum boulder size transport were determined throughout years 2003 to 2011. Clockwise hysteresis loops having average hysteresis index of +1.59 was developed and an average of 40.904±12.453 Megatons (Mt) suspended sediment (SS) have been transported annually from higher Himalayas to hydropower reservoir. The Artificial neural networks (ANNs) was used to predict the daily suspended sediment rate and annual suspended sediment load 35.190±7.018 Mt satisfactorily compared to multiple linear regression (MLR), nonlinear multiple regression (NLMR), general power model, log transform models including sediment rating curve (SRC). Different performance indicators were evaluated to compare the best models and satisfactory fittings were observed in ANNs. The root mean square error (RMSE) 1982 kg/s, percent bias (PBIAS) +14.26, RMSE-observations standard deviation ratio (RSR) 0.55, correlation coefficient (R) 0.84 and Nash- Sutcliffe efficiency (NSE) +0.70 showed that ANNs model performed satisfactorily among all proposed models.

CHAPTER 1. GENERAL INTRODUCTION AND LITERATURE REVIEW

1.1 Research background

Sediment transport in river systems are important to understand the river hydraulics for a variety of disciplines such as hydrology, geomorphology, risk management including reservoir management. Sediment yield from a catchment is dependent on several parameters including topography, terrain slope, river gradient, channel cross section, rainfall, temperature and soil type of the catchment area (Gudino-Elizondo *et al.*, 2019). However, the yield of sediment fluxes is a combination effect of weathering, land sliding, glacial and fluvial erosions (Fort, 2016). Sediment yield from these effects are quite complex (Fort & Cossart, 2013) and varies seasonally. Hydrology of Nepal is primarily dominated by the monsoons characterized by higher precipitation during the summer monsoon from June to September which contributing about 80% of total annual precipitation (Mishra *et al.*, 2014). Studies showed that about 10% of the total precipitation occurs in a single day and 50% of total annual precipitation is occurred within 10 days of monsoon period (Dahal & Hasegawa, 2008) which is responsible for triggering landslides and debris flows in the catchment. The main natural agents for triggering landslides in the Himalayas are monsoon climate, extremities in precipitation, seismic activities, excess internal stress developed and undercutting of slopes by streams (Fort *et al.*, 2010). The sediments are transported by mountain streams in the form of suspended load as well as the bedload (Lenzi *et al.*, 1999). The sediment discharge depend on the intensity of rainfall and number of landslide events occurred within the catchment area (Struck *et al.*, 2015; Gabet *et al.*, 2004). The dam construction regulate the flood magnitudes and limits the downstream transportation of sediments (Asaeda *et al.*, 2011; Kummu & Varis, 2007). However, the annual deposition of sediment in the reservoirs decreases the capacity of reservoir which compromises the operability and sustainability of dam (Guillén-Ludeña *et al.*, 2018; De

Araujo *et al.*, 2006; Annandale, 2006). Basin morphology and lithological formation governs the amount of sediment crossing a stream station at a timepoint, which is generally acted upon by both active and passive forces (Megnounif *et al.*, 2013).

Outburst of glacier and failure of moraine dams trigger flash floods (Fort *et al.*, 2010; Fort, 1987; Costa & Schuster, 1988; O'Connor & Costa, 1993) which is one of the main causes of large boulder transportation in high gradient rivers in mountain region. The different hydraulic parameters such as shear stress, specific stream power and flow velocity can be combined to different ways to form sediment transport predictors (G. Zhang *et al.*, 2009; Ali *et al.*, 2012). Shear stress is a well-known hydraulic parameter that easily determined competence of rivers to transport coarse bedload material (Baker & Ritter, 1975; Lotsari *et al.*, 2015). Similarly, flow competence assessments of floods related to largest particle size transported are described by mean flow stress, specific stream power and mean velocity (Komar & Carling, 1991; Costa, 1983). Studies have been demonstrated relationships of shear stress (Costa, 1983; Komar, 1987; Lenzi *et al.*, 2006; O'Connor, 1993; Williams, 1983) specific stream power (Costa, 1983; O'Connor, 1993; Williams, 1983) and flow velocity (Costa, 1983; O'Connor, 1993; Bradley & Mears, 1980; Helley, 1969) of the river with size of boulder movement in the river system. It is important to perform this study in Kali Gandaki (KG) River as this river originates from the Himalayas and there is limited research in sediment transport by this river and is crucial in Nepal due to difference in terrain within a short distance.

Literature reviews for bed shear stress, specific power and flow velocity are summarized in Table 1, 2 and 3 respectively. The observed data and equations of different researchers are plotted and equations for average, upper and lower boundary are derived (Figure 2a,b and 3).

Table 1. Literature review for bed shear stress

S.No.	Bed shear stress equation	Source	Boundary condition	Compilation
1.	$\tau = 0.728 * d^{1}$ $d > 10\ mm$	Miller (1977) sited in Komar (1987)		
2.	$\tau = 0.17 * d^{1.0}$ $10mm \leq d \leq 3300mm$	Williams (1983)	Lower	Church (1972), Inbar & Schick(1979), Emmett (1976..Snake River), Emmett (1976…Clearwater River), Scott & Graviee (1968), Ritter (1967), Wolman & Eiler (1958), Burrow et al. (1979), Ramette & Heuzel (1962), Fahnestock (1963),Wilcock(1971), Emmett(1980), Milhous (1973)
3.	$\tau = 0.163 * d^{1.213}$(R=0.89) $50mm \leq d \leq 3290mm$	Costa (1983)	Regression line	Ritter (1967), Grimm & Leupold (1939), Fahnestock (1963), Lane (1955),Scott & Graviee (1968), Inbar & Schick 1979, Shroba & Schick (1979), Kellerhals(1967), Glancy & Harmsen (1975), Wolman & Eiler (1958), Milhous (1973), Thompson & Campbell (1979)
4.	$\tau = 0.056 * d^{1.213}$ $50mm \leq d \leq 3290mm$	Costa (1983)	Lower	
5.	$\tau = 0.164 * d^{1.21}$ $50mm \leq d \leq 5000mm$	Komar (1987)	Regression line	Lane & Carlson (1953) $\tau = 4.4 * d^{0.73} (R = 0.66) 2.5cm \leq d \leq 12cm$ Fahnestock 1963 $\tau = 19.3 * d^{0.48}$(R=0.50) 6 $cm \leq d \leq 48cm$ Scott & Gravlee 1968 $\tau = 0.81 * d^{1.56}$(R=0.94)46 $cm \leq d \leq 329cm$ Baker 1973 $\tau = 34.0 * d^{0.84}$(R=0.94) 46 $cm \leq d \leq 152cm$ Milhous 1973 $\tau = 10.8 * d^{0.57}$(R=0.81) 0.8 $cm \leq d \leq 12cm$ Carling(1983)$\tau = 11.0 * d^{0.38} 1\ cm \leq d \leq 20cm$ Hammond et al. (1984) $\tau = 5.5 * d^{0.42} 0.5cm \leq d \leq 4cm$
6.	$\tau = 0.0249 * d^{1.12}$(R=0.71) $270mm \leq d \leq 6240mm$	O'Connor (1993)	Regression line	
7.	$\tau = 86.629 * d^{0.25}$ $20mm \leq d \leq 1000\ mm$	Lenzi (2006)	Regression line	

Table 2. Literature review for specific power

S.No.	Power equation	Source	Boundary condition	Compilation
1.	$\omega = 0.079 * d^{1.3}$ $10 \leq d \leq 1500$	Williams, 1983	Lower	Fahnestock (1963), Milhous (1973), Emmett (1980), Burrow et al. (1979), Wolman & Eiler (1958), Ritter (1967), Emmett (1976..Snake River), Emmett (1976…Clearwater River), Inbar & Schick(1979)
2.	$\omega = 0.030 * d^{1.686}$(R=0.91) $50 \leq d \leq 3290$	Costa, 1983	Regression line	Ritter (1967), Grimm & Leupold (1939), Fahnestock (1963), Lane (1955),Scott & Graviee (1968), Inbar & Schick 1979, Shroba & Schick (1979), Kellerhals(1967), Glancy & Harmsen (1975), Wolman & Eiler (1958), Milhous(1973), Thompson & Campbell (1979)
3.	$\omega = 0.009 * d^{1.686}$ $50 \leq d \leq 3290$	Costa, 1983	Lower	
4.	$\omega = 0.002 * d^{1.71}$ $270 \leq d \leq 6240$	O'Connor 1993	Regression line	Observations
5.	$\omega = 30 * 1.00865^{0.1Di}$ $270 \leq d \leq 6240$	O'Connor 1993	Lower	Observations

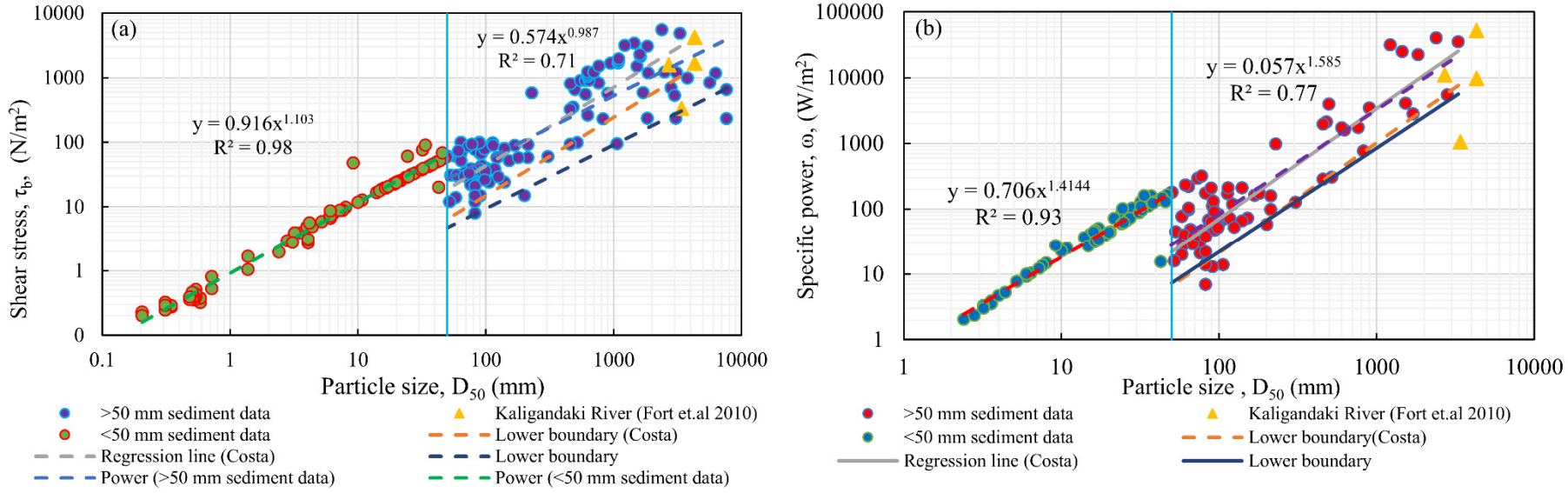

Figure 2. (a) Shear stress and particle size relationship (b) Specific power and particle size relationship

Table 3. Literature review for flow velocity

S.No.	Flow Velocity equation	Researcher	Boundary condition	PublicationsCompilation
1.	$v = 0.065 * d^{0.50}$ $10 \leq d \leq 1500$	Williams, 1983	Lower	Fahnestock(1963), Milhous(1973), Inbar&Schick(1979), Emmett (1976..Snake River), Emmett (1976…Clearwater River), Ritter (1967), Wolman & Eiler (1958), Burrow et al. (1979), Emmett(1980)
2.	$v = 0.20 * d^{0.455}$(R=0.84) $50 \leq d \leq 3290$	Costa, 1983	Regression line	Helley (1969), Ritter (1967), Grimm & Leupold (1939), Fahnestock (1963), Lane (1955),Scott & Graviee (1968), Inbar & Schick 1979, Shroba & Schick (1979), Kellerhals(1967), Glancy & Harmsen (1975), Wolman & Eiler (1958), Milhous(1973), Hooker (1896),Thompson & Campbell (1979)
3.	$v = 0.14 * d^{0.455}$ $50 \leq d \leq 3290$	Costa, 1983	Lower	Proposed from Costa compiled data.
4.	$v = 0.197 * d^{0.46}$ $8mm \leq d \leq 5000mm$	Komar, 1987	Regression line	Hooker (1896) $vc = 0.64 * d^{0.47}(R = 0.95) 5cm \leq d \leq 49cm$ Grimm & Leupold (1939), $vc = 1.02 * d^{0.34}(R = 0.88) 5cm \leq d \leq 52\ cm$ Fahnestock(1963) $vc = 1.28 * d^{0.18}(R = 0.55) 6cm \leq d \leq 48cm$ Helley (1969) $vc = 0.96 * d^{0.26}(R = 0.37) 15cm \leq d \leq 52cm$ Baker (1973) $vc = 1.31 * d^{0.53}(R = 0.77) 46cm \leq d \leq 152cm$ Milhous 1973 $vc = 0.3878 * d^{0.55}$(R=0.78) $0.8\ cm \leq d \leq 12cm$
5.	$v = 0.074 * d^{0.60}$(R=0.72) $270 \leq d \leq 6240$	O'Connor 1993	Regression line	Observations
6.	$v = 1.20 * v_b$ which is equivalent to $v = 0.1545 * d^{0.499}$	Bed velocity Helley(1969)and Flow velocity by Costa (1983)		Balancing forces using turning moments (Helley, 1969) $v_b = 3.276 * \sqrt{\frac{(\gamma_s - 1)d_L(d_s + d_i)^2 * MR_L}{C'_D d_L MR_D + 0.178 d_i d_L MR_L}}$
7.	$v_b = \sqrt{\frac{2 * (\gamma_s - \gamma_f)d_i * g * \mu}{\gamma_f(C_L + C'_D)}}$ $v = 1.20 * v_b$ which is equivalent to $v = 0.1628 * d^{0.5}$	Flow mean velocity by Costa (1983)		Equating fluid drag(F_D) and lift drag(F_L) against gravitational frictional resistance F_R $F_D + F_L = F_R$
8.	$v = 0.1866 * d^{0.50}$ 1 to > 600mm	U.S.B.R.		

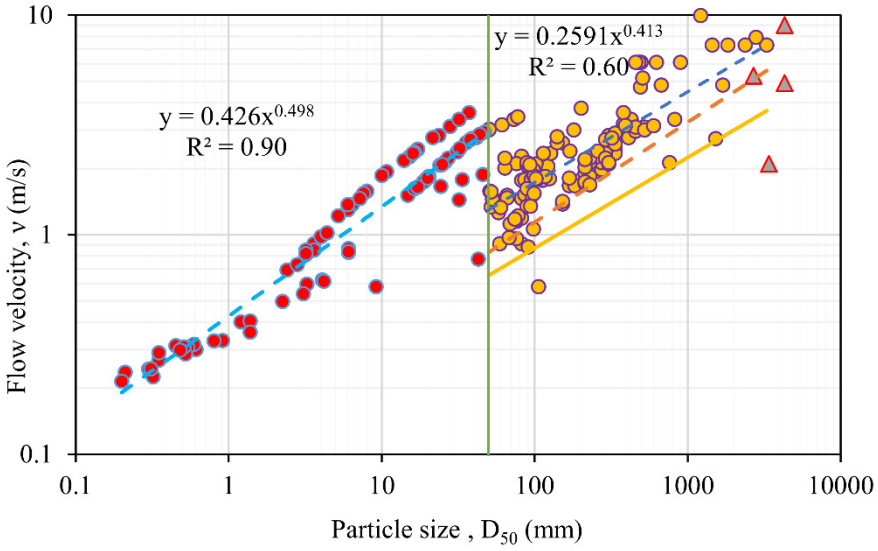

Figure 3. Flow velocity and particle size relationship

1.2 Research objectives

The following are the research objectives of this study (Part-I).

1. To develop the relationships of fluvial discharge and hydraulic parameters such as shear stress, specific stream power and flow velocity.
2. To derive a lowest boundary equation for maximum size of particle transported by fluvial discharge of KG River at 5 km upstream of hydropower dam.
3. To calculate the maximum size of particle transported by fluvial discharge of 2006-2011.
4. To explore the nature of hysteresis loops, developed hysteresis index, quantify the annual suspended sediment load transport (ASSL).
5. To develop different SS transport models for KG River and applied them to predict SS rate as well as average ASSL transport.

CHAPTER 2.0 MATERIALS AND METHODS

2.1 Observation site

The Kali Gandaki (KG) River is a glacier-fed river originating from the Himalaya region, Nepal (Bhusal & Subedi, 2015). The basin has complex geomorphology and watershed topography with rapid changes in elevation ranging from about 529 m MSL to 8143 m MSL. It flows from north to south in the higher Himalayan region before flowing eastward through the lower Himalayan region entering the Terai plains of Nepal with connection of Narayani River, which ultimately merge with the Ganges River in India. Figure 4a shows the different altitude area coverage map showing river networks with locations of meteorological stations created in ArGIS10.3.1(ERSI Inc., USA) software. The elevations of KG River decreases from 5039 m MSL in higher Himalaya to 529 m MSL at Setibeni, 5 km upstream of hydropower dam (Figure 4b) encompasses with wide variation in mean rainfall ranging less than 500 mm yr^{-1} in Tibetan Plateau and about 2000 mm yr^{-1} in the monsoon-dominated Himalayas (Struck *et al.*, 2015). The SS is measured at the hydropower dam.

The main physiographic characteristics of KG River basin at hydropower station is shown in Table 4.

Table 4. Main characteristics of river basin

Parameters	Descriptions
Catchment area	7060 km^2
Length of river up to dam	210 km
Mean gradient of river	2.20%
Extreme Discharge	3280 m^3/s in 1975, 2824.5 m^3/s in 2009
Elevation ranges	529 m MSL -8143 m MSL
Precipitation	Tibetan plateau < 500 mm/yr, Monsoon dominated Himalayas ~ 2000 mm/yr

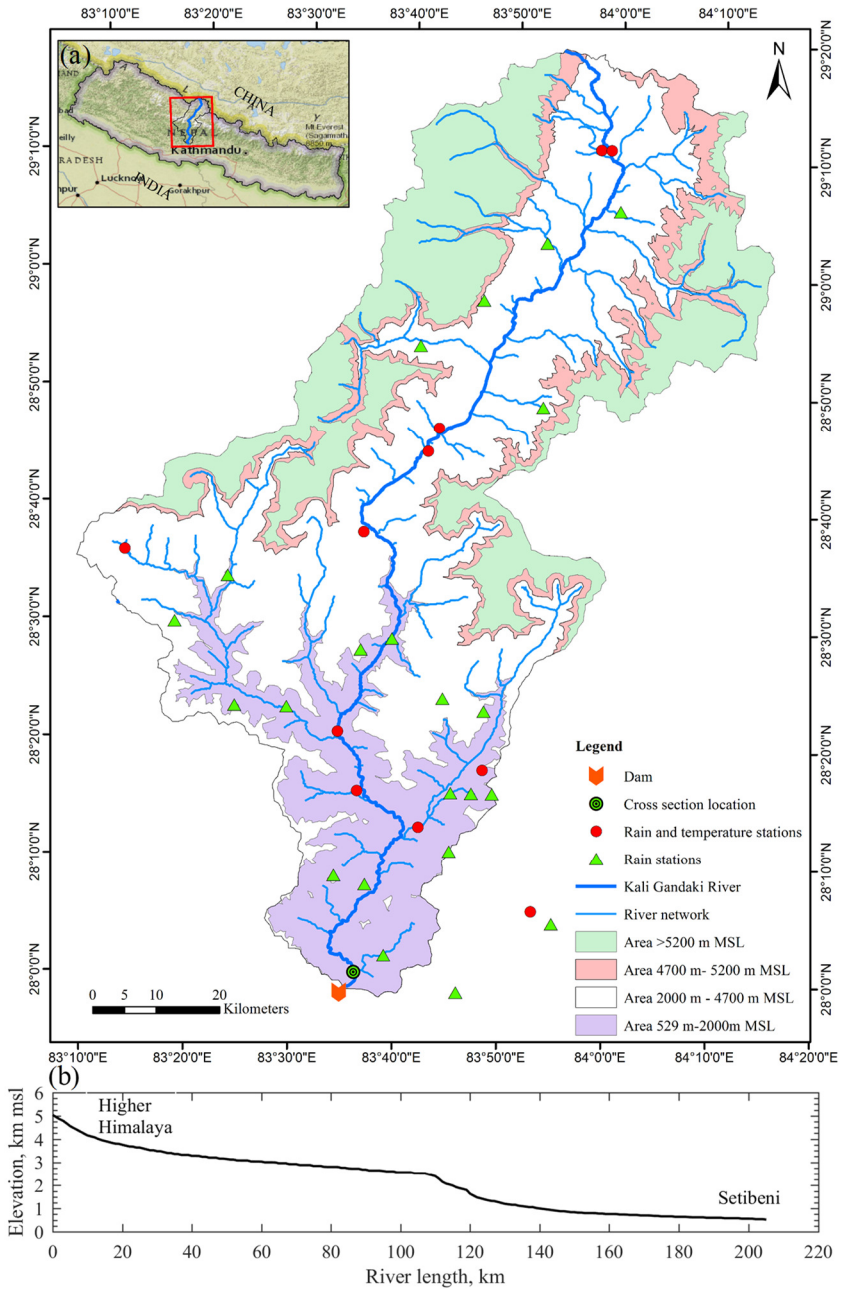

Figure 4. (a) Map of KG River catchment area (b) Longitudinal profile of KG River

The characteristics of basin area is separated as elevation ranges less than 2000 m MSL with no snow cover, 2000 ~ 4700 m MSL with seasonal snow, 4700 ~ 5200 m MSL with completely snow except 1 or 2 month and elevation greater than 5200 m MSL with permanent snow (Mishra *et al.*, 2014). The KG catchment basin at Setibeni outlet has 7060 Km^2 area comprises of elevations 529~2000 m MSL is 1317 Km^2 (19% coverage), 2000~4700 m MSL is 3388 Km^2 (48% coverage), 4700~5200 m MSL is 731 Km^2 (10% coverage) and elevation greater than

5200 m MSL is 1624 Km^2 (23% coverage). The area coverage details of catchment area is shown in Figure 5.

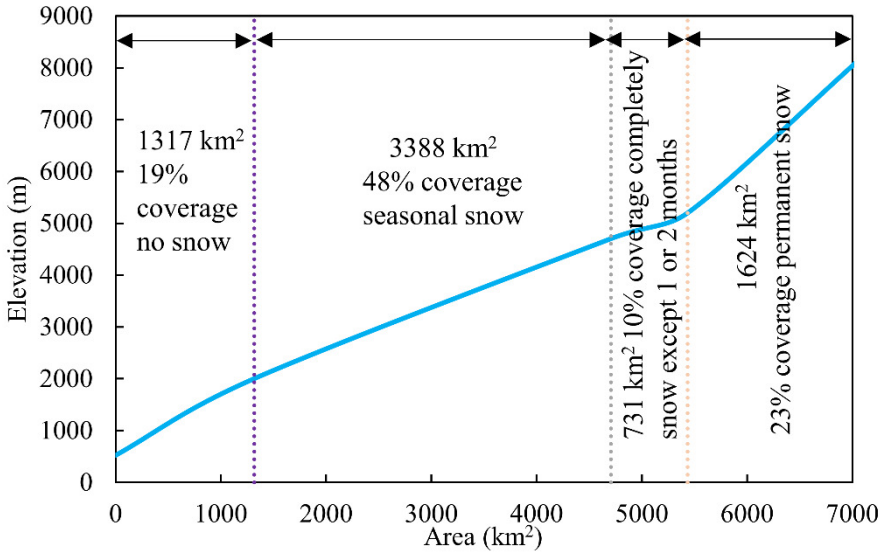

Figure 5. Elevation wise catchment area and snow contribution

2.2 Data collection and acquisition

The discharge of KG River varies seasonally and is dependent on the rainfall received within its tributary catchments in addition to the amount of snow melting from the Himalayas. A hydropower dam (27°58'44.88" N, 83°34'49.68" E) was constructed in 2002 for 144 MW power generation, at Mirmi, Syangja. Department of Hydrology and Meteorology (DHM), Nepal installed a river hydrometric station (28°00'30" N, 83°36'10" E) in 1964 (www.dhm.gov.np) and operated up to 1995. The station was not operated during hydropower dam construction period (1997-2002). The bed level of dam was increasing yearly due to trapping of bedload as well as suspended sediment load by dam, which reduced sediment load in the downstream. The cross-sectional areas of different years were calculated from area-discharge regression equations obtained from historical discharge rating data sourced from DHM (1964-1995) as shown in Figure 6a,b. The sedimentation lowers the reservoir capacity of dam annually.

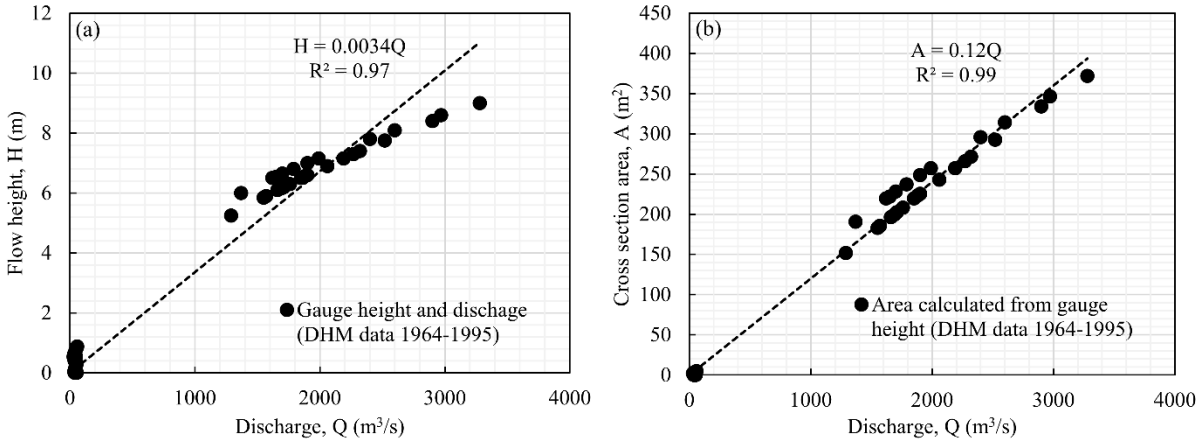

Figure 6.(a) Flow height and discharge relationship (b) Cross section area (calculated from height) and discharge relationship

2.3 Analysis of hydraulic parameters for sediment transport

Historical fluvial discharges and cross profile elevations data sourced from Nepal Electricity Authority(NEA), Nepal were used to calculate bed shear stress, specific power developed and flow velocity by using following well- known equations (Kale & Hire, 2004; Mao *et al.*, 2008; Wicher-Dysarz, 2019).

$$\text{Bed shear stress, } \tau_b = \rho * g * R * i \tag{I.1}$$

The mean available power supply over unit bed area is calculated by

$$\omega = \frac{\Omega}{w_t} = \frac{\rho * g * Q * i}{w_t} \tag{I.2}$$

where, w_t represents width of flow, Ω is available stream power supply or time rate of energy supply to the unit length of stream in w/m and is given by,

$$\Omega = \rho * g * Q * i \tag{I.3}$$

Flow velocity is calculated by Manning's formula,

$$v = \frac{1}{n} R^{2/3} * S^{1/2} \tag{I.4}$$

Where, τ_b is Bed shear stress (N/m^2), ρ is density of water (1000 kg/m^3), g is acceleration due to gravity (9.81 m/s^2), R is hydraulic radius (m), i is slope of river bed (m/m), ω is mean available specific stream power per unit area (w/m^2), Q is observed discharge (m^3/s), v is flow velocity (m/s), and n is Manning's constant. Manning's constant n in steep natural channel, calculated by equation proposed by Jarrett (Jarrett, 1984).

$$n = 0.39S^{0.38}(3.28R)^{-0.16} \tag{I.5}$$

2.4 Model development for suspended sediment predictions

Daily suspended sediment load transported by river in the catchment area is a key numerical indicator to picturize the sediment loss from higher Himalayas and assess the reservoir management in hydropower projects. Different researchers have developed different models such as Multiple Linear Regression (MLR) and Nonlinear Multiple Regression (NMLR), Sediment Rating Curve (SRC) and Artificial Neural Networks (ANNs) models for prediction of daily suspended sediment (Uca *et al.*, 2018; Ulke *et al.*, 2009).

2.4.1. Multiple Linear Regression

Multiple linear regression assumes that the sediment load transported by river is in the linear form. In the model, SS load Q_{s_t} is a dependent variable which depends on two independent variables as daily average discharge of river (Q_{w_t}) and average rainfall (R_t) of catchment area. MLR model is expressed in the form of regression equation (Uca *et al.*, 2018; Ulke *et al.*, 2009).

$$Q_{s_t} = \beta_0 + \beta_1 Q_{w_t} + \beta_2 R_t \quad \text{(I.6)}$$

The different linear models were developed by considering Q_{w_t}, a day lag discharge $Q_{w_{t-1}}$and R_t ,and a day lag rainfall R_{t-1}. Fluvial discharges and rainfalls were input variables of the model. The performance of different MLR models were also evaluated by different performance indicators and will describe in coming subheading.

2.4.2. Nonlinear Multiple Regression

The suspended sediment transported by river shows the dynamic state in the form of nonlinear so that it is expressed in the form of polynomial equation (Uca *et al.*, 2018; Ulke *et al.*, 2009).

$$Q_{s_t} = \beta_0 + \beta_1 Q_{w_t} + \beta_2 R_t + \beta_{11} {Q_{w_t}}^2 + \beta_{22} {R_t}^2 \quad \text{(I.7)}$$

The different NLMR models were also developed and performance indicators of different models were evaluated separately.

2.4.3. Sediment rating curve

SRC is expressed (Glysson, 1987) in the form as

$$Q_{s_t} = a {Q_{w_t}}^b \quad \text{(I.8)}$$

Where Q_{s_t} is suspended sediment load (kg/s), Q_{w_t} is daily average discharge of river, a and b are coefficients that depend on characteristics of river.

2.4.4. Artificial Neural Networks

An artificial neural network is capable of solving complex nonlinear relationships between

input and output parameters which consists of three different layers known as input, hidden and output layer respectively (Ulke *et al.*, 2009). MATLAB(R2016a) software was used for developing different artificial neural networks, where input consists of average daily river discharge (Q_{w_t}), a day lag discharge ($Q_{w_{t-1}}$) and average daily rainfall (R_t), a day lag rainfall (R_{t-1}) , whereas output consists of an average daily suspended sediment load (Q_{s_t}). Out of 2191 fluvial and sediment data sets of duration 2006-2011, 70% data was used for training purpose, 15% for validation purpose and 15% for testing purpose in ANNs calibration.

2.5 Model performance indicators

The performance of different models are evaluated in terms of root mean square (RMSE), percent BIAS (PBIAS), RMSE-observations standard deviation ratio (RSR), correlation coefficient (R)and Nash- Sutcliffe efficiency (NSE) (Uca *et al.*, 2018; Moriasi *et al.*, 2007; Pandey *et al.*, 2018).

$$RMSE = \sqrt{\frac{\sum_{i=1}^{n}\left(Q_{s_{o,i}} - Q_{s_{p,i}}\right)^2}{N}} \tag{I.9}$$

Lower the *RMSE* value, better the model performance.

$$PBIAS = \left\{\frac{\sum_{i=1}^{n}\left(Q_{s_{o,i}} - Q_{s_{p,i}}\right)}{\sum_{i=1}^{n} Q_{s_{o,i}}}\right\} * 100 \tag{I.10}$$

Where optimal PBIAS value is 0.0, positive values indicate model underestimation bias and negative values indicate model overestimation bias.

$$RSR = \frac{RMSE}{STDEV_o} = \frac{\left\{\sqrt{\sum_{i=1}^{n}\left(Q_{s_{o,i}} - Q_{s_{p,i}}\right)^2}\right\}}{\left\{\sqrt{\sum_{i=1}^{n}\left(Q_{s_{o,i}} - \bar{Q}_{s_{p,i}}\right)^2}\right\}} \tag{I.11}$$

The optimal value for RSR is 0.0, lower the RSR, the lower the RMSE and better the model performance.

Correlation coefficient

$$R = \left\{\frac{\sum_{i=1}^{n}\left(Q_{s_{o,i}} - \bar{Q}_{s_{o,i}}\right)\left(Q_{s_{p,i}} - \bar{Q}_{s_{p,i}}\right)}{\sqrt{\sum_{i=1}^{n}\left(Q_{s_{o,i}} - \bar{Q}_{s_{o,i}}\right)^2 \sum_{i=1}^{n}\left(Q_{s_{p,i}} - \bar{Q}_{s_{p,i}}\right)^2}}\right\} \tag{I.12}$$

The optimal value for R is 1.0, higher the value of R, better the model performance.

$$NSE = \left\{1 - \frac{\sum_{i=1}^{n}\left(Q_{s_{o,i}} - Q_{s_{p,i}}\right)^2}{\sum_{i=1}^{n}\left(Q_{s_{o,i}} - \bar{Q}_{s_{o,i}}\right)^2}\right\} \quad \text{(I.13)}$$

The optimal value for NSE is 1.0 and its value ranges from -∞ to 1. Values between 0.0 and 1.0 are taken as acceptable levels of performance whereas negative values indicate that the mean observed value is a better predictor than the predicted value, which shows unacceptable performance. Where $Q_{s_{o,i}}$ and $Q_{s_{p,i}}$ are observed and predicted suspended sediment and $\bar{Q}_{s_{o,i}} and\ \bar{Q}_{s_{p,i}}$ are average observed and average predicted suspended sediment respectively.

CHAPTER 3.0 RESULTS AND DISCUSSION

3.1 Historical fluvial discharge and cross section of river

The average discharge of KG River from year 2003 to 2012 was 306 m^3/s with minimum discharge of 40.73 m^3/s during winter in 2009 and maximum discharge 2825 of m^3/s during monsoon in 2009. There was a decreasing trend of maximum discharge from 2003 to 2006 whereas increasing trend from 2007 onwards (Figure 7a). The transported sediment load increases nearby upstream riverbed level elevations of reservoir (Figure 7b) and sediment deposited into the reservoir decreases reservoir's capacity. The climate change effects in higher Himalayas appear in the form of uneven patterns of increasing rainfall, glacial- rate erosion and permafrost degradation resulting in an increase in landslides and debris flows (Fort, 2016; U. B. Shrestha *et al.*, 2012; Singh & Kumar, 1997), which also reflects on the temporal and spatial variation of water balance components in the KG basin (Bajracharya *et al.*, 2018). The amount and intensity of rainfall around its catchment affects the discharge rating curve (Bhusal & Subedi, 2015).

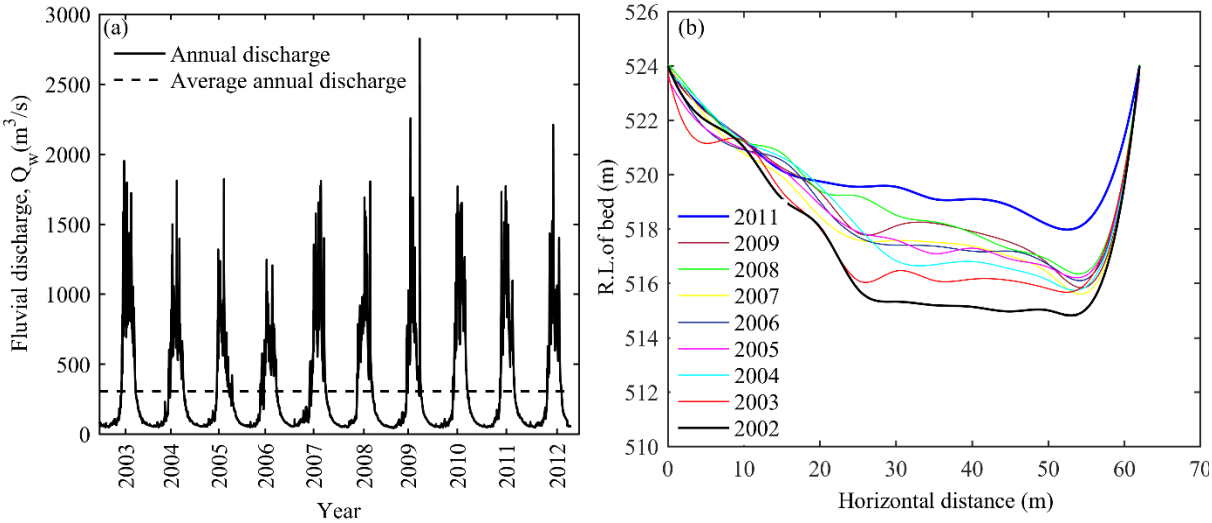

Figure 7.Yearly (a) discharge (NEA 2003- 2012) (b) Cross profiles (2002-2011) of KG River

3.2 Shear stress, Specific stream power and Flow velocity relationship with discharge

The calculated shear stress, specific stream power and flow velocity of KG River at discharge gauge station located about 5 Km upstream from dam within limited data 2003 – 2011 years

was increasing function with fluvial discharge and related as

$$\tau_b = 3.143 * Q^{0.621} \ (R^2 = 0.72) \quad \text{(I.14)}$$

$$\omega = 27.40 * Q^{0.612} \ (R^2 = 0.65) \quad \text{(I.15)}$$

$$v = 0.108 * Q^{0.519} \ (R^2 = 0.95) \quad \text{(I.16)}$$

The highest shear stress, specific stream power and flow velocity was observed during 2008 whereas lowest during 2007. These parameters were directly related with hydraulic radius in case of shear stress and flow velocity, whereas fluvial discharge in case of specific power (Equations I.1, I.2 and I.4). The sedimentation of transported sediment increased the bed level elevation, changed the cross geomorphology of bed (Figure 7b). These parameters were followed nearly the same trends during the remaining years. The hydraulic parameters: shear stress, specific power and flow velocity of river were increasing function of fluvial discharge (Figures 8a,b and 9a).

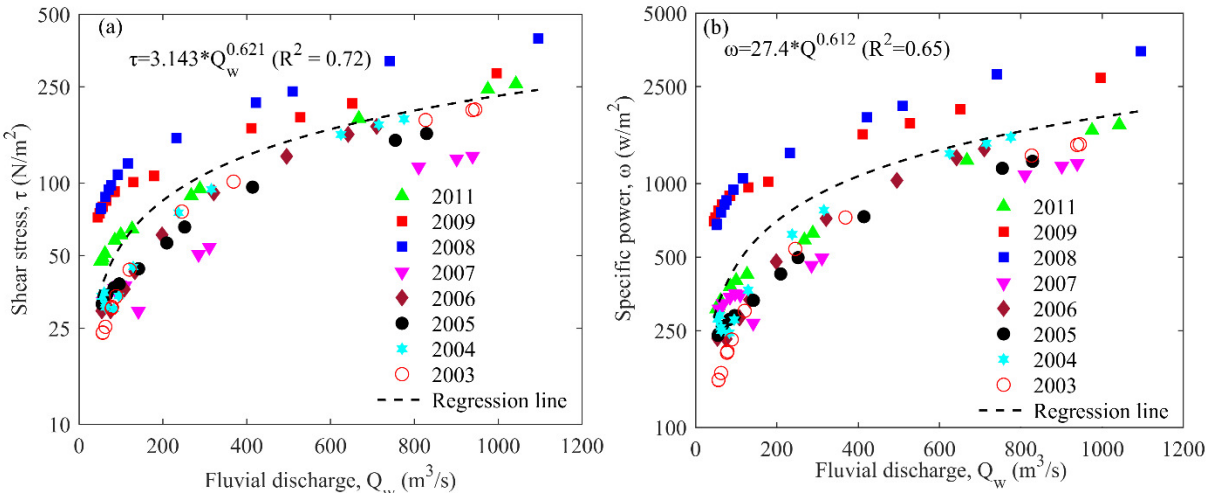

Figure 8. Relationship of fluvial discharge and (a) Shear stress (b) Specific power

3.3 Particle sizes and fluvial discharge relationship

Hydraulic parameters: shear stress, specific stream power and flow velocity depict transportation of different particle sizes. Subjected to same fluvial discharge, specific power showed transportation of 327 mm to 2062 mm particle size whereas flow velocity depicted

transportation of 37 mm to 1794 mm particle size. The shear stress exhibited transportation of 147 mm to 1492 mm particle which covered lowest maximum particle sizes compared to specific power and flow velocity (Figure 9b). These three parameters were derived from fluvial discharge and to cover all particle sizes, a lowest boundary equation with fluvial discharge was derived as shown in Figure 9b:

$$d_{mm} = 0.4 * Q^{1.093} \ (25mm \leq d \leq 840\ mm) \qquad \text{(I.17)}$$

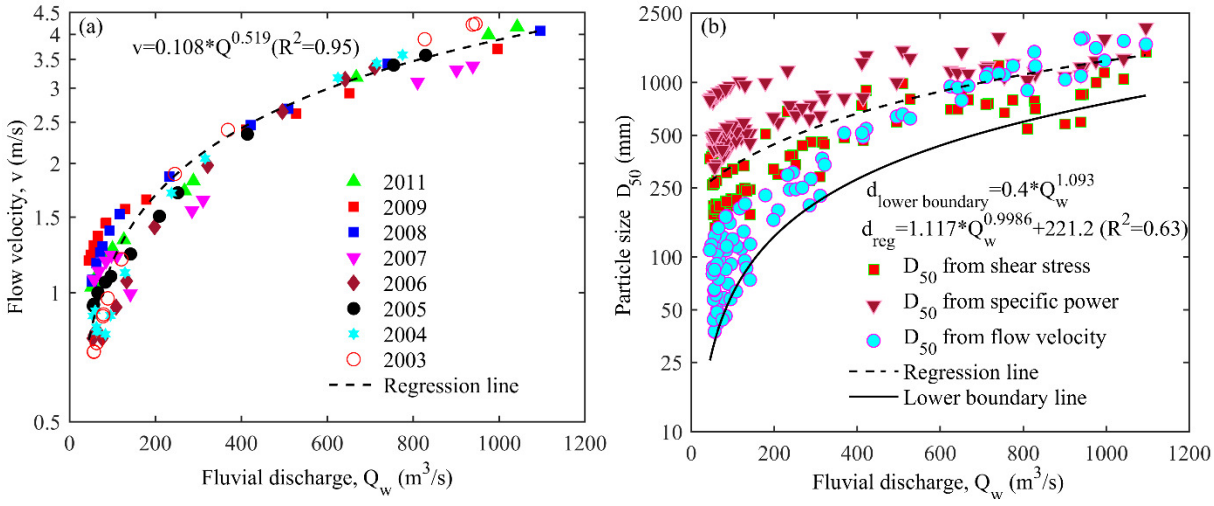

Figure 9. Relationship of fluvial discharge and (a) Flow velocity (b) Particle size (D_{50})

Equation (I.17) predicted that from the year 2003 to 2011, the discharge during monsoon was capable of transporting 840 mm particle size. Hydraulic parameters such as bed shear stress, specific stream power and flow velocity have gained wider acceptability among different researchers (Costa, 1983; Komar, 1987; Lenzi *et al.*, 2006; O'Connor, 1993; Williams, 1983; Bradley & Mears, 1980; Helley, 1969) regarding their useful contribution in derivation of relationship between particle sizes and hydraulic parameters. The shear stress and particle size relationship of this study was compared with Costa's (Costa, 1983) average $\tau_b = 0.163d^{1.213}$, lower boundary $\tau_b = 0.056d^{1.213}$ for 50 mm $\leq d \leq$ 3290 mm, Komar's (Komar, 1987) $\tau_b = 0.164d^{1.21}$for 50 mm $\leq d \leq$ 5000 mm, Lenzi's (Lenzi *et al.*, 2006) $\tau_b = 86.629d^{0.25}$ for 20 mm $\leq d \leq$ 1000 mm, O'Connor's (O'Connor, 1993) average $\tau_b = 0.0249d^{1.12}$ for 270 mm $\leq d \leq$ 6240 mm and Williams's (Williams, 1983) lower boundary $\tau_b = 0.17d^{1.0}$ for 10 mm $\leq d \leq$ 3300 mm

(Figure 10).

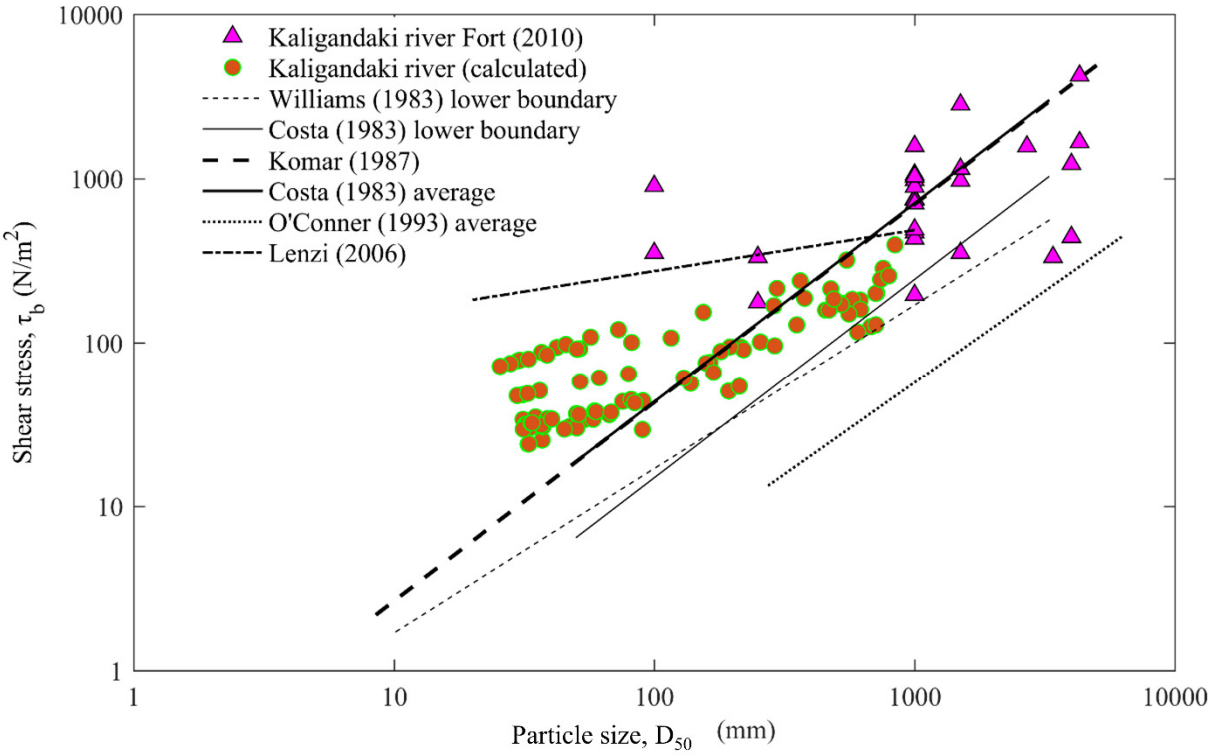

Figure 10. Relationship of shear stress and particle size (D_{50}) and comparison with different researchers

For comparative study of specific stream power and particle size relationship of this river was compared with Costa's (Costa, 1983) average $\omega = 0.030d^{1.686}$, lower boundary $\omega = 0.009d^{1.686}$for 50 mm $\leq d \leq$ 3290 mm, O'Connor's (O'Connor, 1993) average $\omega = 0.002d^{1.71}$, lower boundary $\omega = 30 * 1.00865d^{0.1d}$ for particle size 270 mm $\leq d \leq$ 6240 mm and Williams's (Williams, 1983) lower boundary $\omega = 0.079d^{1.3}$ for 10 mm $\leq d \leq$ 1500 mm (Figure 11).

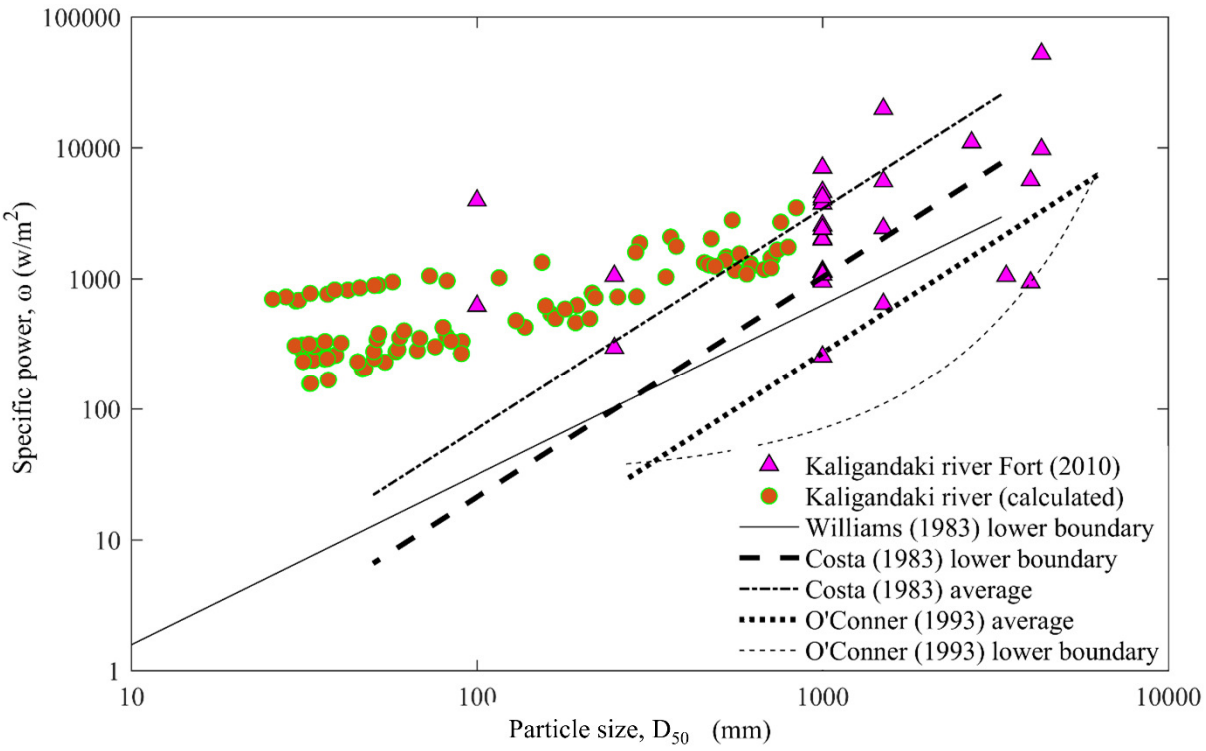

Figure 11. Relationship of specific power and particle size (D_{50}) and comparison with different researchers

The flow velocity and particle size relationship of this study was compared with Costa's (Costa, 1983)average $v = 0.20d^{0.455}$, lower boundary $v = 0.14d^{0.455}$ for 50 mm $\leq d \leq$ 3290, U.S.B.R.'s (Costa, 1983) $v = 0.187d^{0.50}$ for 1 mm $\leq$ d $\leq$ 600 mm, Komar's (Komar, 1987) $v = 0.197d^{0.46}$for 8 mm $\leq$ d $\leq$ 5000 mm, O'Connor's (O'Connor, 1993) average $v = 0.074d^{0.60}$ for 270 mm $\leq$ d $\leq$ 6240 mm, Williams's (Williams, 1983) lower boundary $v = 0.065d^{0.50}$ for 10 mm $\leq$ d $\leq$ 1500 mm, Bradely and Mears's (Bradley & Mears, 1980) $v = 0.163d^{0.5}$ for 50 mm $\leq d \leq$ 3290 and Helley's (Helley, 1969) $v = 0.1545d^{0.499}$for 1 mm $\leq d \leq$ 600 mm (Figure 12).

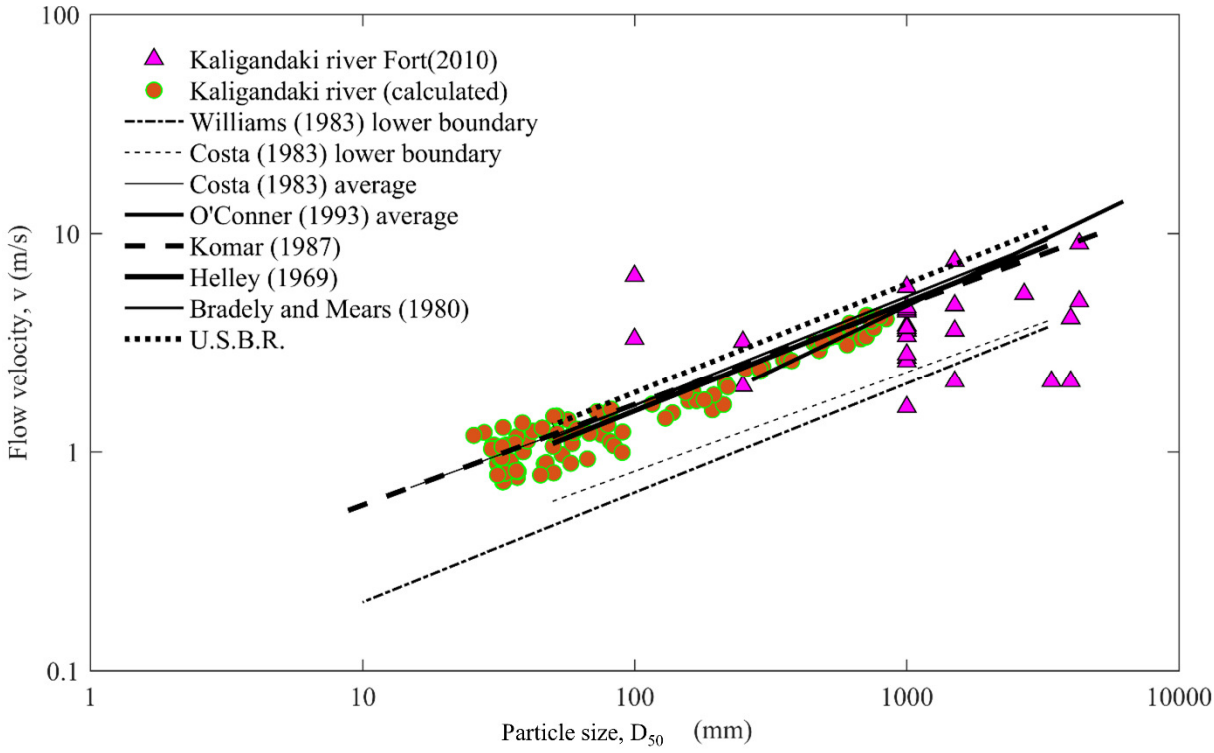

Figure 12. Relationship of flow velocity and particle size (D_{50}) and comparison with different researchers

The calculated values of shear stress, specific stream power and flow velocity were lesser than the observed values by Fort (2010), reconstructed 1998 landslide dam located about 76 km upstream of existing hydropower dam of KG River and estimated hydraulic parameters with exceptional dam breach discharge as 10,035 m^3/s. This high discharge was responsible for movement of maximum boulder size 4300 mm (Fort *et al.*, 2010). The higher shear stress, specific stream power and flow velocity observed due to higher fluvial discharge after breaching of landslide dam were responsible for transport of higher sizes of boulder (Figures 10, 11 and 12).

3.4 Flood return period estimation by Gumbel's distribution

Flood return period from historical data of DHM, Nepal can be forecasted by Gumbel method (Onen & Bagatur, 2017) as $Q_T = \bar{Q} + k\sigma_n$, where $\bar{Q}$ is mean discharge, k is frequency factor and σ_n is standard deviation of maximum instantaneous flows respectively. The frequency factor is

given by $k = \left(\frac{y_t - \bar{y}_n}{s_n}\right)$,where $\bar{y}_n$ is mean and s_n is standard deviation of Gumbel's reduced variate, $\bar{y}_n$ is given by $y_t = -ln\left[ln\left(\frac{T}{T-1}\right)\right]$. The observed highest flood in 1975 was 3280 m^3/s. According to Gumbel frequency of flood distribution, it is estimated that a highest flood will be occurred after 40 years return period shown in Figure 13a and the observed extreme discharge is shown in Figure 13b.

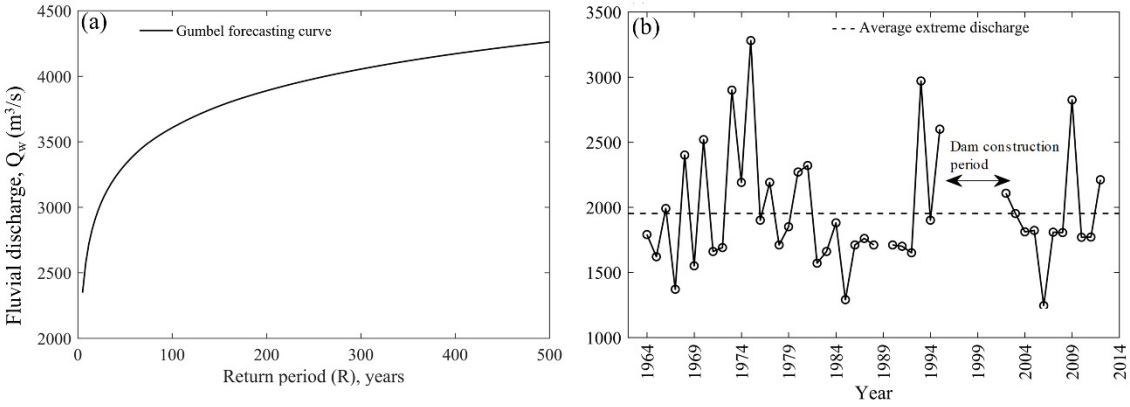

Figure 13. (a) Gumbel flood return period, (b) Extreme fluvial discharge

3.5 Boulder movement mechanisms by high gradient river

High gradient river hydraulics are strongly influenced by large boulders with the diameters on the same scale as channel depth or even width (Grant *et al.*, 1990). Williams (Williams, 1983) described five possible mechanisms of boulder transport by high gradient river are by ice, mudflow, water stepwise creep by periodic erosion, undermining of stream banks and avalanches. The bed forming material remain immobile during typical flows and larger bed forming particles in steep gradient channels typically become mobile only in 50-100 years of hydrologic event (Montgomery & Buffington, 1997). After that the gravel stocked in low energy sites during lower floods, is mobilized and travelled as bedload (Montgomery & Buffington, 1997).

The failure of mountain slope of KG catchment in 1988, 1989 and 1998 evolved rock avalanche and caused damming of the KG River (Monique Fort, 2016). The shockwaves after a massive

7.8 M_w Gorkha earthquake, Nepal on April 25, 2015 and its aftershocks on May 23, 2015 have created cracks in the weathered rocks and weakened the mountain slopes of this catchment that brought rocks, debris and mud down in to the river (Marahatta, 2015; Bricker *et al.*, 2017). The river was blocked about 56 Km upstream from the hydropower dam by landslide on May 24, 2015 for 15 hours (Marahatta, 2015) (Figures 14a,b). The downstream fluvial discharge after blockage was almost zero and a flash flood generated after outburst of natural landslide dam (Figures 14c,d). The extreme flood during monsoon period due to high rainfall event and the flash flood (Figure 13b) generated by overtopping of landslide dams (Bricker *et al.*, 2017) were responsible to noticeable transport of large boulders in the river bed of KG River.

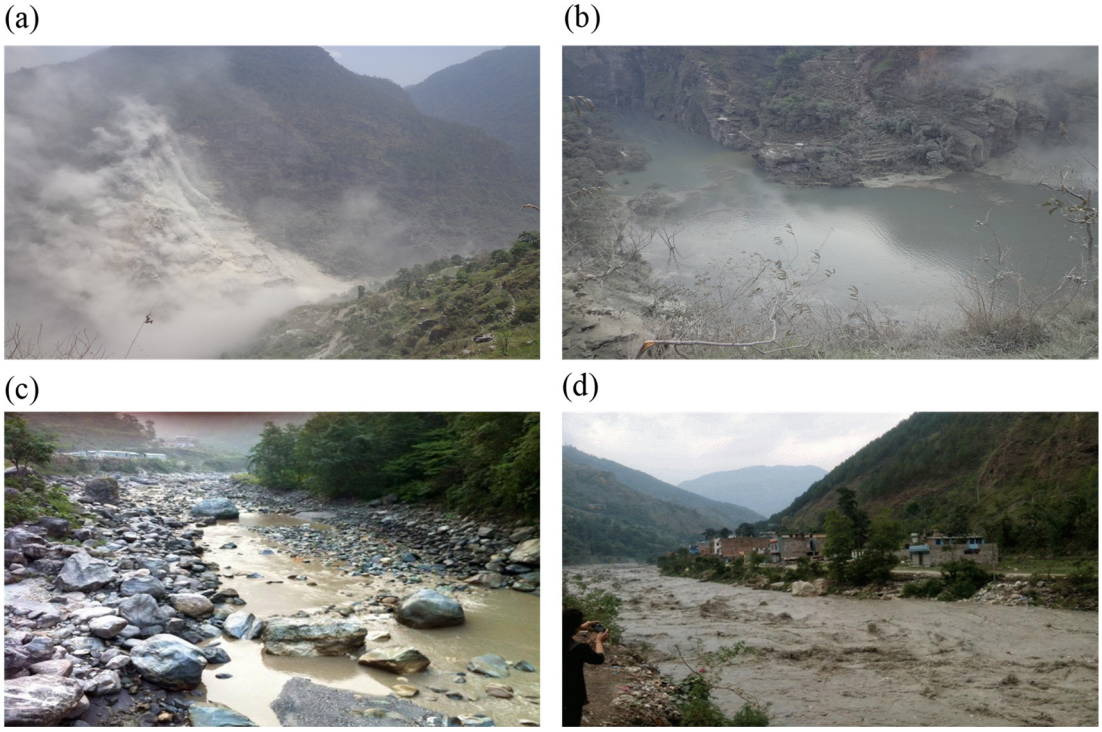

Figure 14. (a) Natural landslide dam formation on May 24, 2015 (~ 56 km upstream of dam) (b) Lake formation after blockage of river (c) Downstream fluvial discharge after blockage of river (d) Flash flood after breaching of landslide dam May 25, 2015

(Source: http://kathmandupost.ekantipur.com/news/2015-05-24/blocked-kali-gandaki-river-flows-again-with-photos.html)

The combination of fluid stress, localized scour and undermining of the stream banks may effect small near vertical displacements of large boulders (Griffiths, 1977). The catastrophic events such as natural dam breaks, debris flows are responsible for larger translations of boulders in the rivers (Montgomery & Buffington, 1997; Griffiths, 1977).

3.6 Suspended sediment quantification and prediction

3.5.1 Hysteresis curve and hysteresis index (HI_{mid}) analysis

Relationship between suspended sediment concentration and fluvial discharge are studied by a nonlinear relationship between them known as hysteresis (Williams, 1989). Generally, a clockwise hysteresis loop is formed due to increasing concentration of sediment more rapidly during rising limb which suggests a source of sediment close to the monitoring point and sediment depletion in channel system. Conversely, anticlockwise hysteresis loop shows a long gap between discharge and concentration peak, which suggests that the source was located far from monitoring point or bank collapse (Bača, 2008; Lloyd *et al.*, 2016).

The clockwise hysteresis loops were developed, increasing suspended sediment load on the rising limb of hysteresis from December to July, leads to a maximum value of suspended sediment load 10691 kg/s for fluvial discharge 1053 m^3/s on August 2009. The suspended sediment load decreases on the falling limb of hysteresis from July/September to November. The different years between 2006-2011 were characterized by distinct clockwise hysteresis patterns (Figure 15a).

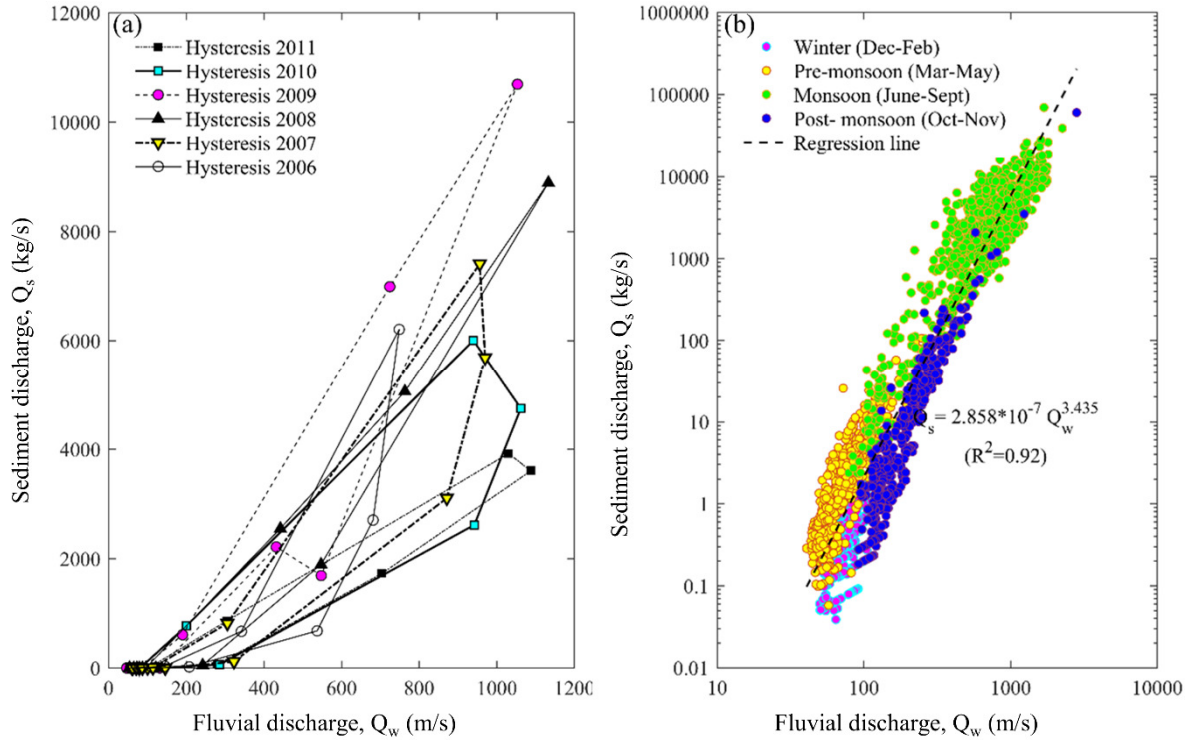

Figure 15. (a) Seasonal hysteresis loop of sediment load (b) Suspended sediment – discharge rating curve.

The hysteresis index (HI_{mid}) is a numerical indicator of hysteresis which effectively shows the dynamic response of suspended sediment concentrations to flow changes during storm events (Lawler *et al.*, 2006). A clockwise hysteresis loop and HI calculation is illustrated in Figure 16.

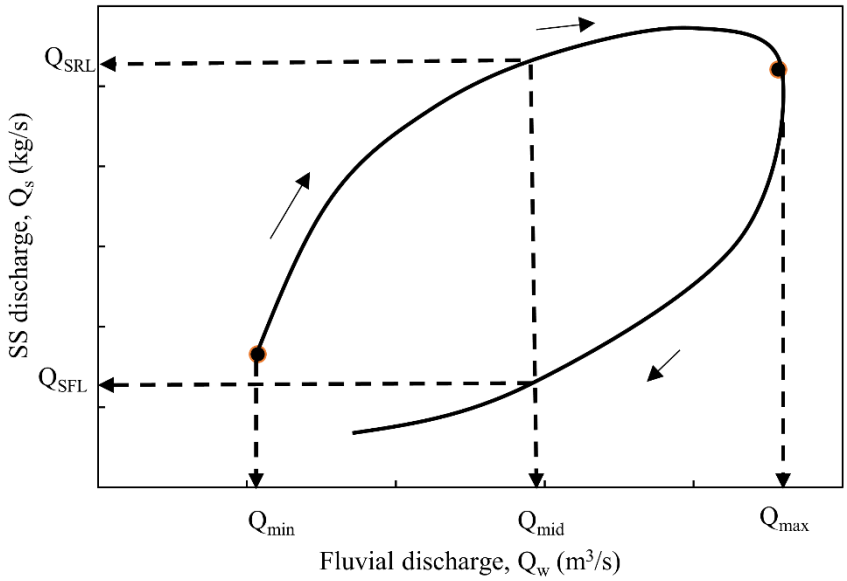

Figure 16. Hysteresis index derivational demonstration

The midpoint discharge is calculated as

$$Q_{mid} = k(Q_{max} - Q_{min}) + Q_{min} \quad \text{(I.18)}$$

Where k is 0.5, Q_{max} is peak discharge and Q_{min} is the starting discharge of event.

The hysteresis index value is calculated by Lloyd (Lloyd *et al.*, 2016) and Lawler (Lawler *et al.*, 2006).

$$HI_{mid} = \left(\frac{Q_{s_{RL}}}{Q_{s_{FL}}}\right) - 1 \text{ for clockwise loop} \quad \text{(I.19)}$$

$$HI_{mid} = \left(-1 \Big/ \left(\frac{Q_{s_{RL}}}{Q_{s_{FL}}}\right)\right) + 1 \text{ for anticlockwise loop} \quad \text{(I.20)}$$

Where $Q_{s_{RL}}$ and $Q_{s_{FL}}$ are suspended sediment on rising and falling limb respectively.

3.5.2 Yearly SS yield

A regression equation derived from observed data (2006-2011) of SS versus discharge of river shown in Figure 15b.

$$Q_s = 2.858 * 10^{-7} * Q_w^{3.435} (R^2 = 0.92) \quad \text{(I.21)}$$

The total suspended sediment yield from catchment is given by

$$Y_s = \int_{t=0}^{T} C_{w_i} Q_{w_i} dt = \sum_{i=1}^{365} C_{w_i} Q_{w_i} * 10^{-3} * (t_{i+1} - t_i) \quad \text{(I.22)}$$

Where Y_s is total annual sediment yield from the catchment, C_{w_i} is suspended sediment concentration in mg/l, $Q_{w_i}$is fluvial discharge in m^3/s, dt is time interval, t_i and t_{i+1} are preceding and succeeding time in seconds respectively.

This study showed that the median ASSL transported by KG River in hydropower reservoir was 0.003 Mt during winter, increased to 0.026 Mt during pre-monsoon, 41.405 Mt during monsoon season respectively and decreased 0.175 Mt during post-monsoon season (Figure 17a). Compared to seasonal transport of SS, more than 96% of SS was transported during monsoon season. This depicts a wide seasonal variability of SS caliber which was nearly fourteen thousand times higher than winter season (Figure 17a). The maximum observed ASSL

transported by river was occurred 58.426 Mt in 2009, after that it was decreased (Figure 17b).

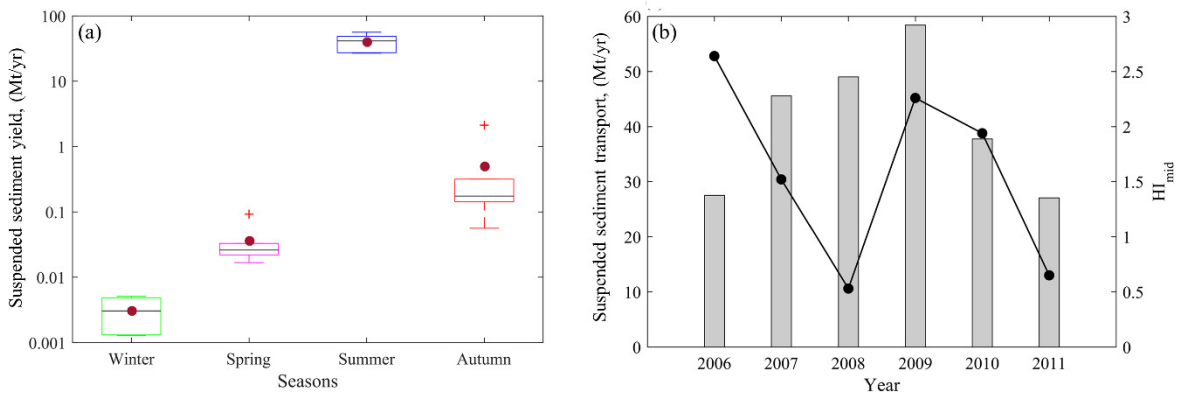

Figure 17. (a) Seasonal SS yield (b) Yearly SS transport and hysteresis index (HI_{mid})

Central lines indicate the median, bottom and top edges of the box indicate the 25th and 75th percentiles respectively. The whiskers extend to the most extreme data points not considered outliers, '+' symbol represents outliers (1.5-fold interquartile range), circle shows the mean value.

The $HI_{mid} \approx 0$ indicated weak hysteresis loop whereas $HI_{mid} > 0$, a clockwise hysteresis loop, and $HI_{mid} < 0$ an anticlockwise hysteresis loop. Moreover, the maximum HI_{mid} developed was +2.64 in 2006 depicted the higher sediment transport rate in rising limb but lower sediment transport rate in falling limb (Figure 15a), whereas the minimum HI_{mid} developed was +0.53 in 2008 depicted the nearly same paths of rising and falling limb indicated a weak hysteresis loop (Figure 15a and 17b) .

3.5.3 SS prediction by different models

Different types of MLR, NLMR, General power, log transform linear and ANNs models with different equations having inputs of fluvial discharge and average rainfall of catchment were developed to select most suitable model and results are shown in Tables 5, 6, 7, 8 and 9 respectively. The performance indicators of MLR and NLMR falls on satisfactory but predicts negative sediment values for low fluvial discharges and low rainfall so that these models are categorized as unacceptable.

Table 5. MLR models

Model scenario	RMSE (kg/s)	PBIAS	RSR	R	NSE	Model equation
Q_t	2498	+0.47	0.66	0.73	+0.56	$Q_s = 7.12Q_t - 920.70$
R_t	2729	+0.34	0.73	0.66	+0.47	$Q_s = 199.54R_t - 229.07$
Q_tR_t	2442	+0.22	0.64	0.74	+0.59	$Q_s = 5.31Q_t + 71.0R_t - 897.03$
Q_tR_{t-1}	2494	+0.35	0.66	0.73	+0.56	$Q_s = 6.68Q_t + 18.12R_{t-1} - 920.66$
$Q_tQ_{t-1}R_tR_{t-1}$	2339	+0.29	0.59	0.77	+0.65	$Q_s = 13.47Q_t - 8.02Q_{t-1} - 14.02R_t + 64.44R_{t-1} - 784.15$

Table 6. NLMR models

Model scenario	RMSE (kg/s)	PBIAS	RSR	R	NSE	Model equation
Q_t	2314	+0.33	0.57	0.77	+0.67	$Q_s = 5.02 * 10^{-3}Q_t^2 + 0.71Q_t - 111.61$
R_t	2697	+0.66	0.71	0.68	+0.49	$Q_s = 1.30R_t^2 + 138.75R_t - 36.72$
Q_tR_t	2280	+0.15	0.56	0.78	+0.68	$Q_s = 4.04 * 10^{-3}Q_t^2 + 0.74Q_t + 0.57R_t^2 + 24.10R_t - 188.70$
Q_tR_{t-1}	2303	+0.32	0.57	0.77	+0.67	$Q_s = 5.14 * 10^{-3}Q_t^2 - 0.17Q_t - 0.024R_{t-1}^2 + 30.46R_{t-1} - 93.99$
$Q_tQ_{t-1}R_tR_{t-1}$	2250	+0.43	0.55	0.79	+0.69	$Q_s = 3.73 * 10^{-3}Q_t^2 - 8.10 * 10^{-4}Q_{t-1}^2 + 4.97Q_t - 3.02Q_{t-1} + 8.18 * 10^{-2}R_t^2 + 0.91R_{t-1}^2 + 8.27R_t + 0.28R_{t-1} - 272.04$

Table 7. General power model

Model scenario	RMSE (kg/s)	PBIAS	RSR	R	NSE	Model equation
General power model 1 Q_t	2039	+3.81	0.56	0.82	+0.68	$Q_s = 1.027 * 10^{-3}Q_t^{2.238}$
General power model 2 Q_t	2039	+0.22	0.56	0.82	+0.68	$Q_s = 0.847 * 10^{-3}Q_t^{2.263} + 71.08$

Table 8. Log transform models

Model scenario	RMSE (kg/s)	PBIAS	RSR	R	NSE	Model equation
Linear model (SRC) $logQ_t$	4451	-21.65	1.23	0.77	-0.51	$logQ_s = 3.435\log Q_t - 6.544$ $Q_s = 2.858 * 10^{-7}Q_t^{3.435}$
General power model 2 $logQ_t$	4039	-17.50	1.12	0.77	-0.25	$logQ_s = 3.915logQ_t^{0.931} - 7.131$
Linear model $logQ_tlogR_t$	3715	-15.47	1.03	0.78	-0.05	$logQ_s = 3.112\log Q_t + 0.10logR_t - 5.714$

Table 9. ANN models

Model scenario	RMSE (kg/s)	PBIAS	RSR	R	NSE	Model equation
$logR_t$ $1-10-1-1$	2768	+54.07	0.77	0.67	+0.41	Levenberg- Marguardt
$logQ_t$ $1-10-1-1$	2070	+14.91	0.57	0.82	+0.66	Levenberg- Marguardt
$logQ_tlogR_t$ $2-10-1-1$	2052	+15.99	0.56	0.84	+0.68	Levenberg- Marguardt
$logQ_tlogR_{t-1}$ $2-10-1-1$	2123	+22.95	0.59	0.83	+0.66	Levenberg- Marguardt
$logQ_tlogQ_{t-1}logR_tlogR_{t-1}$ $4-10-1-1$	1982	+14.26	0.55	0.84	+0.70	Levenberg- Marguardt

The RMSE, PBIAS, RSR, R and NSE values of general power model, log transform models

and ANNs are shown in Tables 7, 8 and 9. In general, model simulation can be judged as "satisfactory" if NSE >0.50 and RSR ≤ 0.70, and if PBIAS ±25% for stream flow, PBIAS ±55% for sediment (Moriasi *et al.*, 2007). In this study, the predicted values from ANNs (4−10−1−1) showed RMSE value 1982 kg/s, PBIAS value +14.26, RSR value 0.55, R value 0.84, NSE value +0.70 which indicates that the ANNs model performance is satisfactory. Figures 18a, 18b, 18c and 18d showed the comparison between observed SS and model predicted transport rates of suspended sediment discharge in kg/s of SRC, log transform power model, log transform linear models and ANNs respectively.

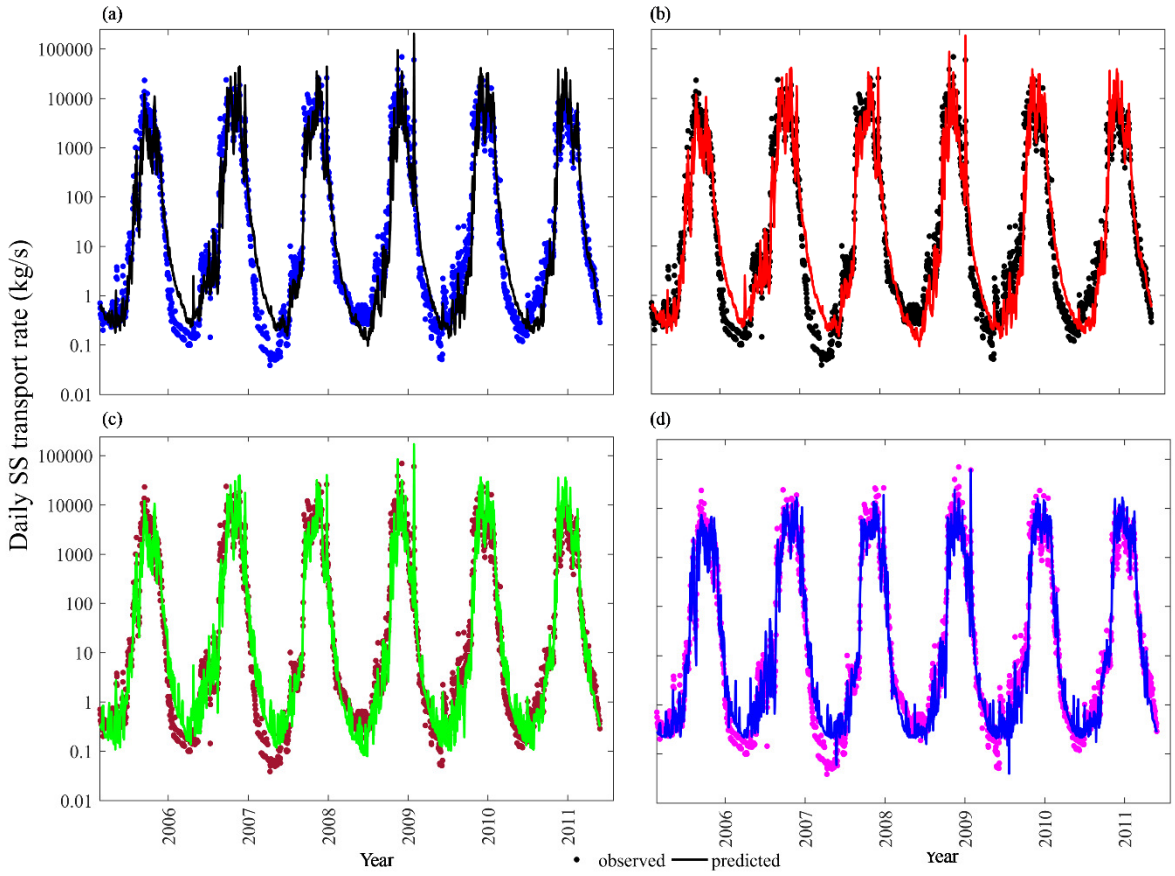

Figure 18. Observed and predicted daily suspended sediment rate (a) SRC (Q_w and Q_s) model (b) Power model (Q_w) (c) Log transform linear model (Q_w and R_t) (d) ANN model

Among SRC, Power, Log transform and ANN models, the best median ASSL predicted by ANN model was 37.611 Mt for the period 2006 to 2011, whereas the observed median ASSL was 41.678 Mt. The mean ASSL transported by river to hydropower reservoir was 40.904±12.453

Mt for 2006 to 2011 and ANNs predicted mean value is 35.190±7.018 Mt (Figure 19). Struck (Struck *et al.*, 2015) reported that the average annual SS transported by this river 36.9±10.6 Mt.

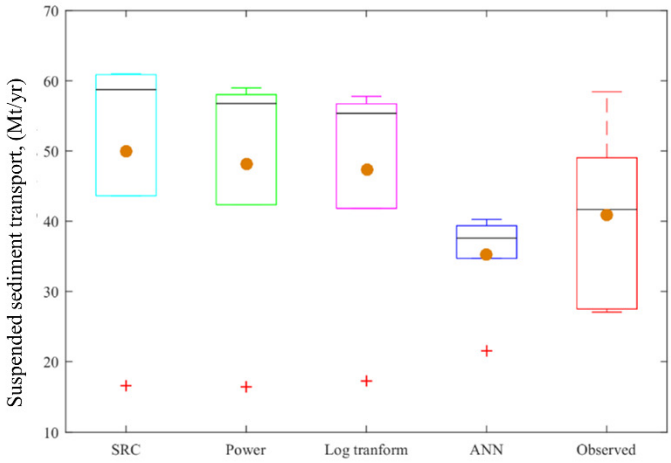

Figure 19. Comparison of annual observed and different model predicted SS

Central lines indicate the median, and bottom and top edges of the box indicate the 25th and 75th percentiles respectively. The whiskers extend to the most extreme data points not considered outliers, '+' symbol represents outliers (1.5-fold interquartile range), circle shows the mean value.

CHAPTER4.0 GENERAL CONCLUSIONS AND RECOMMENDATIONS

4.1 Conclusion

Shear stress, specific stream power and flow velocity are important key hydraulic parameters to describe sediment transport in river systems. The monsoonal fluvial discharge and the landslide dam outburst flood (LDOF) were responsible for boulder movements in KG River, Nepal. The lower boundary equation derived from a broad range of observed and calculated data sets estimate the maximum particle size of 840 mm can be transported by the monsoonal fluvial discharge during 2003 to 2011. The ASSL transported by KG River in hydropower reservoir was increased from winter, pre-monsoon, monsoon respectively and decreased in post-monsoon and estimated as 40.904±12.453 Mt SS losses annually from higher Himalayas. Additionally, the ANNs model perform satisfactory results for prediction of SS transport rate by KG River, where the annual predicted mean ASSL 35.190±7.018 Mt.

4.2 Application of study

The study is important for visualising the sediment loss from higher Himalaya to sea and monitoring the dead storage volume of reservoir for hydroelectric power generation.

4.3 Recommendations

The elevation difference, climate, geology of Himalaya is complex. The sediment loss from tributaries of KG River are not quantified separately, which is important to understand it from whole to part.

PART II- EFFECTS OF RAINFALL ON FLUVIAL DISCHARGE AND SUSPENDED SEDIMENT TRANSPORT IN KALI GANDAKI RIVER BASIN, HIMALAYA, NEPAL

ABSTRACT

Fluvial discharge is a principal driver of suspended sediment (SS) transport in Himalaya mountain catchment of Kali Gandaki (KG) River, Nepal. Stream flow with SS transport rate variation is one of the most remarkable effects of seasonal rainfall changing patterns in Himalaya. The synopsis of this study is to analyse relationship of specific discharge of three hydrometric stations of main KG River, four hydrometric stations of its tributaries with rainfalls of the whole basin and its sub basins together with SS transport at hydropower reservoir. An annual anticlockwise hysteresis loops were developed between specific discharge and rainfall at three hydrometric stations of main KG River, whereas its tributaries namely Aandhi Khola, Seti Khola and Modi Khola followed anticlockwise, and Myagdi Khola showed an eight-shaped hysteresis loop. The clockwise hysteresis developed between SS concentration and fluvial discharge was changed to linear relationship with the direct runoff discharge. The total average monthly rainfalls of June (388.39±84.24 mm), July (674.91±105.24 mm), August (571.81±110.77 mm) and September (356.50±104.39 mm) transported an average of 2.469±1.641, 12.952±4.932, 12.629±7.937 and 4.406±2.363 mega tons (Mt) of SS respectively over the period 2006-2017 from the KG catchment in to hill-side dam reservoir. This result showed that about 97% of suspended sediment was transported during monsoon season (June-September), comprising an annual weathering rate of KG basin estimated to be 4390 tons/km^2/yr which is equivalent to 1.66 mm/yr. Particularly, specific direct runoff discharge and monsoonal daily erosion rate of major rainfall events (>30 mm/day) showed linear increasing trend with rainfall in KG basin.

CHAPTER 1. GENERAL INTRODUCTION AND LITERATURE REVIEW

1.1 Research background

Fluvial discharge of river systems and the rainfall inside basins play an important role in the sedimentary as well as hydrological budget in a basin. Fluvial discharge is a main driver of suspended sediment transport from Himalayan catchment, Nepal. Stream flow with suspended sediment transport rate variation is one of the key noticeable effects of seasonal rainfall change patterns in Himalayan mountain catchment of Kali Gandaki (KG) River. The hydrology of Nepal is primarily dominated by the monsoon season (June- September), unique in higher rainfall contributing 80% of total annual rainfall (Mishra *et al.*, 2014; Burbank *et al.*, 2012). Researches showed about 10% of the total rainfall occurs in a single day (Talchabhadel *et al.*, 2018) and 50% of total annual rainfall is occurred within 10 days of monsoon season (Dahal & Hasegawa, 2008), responsible for triggering erosion, landslides, gullies formation and debris flows. The hydrological budget specially in Himalayan river is primarily governed by monsoonal rainfall (Bookhagen *et al.*, 2005), snow and glaciers melt, and secondarily by evapotranspiration forming minor component (Andermann, Longuevergne, *et al.*, 2012; Bookhagen & Burbank, 2010).

An alterations in regional hydrological cycles and changes in river flow such as flood or low flow are the significant potential consequences of climate change (Q. Zhang *et al.*, 2008). Climate change is threatening Nepal's as well as worldwide food security, water resources, human habitats and tourism sectors seriously (M. Karki *et al.*, 2009; Langat *et al.*, 2017). The Himalayan regions are more vulnerable because of varying altitudes within a short distance. The increasing temperature and shifting of rainfall patterns affected the livelihoods of people in the KG basin where monsoon is a major source of water and water budget depends on annual rainfall to recharge the aquifers that fed them (Dandekhya *et al.*, 2017). The availability of water

in KG basin is of major importance for hydropower as well as the small farmer managed irrigation scheme along the river and water transportation on hydropower reservoir for surrounding villages. Because of less availability data and limited numbers of meteorological stations in Himalayan region, Nepal, only few researches of climate change and its impacts were conducted (U. B. Shrestha *et al.*, 2019). The effects of climate changes in Nepal have been documented by different researchers in terms of temperature and precipitation scenario (Duncan *et al.*, 2013; R. Karki *et al.*, 2017; A. B. Shrestha *et al.*, 2017; Talchabhadel & Karki, 2019).

Himalayan Rivers transport tremendous amount of sediments in the form of bedload as well as suspended load (Thapa *et al.*, 2005). Several factors including topography, catchment slope, runoff, temperature, lithology, drainage length, tectonic activities, and number of landslides inside the catchment determine the sediment load in the fluvial systems (Baniya *et al.*, 2019; Chakrapani & Saini, 2009; Temple & Sundborg, 1972; Pagano *et al.*, 2019; Ayadi *et al.*, 2010). The dam construction curtails the sediment transport in to the downstream (Asaeda *et al.*, 2011; Yonggui *et al.*, 2013). Sedimentation in hydropower reservoirs is a global challenge, estimated as 1% of hydropower reservoir capacity being lost annually (Haun & Olsen, 2012). The capacity of hydropower plants developed in Himalayan region are decreased by decreasing reservoir capacity through sedimentation and wear and tear of underwater parts such as turbine, which are crucial issues in the context of operation, maintenance and rehabilitation (Koirala *et al.*, 2016; Chhetry & Rana, 2015).

A nonlinear relationship between specific discharge and rainfall or suspended sediment concentration and fluvial discharge known as hysteresis loops, which can be affected by the spatial and temporal rainfall distribution, seasonal rainfall changing patterns and geomorphological characteristics of catchment (Williams, 1989; Lawler *et al.*, 2006; Yang & Lee, 2018). The main drivers of streamflow trends are climatic variability and changes, and the

streamflow trend identification in a catchment is important for understanding the impact of climatic variability and changes in the region (Gautam & Acharya, 2012). It is of paramount importance to conduct this study in KG River catchment as this river originates from Himalayas and there are only limited studies about linkage of rainfall on fluvial discharge and sediment erosion and transport from Himalayas to hydropower reservoir. In this study, we examined seasonal patterns of fluvial discharges of main KG River and its tributaries and rainfalls received inside the basin. We also observed the relationships of specific discharge, fluvial discharges of three hydrometric stations of main KG River, four hydrometric stations of its tributaries with rainfalls of main basin and its sub basins together with suspended sediment transport from Himalayan basin and hysteresis effects developed at different hydrometric stations.

1.2 Research objectives

The following are the research objectives of this study (Part-II).

1. To know the behaviour of specific discharge and rainfall, SS and discharge hysteresis developed in different catchments.
2. To analyze the direct runoff discharge of KG River and relation with rainfall.
3. To analyze hysteresis during extreme events of KG River.
4. To study the seasonal, monthly flow duration curve (FDC) and seasonal suspended sediment load duration curve (SSLDC) of KG River.
5. To link up the effects of rainfall on fluvial discharge and sediment yield of catchment.
6. To quantify suspended sediment yield and annual weathering rate together with erosion rate during major rainfall events of KG basin.

CHAPTER 2.0 MATERIALS AND METHODS

2.1 Observation site

The observation site is Kali Gandaki (KG) River, Nepal. The KG River is a main glacier-fed river originating from the Himalaya region, Nepal. The main river flows from north to south in the higher Himalayan region and entering the Terai plains of Nepal to ultimately merge with the Ganges River in India. The river, upstream of hydropower dam has mainly four tributaries namely: Myagdi Khola (local name of stream), Modi Khola, Seti Khola and Aandhi Khola. Myagdi Khola and Modi Khola are glacier- fed streams that connects to main KG River at middle of the reach whereas Seti Khola and Aandhi Khola are non-glacier-fed streams connect the main river close to hydropower dam. The topography of KG basin is composed of Tibetan, Greater and Lesser Himalayan zones having distinctive in nature lithologically and petrologically (Robinson *et al.*, 2001). Each sub basins have complex geomorphology and watershed topography with rapid changes in elevations (Figure 20a-f).

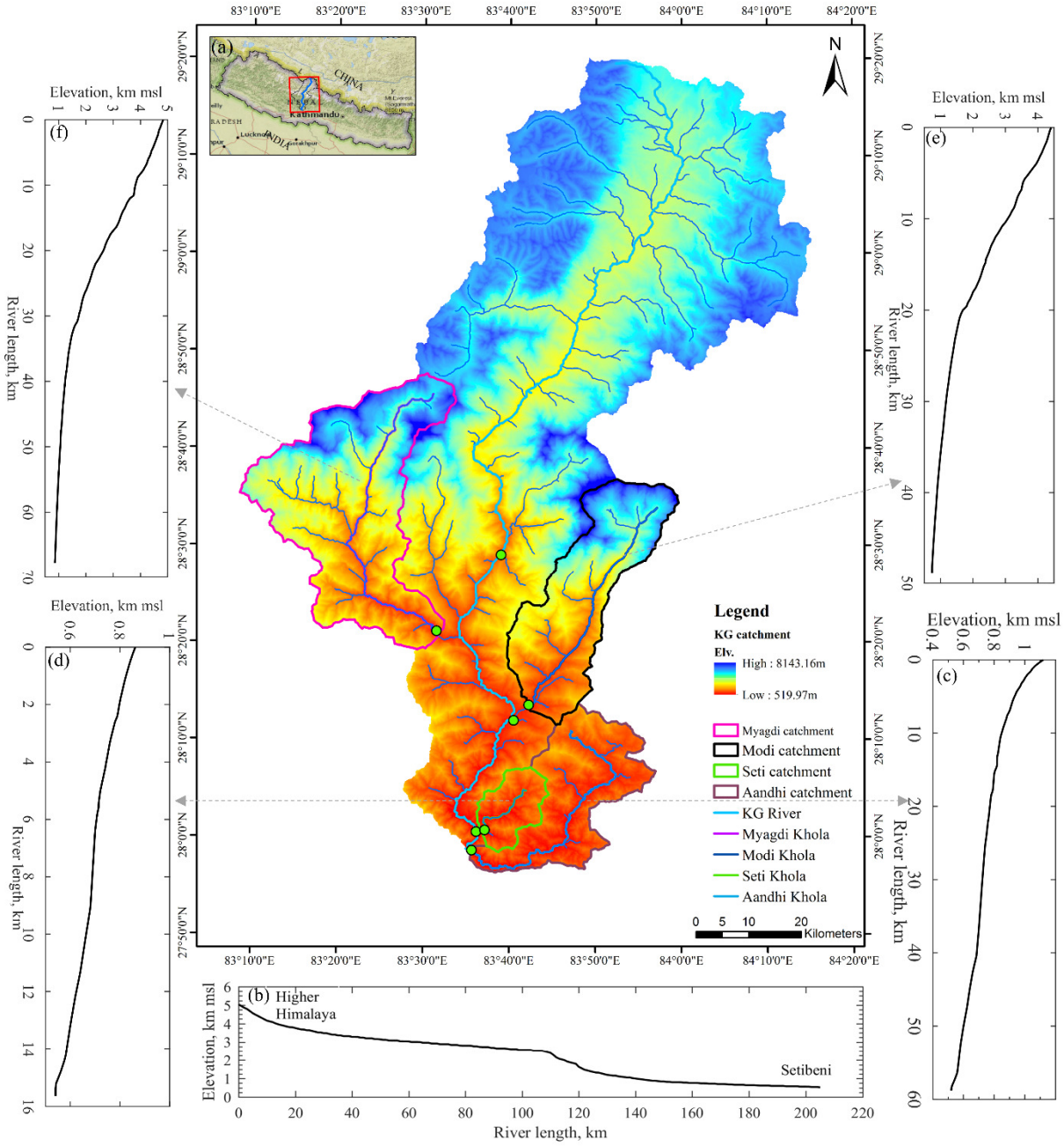

Figure 20. (a) Map of Kali Gandaki River catchment area (b) L- profile of Kali Gandaki River (c) L- profile of Aandhi Khola (d) L- profile of Seti Khola (e) L- profile of Modi Khola (f) L-profile of Myagdi Khola.

2.2 Data collection and acquisition

Department of Hydrology and Meteorology (DHM), Nepal installed different hydrometric gauge stations (www.dhm.gov.np) inside KG catchment and the station 410 was operated up to 1995 and now it is not operated after dam construction. Available historical daily KG River

discharges at three hydrometric stations and four main tributaries Aandhi Khola, Seti Khola, Modi Khola and Myagdi Khola stations were obtained from DHM. The details of hydrometric stations are summarized in Table 10.

Table 10. Details of hydrometric stations

S.No.	Station No.	River	Location	Latitude	Longitude	Elevation (m)	Data availability
1	406	Kaligandaki	Modi khola	28° 12' 00"	83° 42' 00"	667	1992-2013
2	415.1	Andhi Khola	Borlangpol	27° 05' 20"	83° 35' 20"	749	2000-2015
3	403.5	Kali Gandaki	Tatopani	28° 29' 00"	83° 39' 00"	1239	2004-2014
4	404.7	Myagdi Khola	Mangalghat	28° 21' 30"	83° 32' 00"	817	1976-2015
5	406.5	Modi Khola	Nayapul	28° 13' 30"	83° 42' 15"	701	1975-2015
6	409.5	Seti Khola	Seti Beni	28° 00' 40"	83° 37' 10"	550	1989-2009
7	410	Kali Gandaki	Seti Beni	28° 00' 30"	83° 36' 10"	529	2002-2017

Similarly, daily rainfall data of 27 rain gauge stations inside the whole KG basin were also collected from DHM and average daily rainfall of respective basins and sub basins were calculated. The details of meteorological stations are summarized in Table 11.

Table 11. Details of meteorological stations

S.No.	Station Name	Index No.	Types of Station	District	Latitude	Longitude	Elevation (m)	Data availability
1	Jomsom	601	Climatology	Mustang	28° 47'	83° 43'	2744	1958-2018
2	Thakmarpha	604	Agrometeorology	Mustang	28° 45'	83° 42'	2566	1968-2018
3	Baglung	605	Climatology	Baglung	28° 16'	83° 36'	984	1970-2018
4	Tatopani	606	Precipitation	Myagdi	28°29'	83° 39'	1243	1970-2018
5	Lete	607	Climatology	Mustang	28° 38'	83° 36'	2384	1970-2018
6	Beni Bazar	609	Climatology	Myagdi	28° 21'	83° 34'	835	1957-2016
7	Karkineta	613	Precipitation	Parbat	28° 11'	83° 45'	1720	1977-2018
8	Kushma	614	Climatology	Parbat	28° 13'	83° 42'	891	1970-2018
9	Bobang	615	Precipitation	Baglung	28° 24'	83° 06'	2273	1978-2018
10	Gurjakhani	616	Climatology	Myagdi	28° 36'	83° 13'	2530	1979-2016
11	Ghorepani	619	Precipitation	Myagdi	28° 24'	83° 44'	2742	1975-2018
12	Tribeni	620	Precipitation	Parbat	28° 02'	83° 39'	700	1989-2018
13	Darbang	621	Precipitation	Myagdi	28° 23'	83° 24'	1160	1989-2018
14	Rangkhani	622	Precipitation	Baglung	28° 09'	83° 34'	1740	1989-2018
15	Bega	626	Precipitation	Myagdi	28° 28'	83° 36'	1770	1992-2018
16	Kuhun	627	Precipitation	Myagdi	28° 23'	83° 29'	1550	1992-2018
17	Muna	628	Precipitation	Myagdi	28° 30'	83° 18'	1970	1992-2018
18	Baghara	629	Precipitation	Myagdi	28° 34'	83° 23'	2330	1992-2018
19	Sirkon	630	Precipitation	Parbat	28° 08'	83° 37'	790	1992-2018
20	Syangja	805	Climatology	Syangia	28° 06'	83° 53'	868	1973-2018
21	Bhadaure Deurali	813	Precipitation	Kaski	28° 16'	83° 49'	1600	1985-2018
22	Lumle	814	Agrometeorology	Kaski	28° 18'	83° 48'	1740	1970-2018
23	Ghandruk	821	Precipitation	Kaski	28° 23'	83° 48'	1960	1976-2018
24	Walling	826	Precipitation	Syangja	27° 59'	83° 46'	750	1989-2018
25	Sallyan	829	Precipitation	Kaski	28° 16'	83° 45'	1000	1992-2018
26	Pamdur	830	Precipitation	Kaski	28° 16'	83° 47'	1160	1992-2018
27	Dandaswanra	832	Precipitation	Syangja	28° 05'	83° 55'	1432	2000-2018

A hydropower dam (27°58’44.88” N, 83°34’49.68” E) was built in 2002 for 144 MW power generation, at Mirmi, Syangja, Nepal. Also, historical daily fluvial discharge and suspended sediment concentration data sourced from Nepal Electricity Authority (NEA), Kali Gandaki Hydropower station were used for sediment hysteresis and quantification. The bed level of dam was increasing yearly due to trapping of bedload as well as suspended sediment load by dam, which curtail sediment load in the downstream. The sedimentation in reservoir lowers the reservoir’s capacity annually.

The main physiographic characteristics of KG River basin at three hydrometric stations and four tributaries are shown in Table 12.

Table 12. Main characteristics of river basin and sub basins.

Parameters	KG basin at Setibeni (Downstream reach)	KG basin at Modibeni (middle reach)	KG basin at Tatopani (Upper reach)	Aandhi Khola basin	Seti Khola basin	Modi Khola basin	Myagdi Khola basin
Catchment area (km^2)	7579	5899	4044	479	138	642	1076
Length of river (km)	~216	~79	~37	~59	~16	~49	~68
Mean gradient of river (%)	2.20	2.83	4.64	1.02	2.06	7.52	5.87
Extreme Discharge (m^3/s)	3280 in 1975, 2825 in 2009	2978 in 2001, 1694 in 2009	493 in 2009	1590 in 1970, 724 in 2014	682 in 2009	1456 in 1976, 907 in 2014	834 in 2009, 840 in 2010
Elevation ranges (m)	529-8143	683-8143	1184-8143	531-2473	548-2249	747-8019	

The fluvial discharge of main river varies seasonally and is dependent on the discharge of the tributaries and rainfall received in sub basins in addition to the amount of snow melting from the Himalayas.

2.3 Analysis of direct runoff discharge and quantification of monthly sediment transport

The base flow from the fluvial discharge is separated by the recursive digital filter method proposed by Lim et al. (2010). This method is generated by the equation proposed by Eckhardt (2005). The base flow Q_k at time step k is determined by using

$$Q_k = \frac{(1 - BFI_{max})ab_{k-1} + (1 - a)BFI_{max}y_k}{(1 - aBFI_{max})} \quad \text{(II.1)}$$

where BFI_{max} is base flow index, b_{k-1} is base flow in m^3/s at the time step *k-1*, y_k is the total streamflow in m^3/s at time step k, and a is filter parameter. The direct runoff discharge is determined by deducting base flow from total streamflow. For recursive digital filter with perennial streams with hard rock aquifers condition a=0.98 and BFI_{max}=0.25.

The monthly sediment transport for KG River is quantified by

$$Q_s = \int_{t=1}^{t_m} C_t \, Q_t dt \quad \text{(II.2)}$$

where Q_s is the total monthly suspended sediment transport by KG River, C_t and Q_t are suspended sediment concentration and daily discharge of river during time interval dt.

CHAPTER 3.0 RESULTS AND DISCUSSION

3.1 Seasonal fluvial discharge of KG River and its tributaries

The hydrology of both the snow-fed and non- snow-fed river systems is apparently distinctive during the snow melting season. The snow and glacier melts have significant effect on the hydrology of the KG River. The winter, pre-monsoon, monsoon and post-monsoon fluvial discharge of KG River at three hydrometric stations, namely downstream at Setibeni, middle at Modibeni and upstream at Tatopani and four main tributaries are shown in Figure 21a,b. The discharge during winter and pre-monsoon followed the lowest values, whereas monsoon and post-monsoon followed higher discharge. The discharges of non-snow fed tributaries, namely Aandhi Khola and Seti Khola, depend on the amount of rainfall received and its duration occurred in their catchments, whereas the fluvial discharges of snow fed rivers, namely KG, Modi Khola and Myagdi Khola depend on snow and glaciers melts from Himalayas and rainfall events inside hilly area of the catchments.

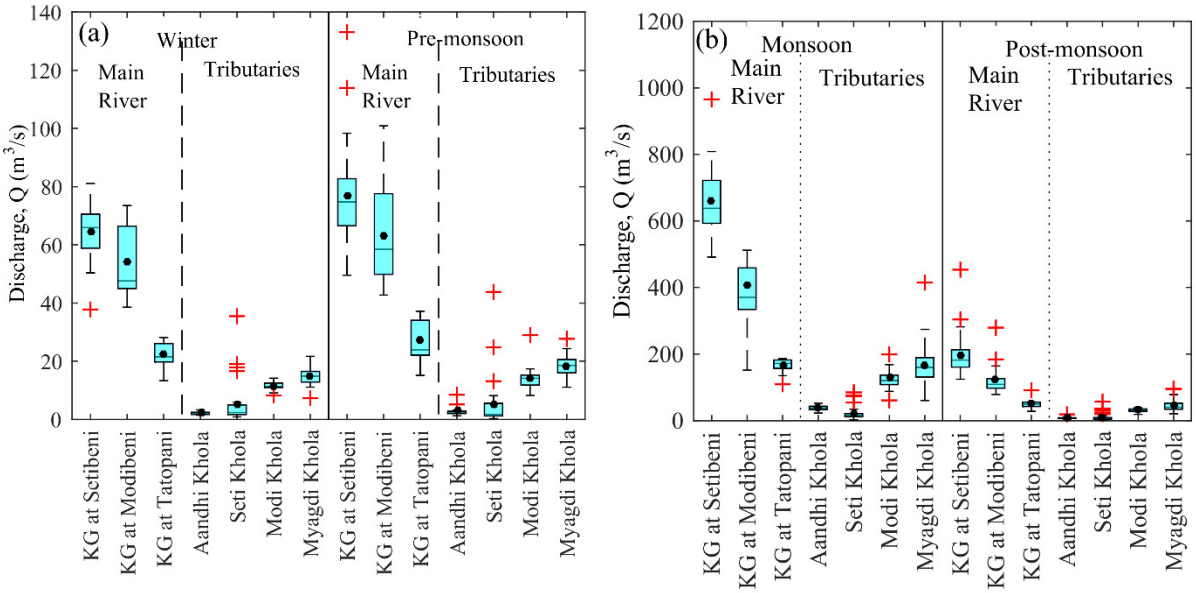

Figure 21. Seasonal discharge of KG River and its tributaries during (a) Winter and Pre-monsoon (b) Monsoon and Post-monsoon.

Central lines indicate the median and bottom and top edges of the box indicate the 25th and 75th percentiles respectively. The whiskers extend to the most extreme data points not considered

outliers, the '+' sign represents outliers (1.5-fold interquartile range), and the circle shows the mean value.

The annual average fluvial discharge and rainfall trends of main KG River, its tributaries Aandhi Khola, Seti Khola, Modi Khola and Myagdi Khola and catchments are shown in Figure 22. The snow-fed river discharges seem consistent compared to non-snow-fed streams followed higher discharge during monsoon season. The monthly flow in the adjacent snow-fed (KG River, Modi Khola and Myagdi Khola) and two non-snow-fed (Aandhi Khola and Seti Khola) sub basins in the KG basin indicate that there is an increasing trend in the runoff of the former during the months of April and May. By contrast, it is exactly, opposite for the later. This indicates that there is an increasing trend in melting of snow and glaciers in these sub basins. However, the wet season flows have an apparently increasing trend in all the sub basins.

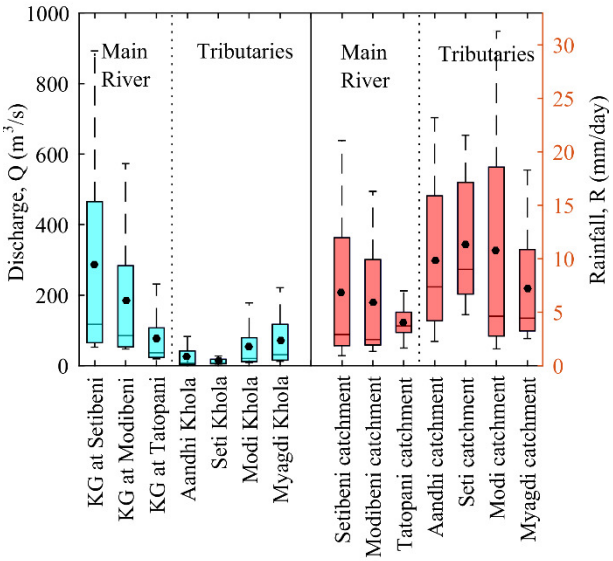

Figure 22. Discharge and rainfall of KG River and its tributaries.

3.2 Fluvial discharge and rainfall relationship

3.2.1 Main river specific discharge and rainfall relationship

Figure 23a-c show daily specific discharge and daily rainfall relationship for KG River catchment at three different hydrometric locations, namely at Setibeni station No.410 (tail of river), Modibeni station No.406 (Middle of river) and Tatopani station No.403.5 (upper portion

of river). As the rainfall and catchment area decreases to upstream, the data were scattered more. However, the same general pattern was observed in all three hydrometric stations. The specific discharge was increased with increasing rainfall from pre-monsoon (March - May) to the monsoon (June - September) and decreasing during post-monsoon (October - November). A clear anticlockwise hysteresis loops were developed between specific discharge (Q/A) and rainfall at three hydrometric stations of main KG River which describe the situation where the rainfall variable increases during rising curve of the rainfall. The higher river discharge during post-monsoon compared with the pre monsoon for a given precipitation rate. These patterns illustrated that part of the last year's rainfall was temporarily reserved within these catchments.

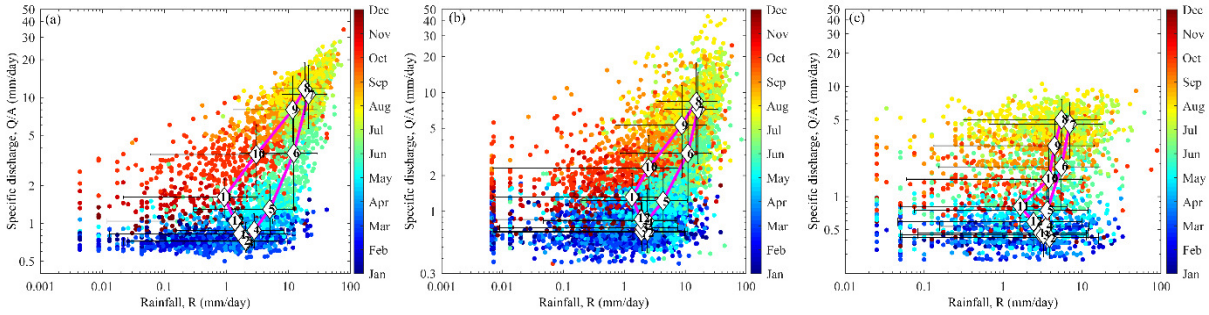

Figure 23. Specific discharge and rainfall relationship for KG River at (a) Setibeni (2002-2017) (b) Modibeni (1992-2013) (c) Tatopani (2004-2014).

The white filled diamonds with numbers (1 for January, …….and 12 for December) show the mean monthly values. The error bars represent the 5% and 95% quantiles of the daily data for each month.

The entire rainfall received in catchments was not transferred directly to the river system during the pre-monsoon and the monsoon seasons, whereas the storage part was drained during the post-monsoon season (Andermann, Longuevergne, *et al.*, 2012). The hysteresis effects are performed due to glacier and snow melt runoff in river system during the pre-monsoon and monsoon seasons (Andermann, Bonnet, *et al.*, 2012). In the Himalayas, higher rainfall during the monsoon is responsible for the recharge of basement aquifers, which are refilled during the monsoon and released in the post monsoon, leading to the observed annual hysteresis

(Andermann, Bonnet, *et al.*, 2012).

3.2.2 Tributaries' specific discharge and rainfall relationship

Figure 24a-d show daily specific discharge and daily rainfall of tributaries Aandhi Khola station No.415.1, Seti Khola station No.409.5, Modi Khola station No.406.5 and Myagdi Khola station No.404.7 respectively for sub basins. Out of them, Aandhi and Seti streams are dry in pre-monsoon, whereas Modi and Myagdi streams are snow feeding streams. Compared to snow feeding streams, the streams which are dry in pre-monsoon showed the specific discharge and rainfall data were scattered more. Anticlockwise hysteresis loops were observed between specific discharge and rainfall for all tributaries except for Myagdi Khola. The Myagdi Khola showed eight shaped anticlockwise hysteresis loops.

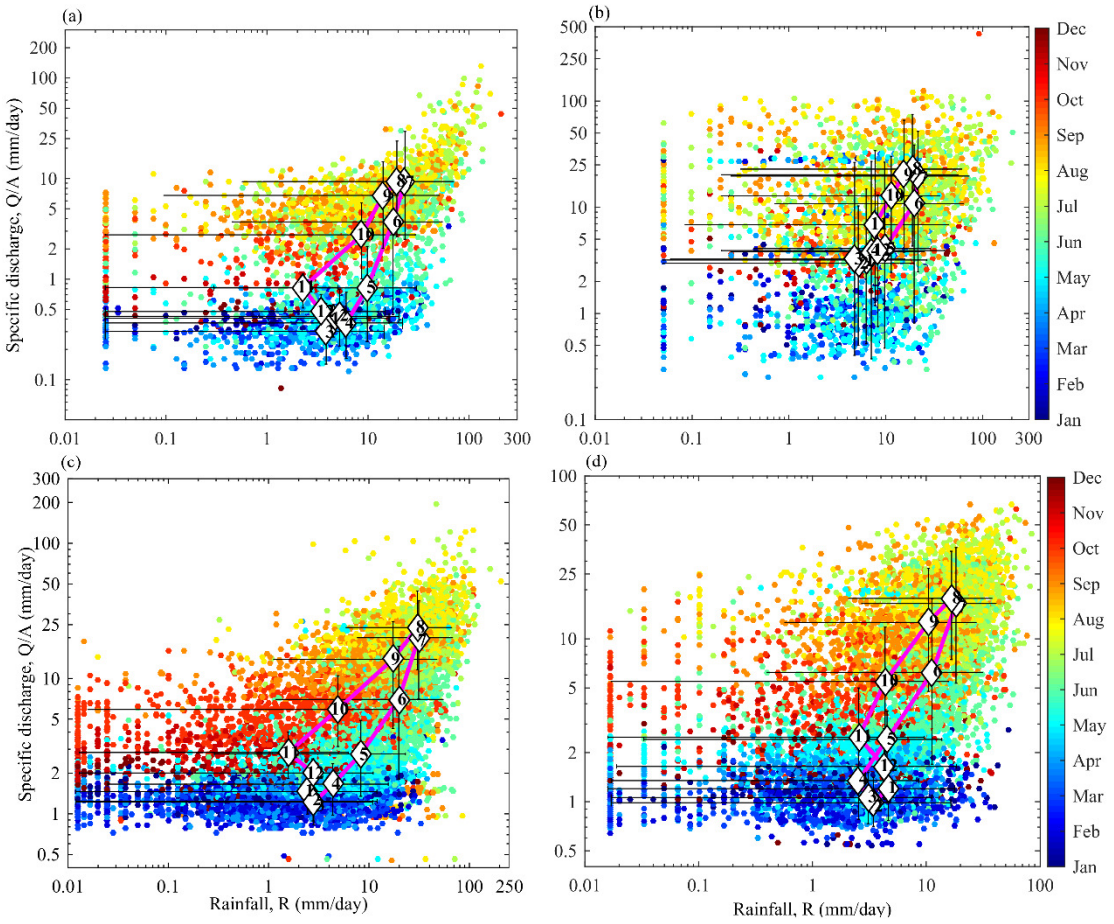

Figure 24. Specific discharge and rainfall relationship (a) Aandhikhola (2000-2015) (b)

Setikhola (1989-2009) (c) Modikhola (1975-2015) (d) Myagdikhola (1976-2015).

The white filled diamonds with numbers (1 for January, …….and 12 for December) show the mean monthly values. The error bars represent the 5% and 95% quantiles of the daily data for each month.

3.3 Suspended sediment, fluvial discharge and direct runoff discharge relationship

The specific discharge calculated from observed fluvial discharge data and catchment area followed an anticlockwise hysteresis loop with rainfall data. In contrast, clockwise hysteresis loops were developed between suspended sediment concentration and fluvial discharge in a catchment (Figure 25a) due to increasing sediment concentration more rapidly with increasing fluvial discharge. This phenomenon indicated that a source of sediment close to the monitoring point. As rainfall during pre-monsoon (March- May) and monsoon (June-September) increases, fluvial discharge in tributaries and main river increases so that high amount of suspended sediment transport in the fluvial system.

Later, during post-monsoon, the fluvial discharge decrease compared to monsoon but higher than pre-monsoon (Figure 21a-b) so that sediment depletion occurs in the river channel. The release of stored water in post-monsoon transported the riverbanks sediment stock so that sediment depletion occurred in the river system. This remobilization of sediment deposits from the banks were responsible for clockwise hysteresis loop (Smith & Dragovich, 2009)(G. P. Williams, 1989)(Lana-Renault & Regüés, 2009).

The base flow and direct runoff discharge from the daily fluvial discharge was separated by Web GIS-based Hydrograph Analysis Tool (WHAT) proposed by Lim et al. (2010). The direct discharges during the post-monsoon and winter seasons are minimum, as the suspended sediment concentration is low, whereas high direct discharge and concentration are observed during the pre-monsoon and monsoon seasons. The suspended sediment concentration and the direct discharge followed a linear relationship, where the hysteresis effect was eliminated (Figure 25b) which demonstrates that the suspended sediment concentration is not dependent

on fluvial discharge in the rivers but depends on the quantity of water draining from vicinity area into the river system (Andermann, Bonnet, *et al.*, 2012). This revealed that the suspended sediment concentration depends on amount of sediment yield from the hillslopes.

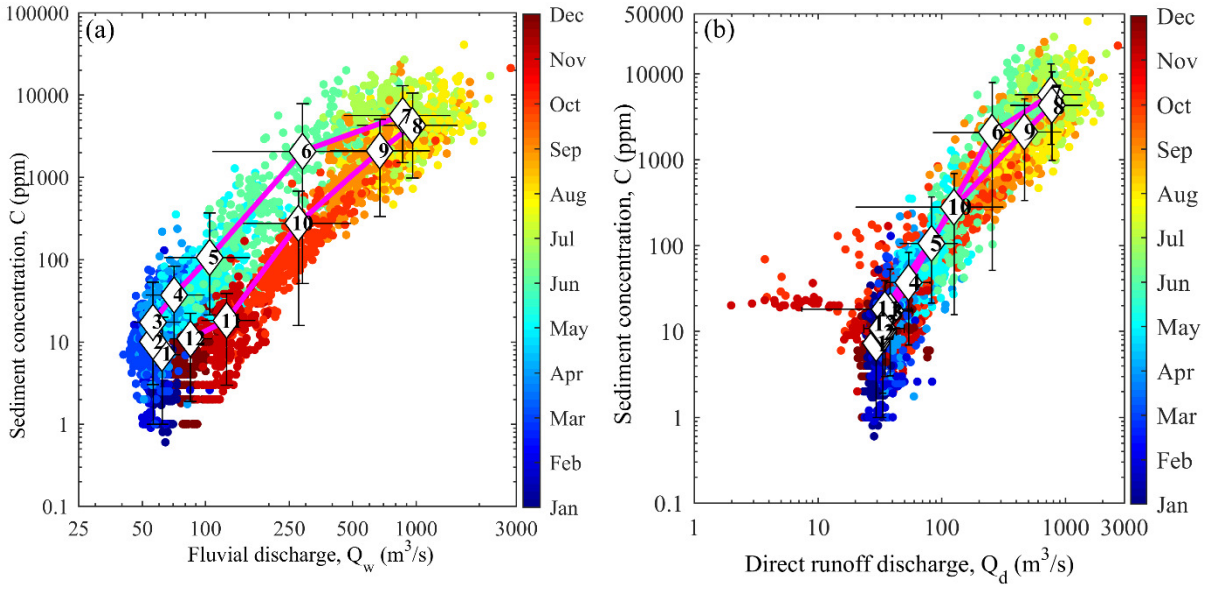

Figure 25. Suspended sediment concentration and fluvial discharge relationship with clockwise hysteresis loop (b) Suspended sediment concentration and direct discharge relationship without hysteresis loop for KG River (2006-2017).

The white filled diamonds with numbers (1 for January, …….and 12 for December) show the mean monthly values. The error bars represent the 5% and 95% quantiles of the daily data for each month.

A single event hysteresis loops showed clockwise patterns were dominant suggesting local sediment sources. The largest suspended sediment concentration spike was often associated with the first in successive discharge events but not necessarily highest discharge event indicating seasonal depletion of local sediment stocks (Martin *et al.*, 2014). The hysteresis loops shifted from clockwise to linear or complex patterns in multi-peaked discharge events pointing that localized sediment stocks are being transported. Hysteresis loops are classified in to five types (Martin *et al.*, 2014; Bussi *et al.*, 2014):

Clockwise loop: These patterns are generated when suspended sediment concentration peaks occurs before fluvial discharge peaks indicating a localized sediment sources or depletion of

sediment source.

Anticlockwise loop: These patterns occur when suspended sediment concentration peaks after fluvial discharge peaks which suggesting a more distant sediment source and a discharge threshold that must be reached to entrain consolidated bank sediments or bank collapse or a rainfall threshold required to initiate overland flow.

Linear loop: These patterns generated where peaks occur simultaneously which imply a sediment source at an intermediate distance, a lower entrainment threshold, or a continuous supply of sediment.

Eight shaped and complex loops: These patterns are generated when there are multiple sediment source locations or multiple erosion processes acting concurrently.

Generally, the SSC and discharge (Q_w) extreme events occur in different time events. The SSC extreme events hysteresis followed clockwise loops for the years 2006, 2007, 2009, 2010, 2012, 2015, 2016 and 2017 whereas years 2008, 2011 and 2014 followed a combination of clockwise and anticlockwise loops immediately (Figure 26a-k).

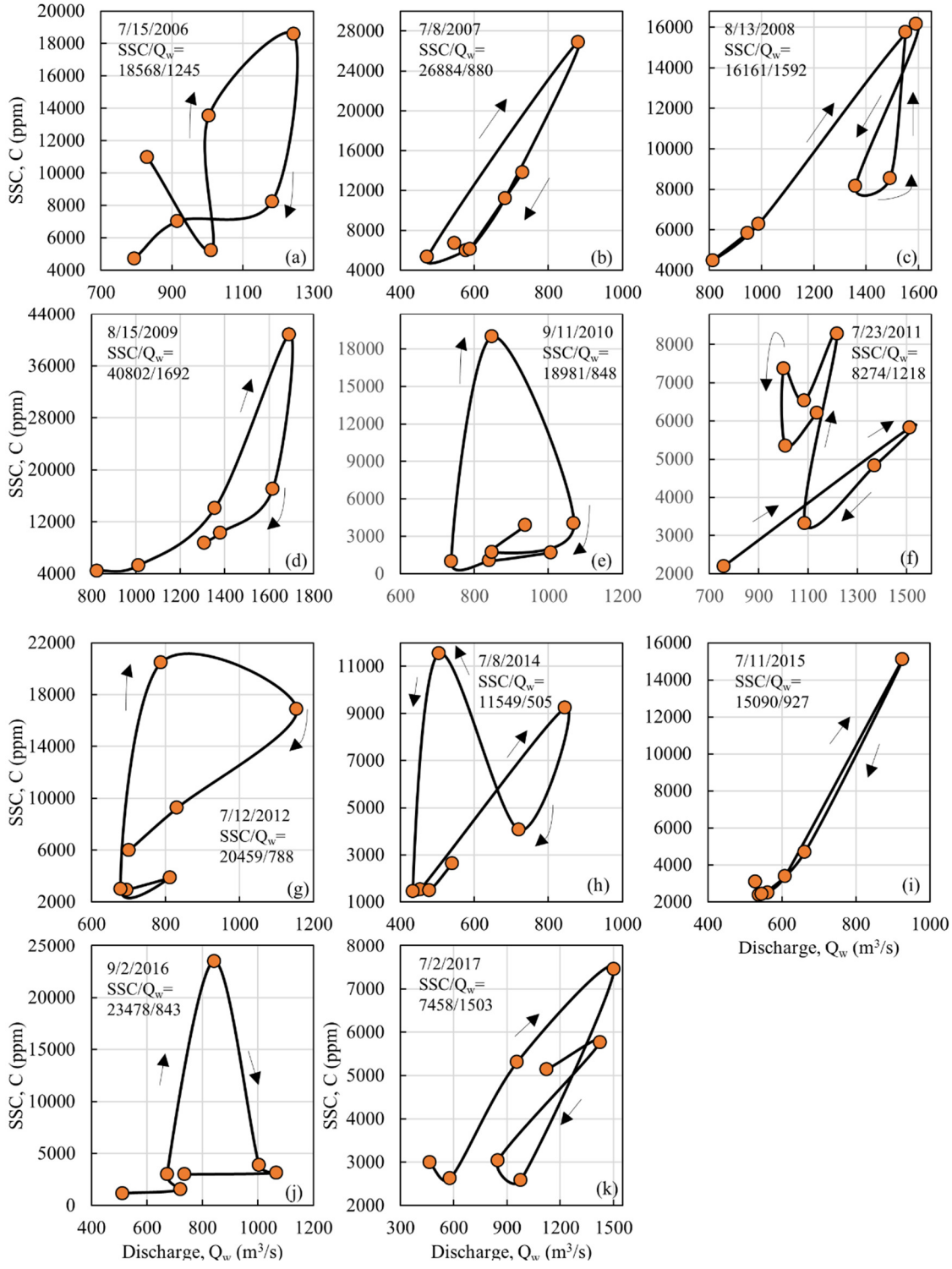

Figure 26. (a-k) Typical hysteresis during SSC_{max} extreme events

Similarly, the Q_w extreme events followed clockwise hysteresis loops for all years except 2010, showed both anticlockwise and clockwise loop (Figure 27a-k).

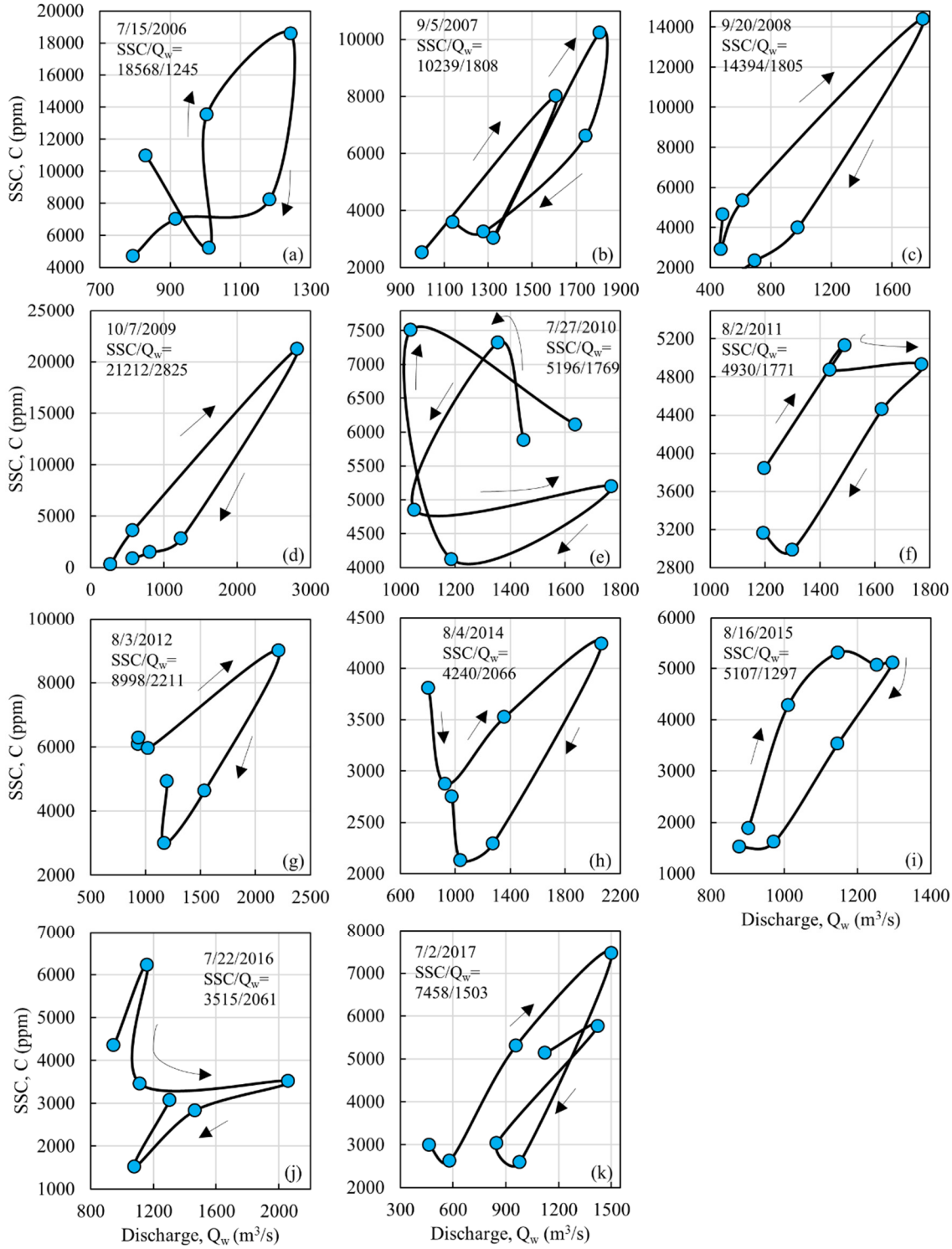

Figure 27. (a-k) Typical hysteresis during discharge, Q_{wmax} extreme events

The maximum SSC occurred in maximum Q_w in 2006 and 2017. The difference in time interval between the two events entered as lag time. Typical features showing extreme events dates, magnitudes and 2, 1, 0-day lag daily average and extreme rainfall inside the basin are shown in

Table 13.

Table 13. Typical features during extreme events

Year	Extreme SS			Extreme discharge Q_w			Lag time (days)
	Event date	SSC/Q_w (ppm/m^3/s)	Average rainfall before 2, 1, 0 day and max rainfall in basin (mm)	Event date	SSC/Q_w (ppm/m^3/s)	Average rainfall before 2, 1, 0 day and max rainfall in basin (mm)	
2006	15-July	18568/1245	35,24,39,98	same	same	same	0
2007	8-July	26884/880	16,11,17,73	5-September	10239/1808	66,21,49,153	+59
2008	13-August	16161/1592	8,23,44,111	20-September	14394/1805	17,25,69,212	+38
2009	15-August	40802/1692	32,53,41,88	7-October	21212/2825	8,34,93,250	+53
2010	11-September	18981/848	4,9,15,79	27-July	5196/1769	28,27,42,160	-46
2011	23-July	8274/1218	16,20,25,84	2-August	4930/1771	31,29,34,88	+10
2012	12-July	20459/788	16,15,25,144	3-August	8998/2211	14,25,54,111	+22
2013	11-June	11272/NA	2,7,44,133	NA	NA	NA	NA
2014	8-July	11549/505	48,24,7,32	4-August	4240/2066	23,40,43,139	+27
2015	11-July	15090/927	16,13,24,80	16-August	5107/1297	25,19,25,80	+36
2016	2-September	23478/843	27,21,27,78	22-July	3515/2061	37,35,52,182	-42
2017	2-July	7458/1503	22,46,53,175	same	same	same	0

The positive lag time means the SS peak event occurred at 'T' time ahead than Q_w event whereas negative lag time shows the SS peak occurred 'T' time after than Q_w event. The highest lag time for year 2007 has value +59 days. The year 2010 and 2016 showed opposite trend compared to other years. The SS and discharge data during 2006-2017 showed a month lag time interval between monthly average SS and discharge as shown in Figure 28a. The particle size distribution of suspended sediment transported by river at different locations dated on 4 June 2012 is shown in Figure 28b.

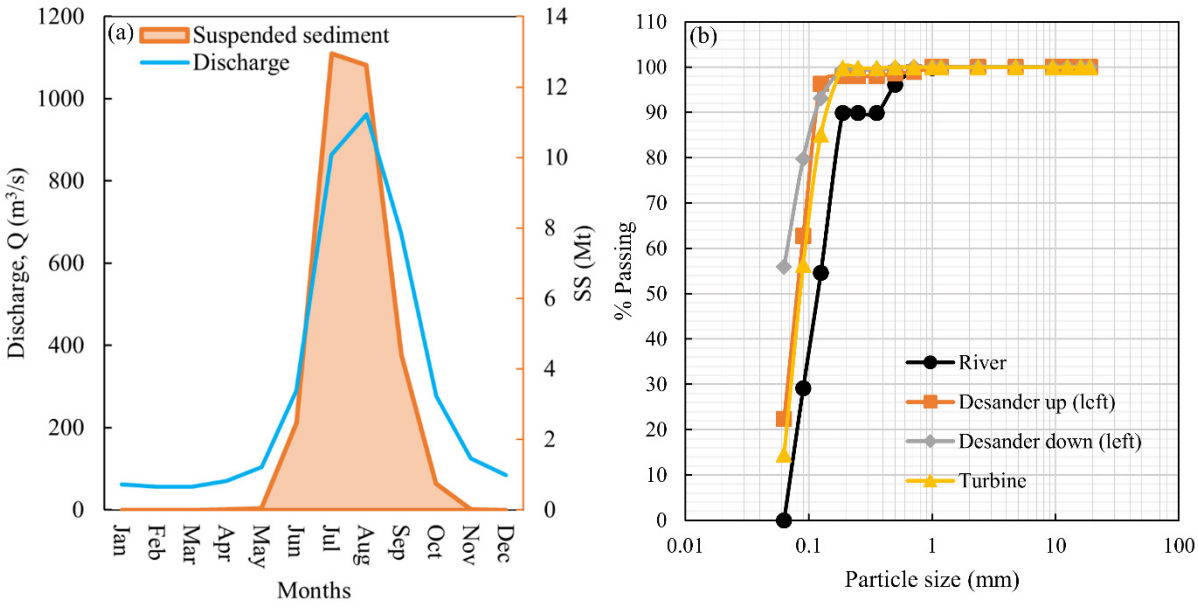

Figure 28. (a)Time lag of discharge and suspended sediment (b) Particle size distribution of SS

3.4 Flow and suspended sediment load duration curve and SS quantification

Flow duration curves (FDCs) are used for summarizing the hydrological characteristics of a river (Banasik & Hejduk, 2013). FDC corresponding to 10%, 50% and 90% dependability were estimated as 91.17, 61.92 and 55.73 m^3/s during winter, 116.83, 69.50 and 53.16 m^3/s during pre-monsoon, 1029.42, 744.13 and 232.88 m^3/s during monsoon and 380.47, 164.29 and 108.79 m^3/s during post-monsoon respectively (Fig.29a,b). The daily SSL transport corresponding to same dependability were also estimated as 96.6×10^{-6}, 48.2×10^{-6}, 34.4×10^{-6} Mt/d during winter, 1614×10^{-6}, 220×10^{-6}, 51.3×10^{-6} during pre-monsoon, 501434×10^{-6}, 278037×10^{-6}, 35923×10^{-6} during monsoon and 20263×10^{-6}, 391×10^{-6}, 125×10^{-6} during post-monsoon respectively (Figure 29c,d).

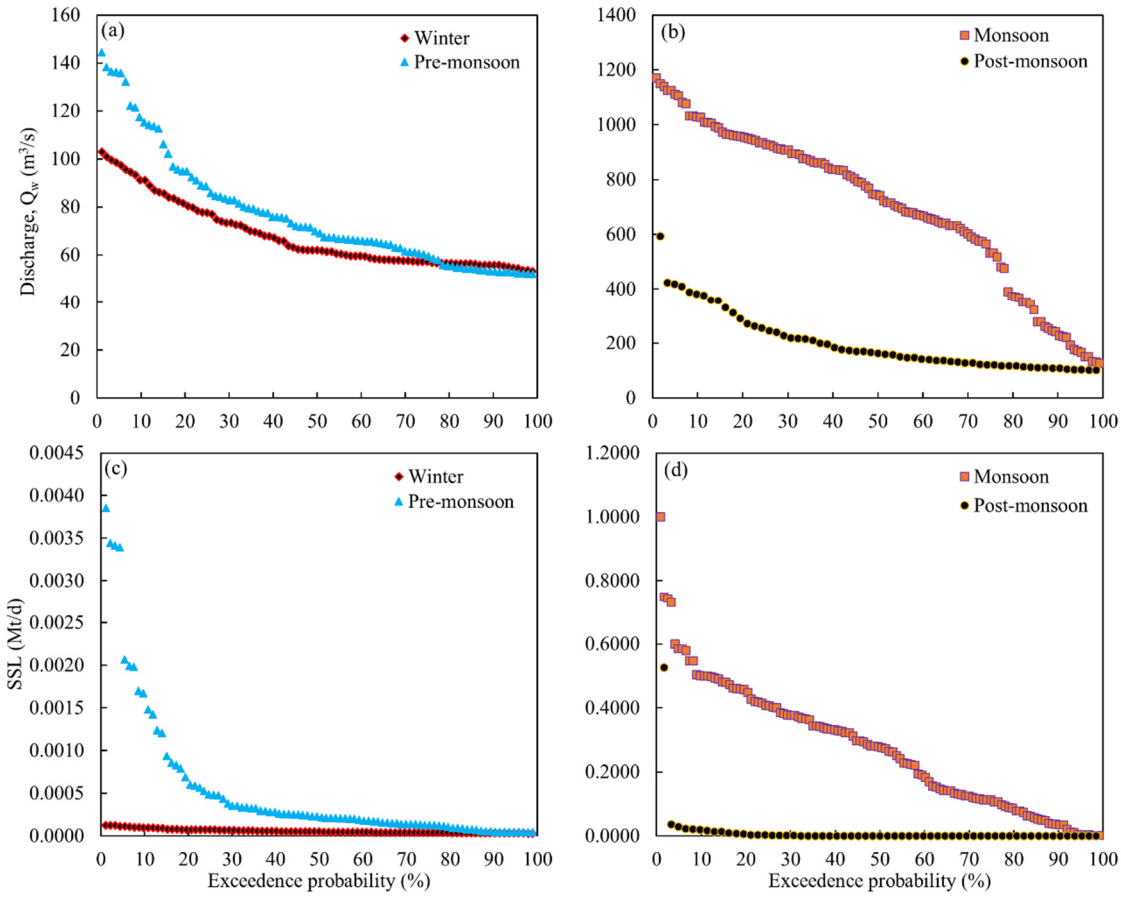

Figure 29. (a-b) Seasonal flow duration curve (c-d) Seasonal suspended sediment load duration curve

Subjected to FDCs for monsoonal months, the discharge flow during August has highest value

among other monsoonal months and followed by July, September and June in decreasing order. Conversely, July showed highest SSL and followed by August (Figure 30a,b). This showed the SS production and transport is high during July whereas flow is higher during August indicating a month peak time difference between them. Significant amount of SS transport during July and August.

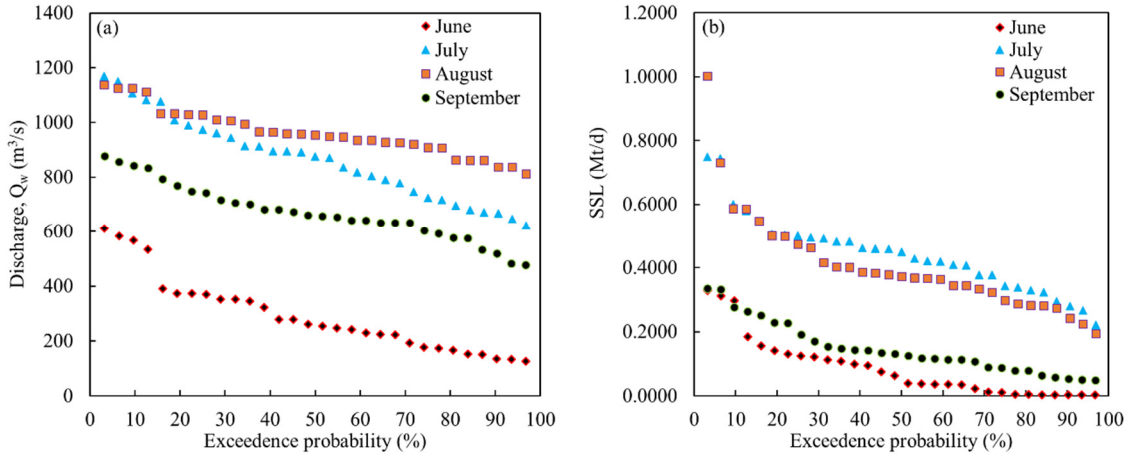

Figure 30. (a) Monthly flow duration curves and (b) Monthly suspended sediment load duration curve

3.5 Seasonal, monthly sediment transport and rainfall

Sediments sources in KG are Tethyan Sedimentary Series (TSS) comprises of Palaeozoic and Mesozoic marine sediments deposited in the Tethian ocean consists of sandstones, limestones, quartzites and shales with fossiliferous beds (Granet *et al.*, 2007; Adhikari & Wagreich, 2011). The origin of sediments in Himalayan river are incision of Late Pleistoncene to Holocene terraces, landslides from hillslopes during and after major rainfall events and erosion of last glacial maximum moraines (Granet *et al.*, 2007; Monique Fort *et al.*, 2010). The scarcely vegetated semi-desert area of upper KG River valley with deep gullies formed in a graben structure storing large amount of unconsolidated sediments, which provide a source during high stream power (Reimann *et al.*, 2019). The middle KG river terraces composed of glacial lake outburst flood (GLOF) deposits (Yoshida *et al.*, 2015). During monsoon season, rainfall intensity and frequency attain increasingly wetter conditions favored the development of

saturated areas producing runoff and deep-seated landslides (Lana-Renault & Regüés, 2009; Morin *et al.*, 2018) and therefore the runoff on the hillslopes provides a large amount of eroded material to the rivers because of their transport limited state. The high transport capacity of the rivers is due to the contribution of runoff to the discharge as well as to the ground water release during post-monsoon into the rivers (Figure 31a,b). The transported sediment from runoff to river deposited in the hydropower reservoir (Figure 31c,d).

Figure 31. (a) Sources of sediment (b) Sediment transport by fluvial discharge (c) Deposited sediment in KG hydropower reservoir (d) Flushing of deposited sediment in KG hydropower reservoir.

Suspended sediment and discharge are expressed in the form of sediment rating curve (SRC) as

$$SSL = a \times {Q_w}^b \quad \text{(II.3)}$$

where SSL is daily suspended sediment load (Mt/d), Q_w is daily average discharge of river, a and b are coefficients that depends on characteristics of river. The peak amount of daily SSL transport was 0.007, 0.023, 5.964 and 5.176 Mt/d during winter, pre-monsoon, monsoon and post monsoon respectively (Figure 32a-d).

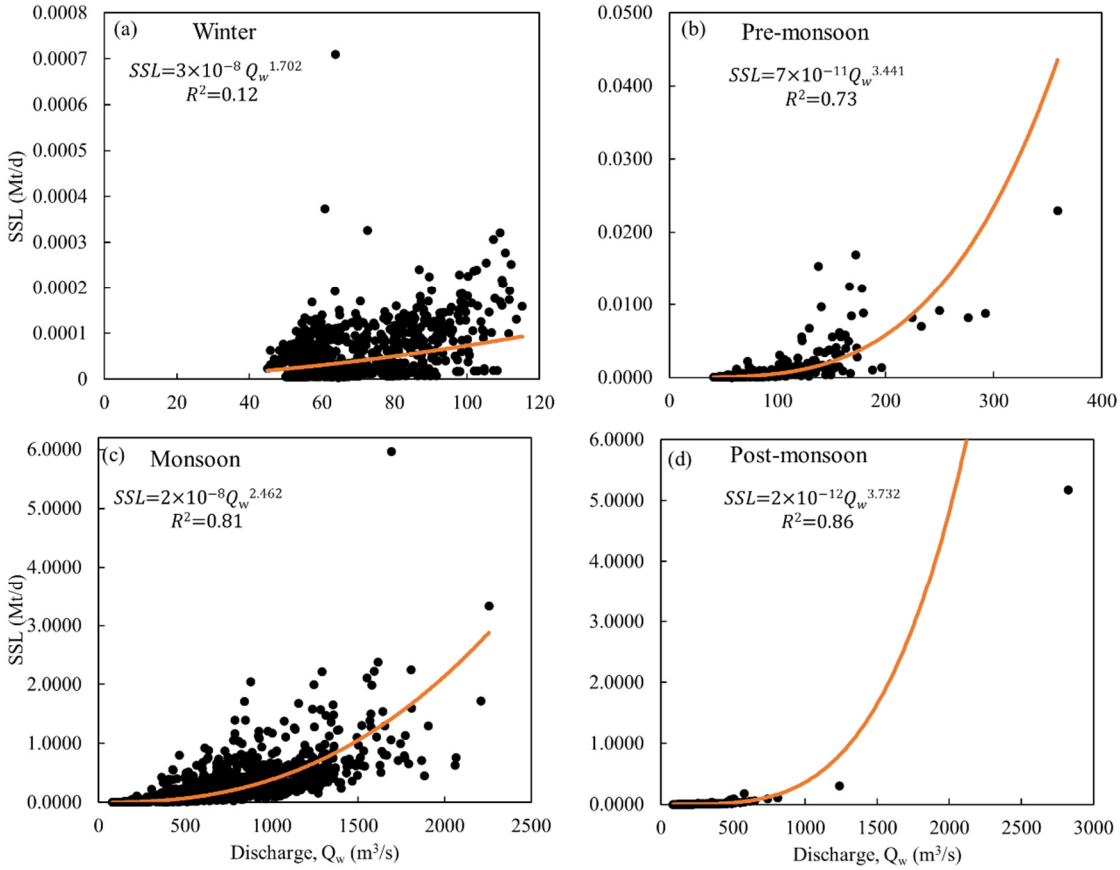

Figure 32. (a-d) Seasonal SSL and discharge relationship

Similarly, the peak daily SSL was 1.035, 3.328, 5.964 and 2.245 Mt/d during June, July, August and September (Figure 33a-d).

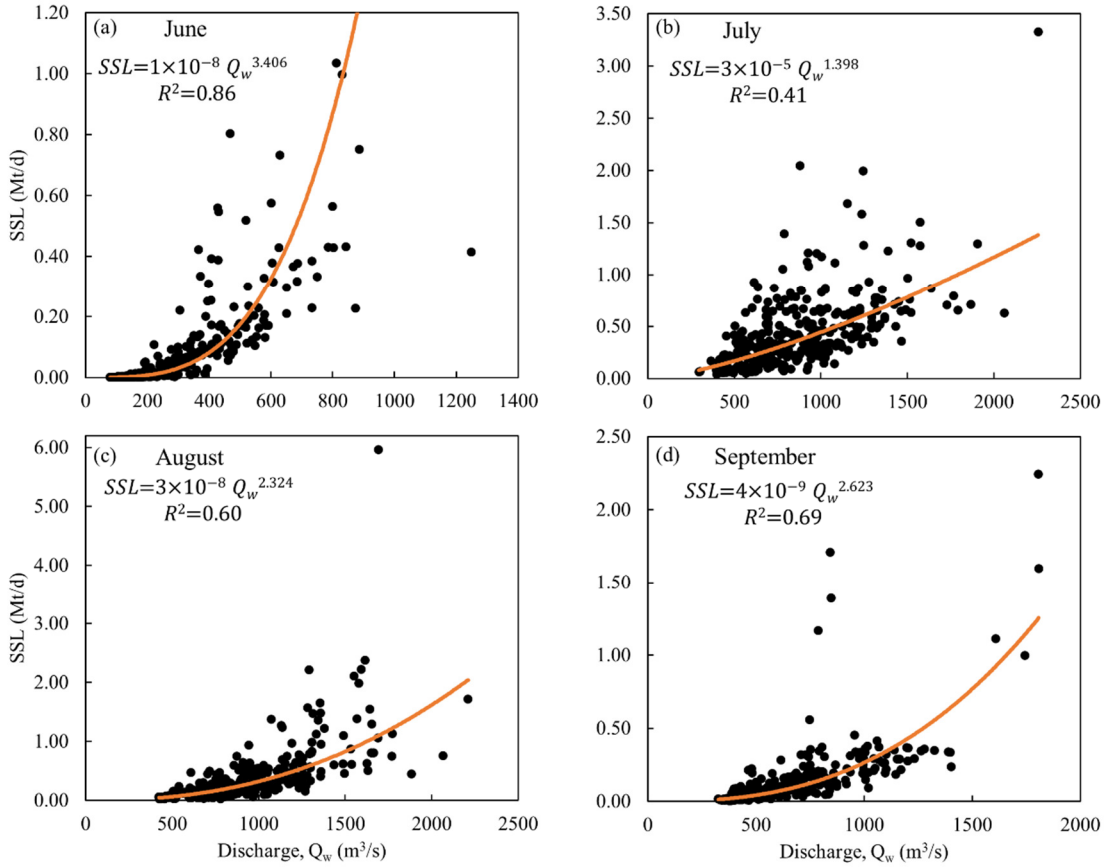

Figure 33. (a-d) Monthly SSL and discharge relationship for monsoon

The seasonal and monthly SRCs equations, coefficient of determination and average suspended sediment (ASSL) are summarized in Table 14. The monsoonal months July and August have the highest ASSL during monsoon.

Table 14. Seasonal sediment rating curves and average suspended sediment load

2006-2017	Equations with discharge	R^2	ASSL(Mt)±SD
Average annual	$SSL = 8 \times 10^{-11} Q_w^{3.235}$	0.91	33.269±4.872
Winter	$SSL = 3 \times 10^{-8} Q_w^{1.702}$	0.12	0.005±0.001
Pre-monsoon	$SSL = 7 \times 10^{-11} Q_w^{3.441}$	0.73	0.048±0.019
Monsoon	$SSL = 2 \times 10^{-8} Q_w^{2.462}$	0.81	32.455±5.459
June	$SSL = 1 \times 10^{-8} Q_w^{3.406}$	0.86	2.469±1.641
July	$SSL = 3 \times 10^{-5} Q_w^{1.398}$	0.41	12.952±4.932
August	$SSL = 3 \times 10^{-8} Q_w^{2.324}$	0.60	12.629±7.937
September	$SSL = 4 \times 10^{-9} Q_w^{2.623}$	0.69	4.406±2.363
Post-monsoon	$SSL = 2 \times 10^{-12} Q_w^{3.732}$	0.86	0.761±0.530

The monthly sediment transport by KG River in hydropower reservoir and monthly average total rainfall are compared in Figure 34. The increase in monthly SS perfectly coincides with

the monthly increase in average total rainfall trend. The total average monthly rainfalls of June (388.39±84.24 mm), July (674.91±105.24 mm), August (571.81±110.77 mm) and September (356.50±104.39 mm) yielded an average of 2.469±1.641, 12.952±4.932, 12.629±7.937 and 4.406±2.363 mega tons (Mt) of SS during respective months over the period 2006-2017 from the KG catchment. The study found higher the rainfall during monsoon months in KG basin, higher the amount of SS was transported from higher Himalayas to hydropower reservoir.

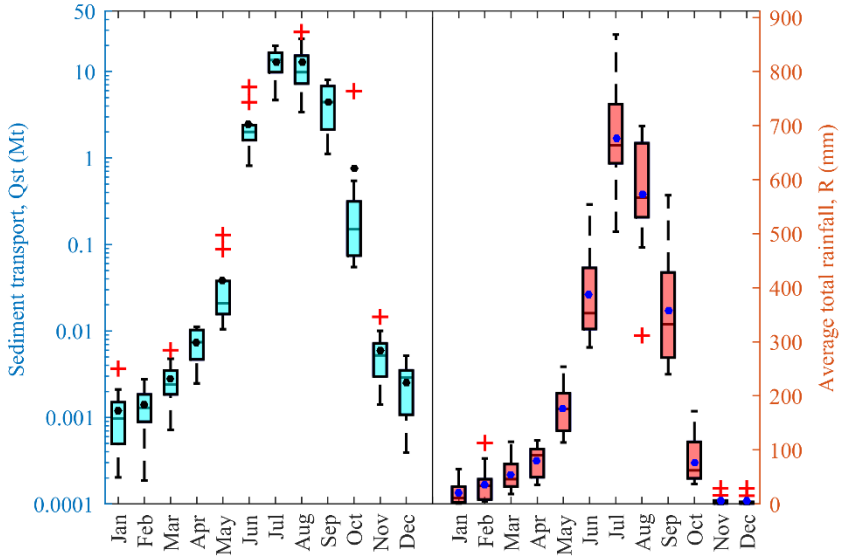

Figure 34. Suspended sediment transport and average total rainfall of KG basin.

3.6 Specific direct runoff discharge, erosion rate and rainfall relationship

In monsoon season (June-September), highest amount of SS was transported from Himalayas with an annual weathering rate estimated as 4390 tons/km^2/yr which was equivalent to 1.66 mm/yr. The upstream erosion rate of KG basin reported as 2-3.5 mm/yr (Struck *et al.*, 2013), whereas its value for the whole basin at hydropower station as 1.9 mm±0.9 mm/yr (Struck *et al.*, 2015). The direct runoff discharge increases linearly with increase in rainfall (Figure 35a) and relate as:

$$\frac{Q_d}{A} = 0.33 \times \mathrm{R} \qquad \text{(II.4)}$$

Where Q_d is fluvial discharge in and A is catchment area, specific discharge, $\frac{Q_d}{A}$ is expressed in

mm/day and R is rainfall in mm.

Noticeably, higher runoff discharges were observed during monsoon season (June- September). Particularly, major rainfall events are defined according to their rainfall threshold values greater than 30 mm/day (Merz *et al.*, 2006; Carver, 1997). In this study, there were 150 number of major rainfall events over the period 2006 - 2017. Out of them, all the major rainfall events were occurred in the monsoon season (June - September) except two events on October 2009. The monsoonal daily erosion rate in mm/day was showed linear increasing trend with major rainfall events (Figure 35b) expressed as:

$$Erosion\ rate = 0.002 \times \mathrm{R} - 0.035 \qquad \text{(II.5)}$$

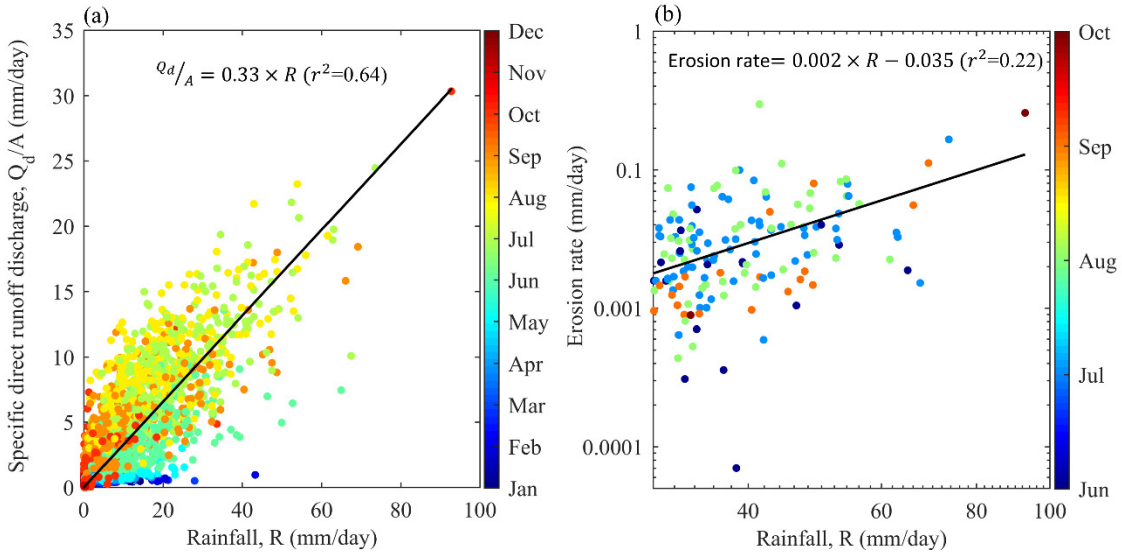

Figure 35. (a) Specific direct discharge and rainfall relationship (b) Erosion rate and major rainfall events (daily rainfall >30 mm) relationship

CHAPTER4.0 GENERAL CONCLUSIONS AND RECOMMENDATIONS

4.1 Conclusion

In this study, the specific discharge versus rainfall relationship at three hydrometric stations of main KG River and four hydrometric stations of its four tributaries and SS versus total and direct runoff discharge at hydropower reservoir were examined. Groundwater has a major impact on the annual hydrological budget and transport of suspended sediment in river system. About 97% of suspended sediment was transported during monsoon season (June - September), comprising an annual weathering rate of KG basin was estimated as 4390 tons/km^2/yr which was equivalent to 1.66 mm/yr. The specific direct runoff discharge and monsoonal daily erosion rate of major rainfall events (>30 mm/day) occurred in KG basin showed linear increasing trend with rainfall in KG basin.

4.2 Application of study

The research findings of seasonal SS budget and linear trends of specific direct runoff discharge and erosion rate will help to quantify seasonal sediment loss from Himalaya and to monitor sediment erosion from Himalayas, which could be useful for hydropower reservoir management.

4.3 Recommendations

The climatic variation within different elevation is complex in Himalaya region. The rainfall events in each sub-basin affects the SS yield. The erosion rate for each sub-basin should be investigated separately so that it is needed to install suspended sediment monitoring stations in the outlet of major tributaries.

PART III- RAINFALL TREND ANALYSIS IN KALI GANDAKI RIVER BASIN, HIMALAYA, NEPAL

ABSTRACT

Stream flow alteration is one of the most noticeable effects of rainfall change patterns in Himalaya mountain catchment of Kali Gandaki (KG) River. Localized rainfall changing trends with climate change in Himalaya zone is a rising issue. The synopsis of this study is to analyse fluvial flow changing patterns of three hydrometric stations of KG River, four hydrometric stations of its major tributaries due to changing seasonal and annual rainfall trends in twenty-seven rain gauge stations located between the elevations ranges of 700 to 2744 m MSL of KG River basin, Nepal over the period of 1957-2017. Monthly rainfall data were used to examine the rainfall and discharge trends. Mann- Kendall trend test (MKT) along with Sen's slope and sequential Mann- Kendall trend (SQMKT) analysis on homogenized time series data were used to evaluate the existence of monotonic trends, magnitude of trend and identify shifting of precipitation trend.

CHAPTER 1. GENERAL INTRODUCTION AND LITERATURE REVIEW

1.1 Research background

Stream flow with suspended sediment transport rate variation is one of the key noticeable effects of rainfall change patterns in Himalaya mountain catchment of Kali Gandaki (KG). Climate change is a remarkable issue globally from past few decades, had a significant impact on higher mountains in the form of extreme weather conditions such as rising temperature, changing of precipitation patterns, decrease of snowfall and decreasing the glaciers numbers. An alterations in regional hydrological cycles and changes in river flow such as flood or low flow are the significant potential consequences of climate change (Q. Zhang *et al.*, 2008). The global monsoon precipitation trend had a tendency to increase from 1901 to 1955 and decreasing trend since the 1950s up to 2001 (L. Zhang & Zhou, 2011). Studies between 1951-1999 (Min *et al.*, 2009) and between 1900 – 2009 (Westra *et al.*, 2013) showed about two-thirds of rainfall stations globally exhibited increasing trends.

Climate change is threatening Nepal's as well as worldwide food security, water resources, human habitats and tourism sectors seriously (M. Karki *et al.*, 2009; Langat *et al.*, 2017). The Himalaya regions are more vulnerable because of changing of altitudes within a short distance. The increasing temperature and shifting of rainfall patterns affected the livelihoods of people in the KG basin where springs are a major source of water and depend on annual rainfall to recharge the aquifers that fed them (Dandekhya *et al.*, 2017). The availability of water in KG basin is of major importance for hydropower as well as the small farmer managed irrigation scheme along the river and water transportation on hydropower reservoir. Because of less availability data and limited numbers of weather stations in Himalayan region, Nepal, only few researches of climate change and its impacts were conducted (U. B. Shrestha *et al.*, 2019). The effects of climate changes in Nepal have been documented by different researchers in terms of

temperature and precipitation scenario (Duncan *et al.*, 2013; R. Karki *et al.*, 2017; A. B. Shrestha *et al.*, 2017).

The main drivers of streamflow trends are climatic variability and changes, and the streamflow trend identification in a catchment is important for understanding the impact of climatic variability and changes in the region (Gautam & Acharya, 2012). It is paramount importance to conduct this study in KG River catchment at hydropower station as this river originates from Himalayas and there are only limited studies about effects of rainfall on hydropower reservoir.

1.2 Research objectives

The following are the research objectives of this study (Part-III).

1. To predict the homogeneous and non-homogeneous rainfall data stations in the catchment.
2. To analyze the rainfall trend of homogenized stations of catchment by Mann Kendall trend (MKT) and sequential Mann Kendall trend (SQMKT) tests.
3. To predict the rainfall trend change time.
4. To determine the magnitude of trend change.

CHAPTER 2.0 MATERIALS AND METHODS

2.1 Observation site

The Kali Gandaki (KG) River is a main glacier-fed river originating from the Himalaya region, Nepal. The main river flows from north to south in the higher Himalayan region and entering the Terai plains of Nepal to ultimately merge with the Ganges River in India. The river, upstream of hydropower dam has mainly four tributaries namely: Myagdi Khola (stream), Modi Khola, Seti Khola and Aandhi Khola. Myagdi Khola and Modi Khola are glacier- fed streams that connects to main KG River at middle of the reach whereas Seti Khola and Aandhi Khola are non-glacier-fed streams connect the main river close to hydropower dam. Each sub basins have complex geomorphology and watershed topography with rapid changes in elevations. The snowfall area is separated as elevation ranges less than 2000 m MSL with no snow cover, 2000 ~ 4700 m MSL with seasonal snow, 4700 ~ 5200 m MSL with completely snow except 1 or 2 month and elevation greater than 5200 m MSL with permanent snow. The KG catchment basin has 7060 Km^2 area comprises of elevations 529~2000 m MSL is 1317 Km^2 (19% coverage), 2000~4700 m MSL is 3388 Km^2 (48% coverage), 4700~5200 m MSL is 731 Km2 (10% coverage) and elevation greater than 5200 m MSL is 1624 Km^2 (23% coverage). Figure 36(a) shows the different altitude area coverage map showing river networks with locations of meteorological stations created in ArGIS10.3.1(ERSI Inc., USA) software. The elevations of KG decreases from 5039 m MSL in higher Himalaya to 529 m MSL at Setibeni, 5 km upstream of hydropower dam (Figure 36b) encompasses with wide variation in mean rainfall ranging less than 500 mm/yr in Tibetan Plateau and about 2000 mm/yr in the monsoon-dominated Himalayas.

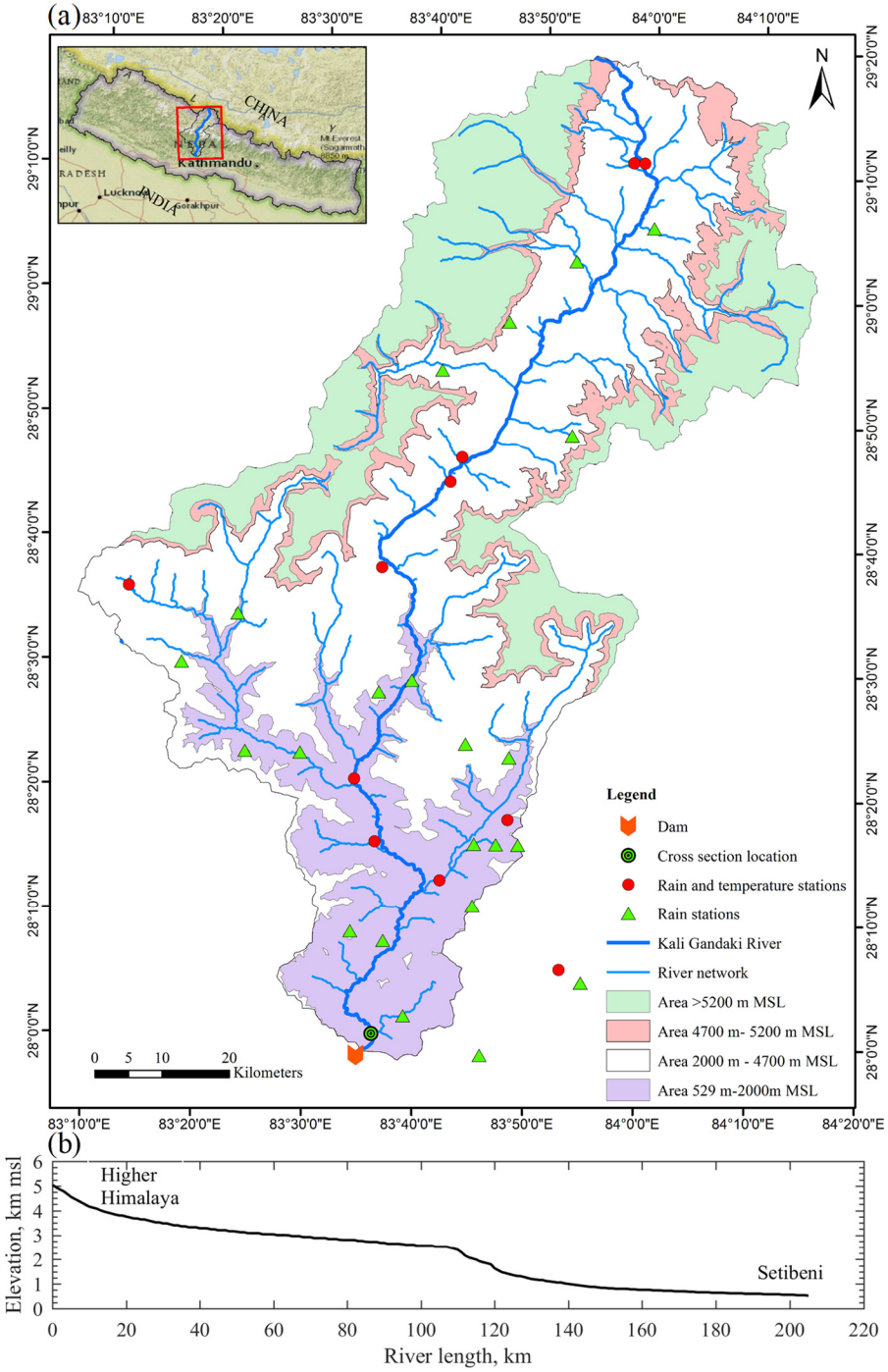

Figure 36. (a) Map of Kali Gandaki River catchment area (b) Longitudinal profile of Kali Gandaki River.

2.2 Data collection and acquisition

Department of Hydrology and Meteorology (DHM), Nepal set different hydrometric gauge stations (www.dhm.gov.np) and the station 410 was operated up to 1995 and now it is not

operated after dam construction. The bed level of dam was increasing yearly due to trapping of bedload as well as suspended sediment load by dam, which curtail sediment load in the downstream. The sedimentation lowers the reservoir capacity of dam annually.

The main physiographic characteristics of Kali Gandaki River basin at hydropower station is shown in Table 4.

The fluvial discharge of main river varies seasonally and is dependent on the discharges of the tributaries and rainfall received in sub basins in addition to the amount of snow melting from the Himalayas. A hydropower dam (27°58'44.88" N, 83°34'49.68" E) was built in 2002 for 144 MW power generation, at Mirmi, Syangja.

2.2.1. Missing Data Analysis

Monthly precipitations time series data from 1980 to 2018 were obtained by summing the daily rainfall data measured in the 27 rainfall stations located by Department of Hydrology and Meteorology (DHM). The details of meteorological stations are summarized in Table 11. The annual total rainfall data were calculated by adding monthly total rainfall data after filling the missing values. The monthly missing data during the period were filled using estimation technique. Generally, rainfall for the missing period was estimated by using normal ratio method (NRM) (Abdulkareem & Sulaiman, 2016), which assumes the precipitation P_x at a station X is estimated as a function of the normal monthly precipitation of the station under consideration and the neighbouring stations for the period of missing data at the station under consideration.

$$P_x = \frac{\sum_{i=1}^{n} \frac{NP_x}{NP_s} \times P_s}{n} \quad \text{(III.1)}$$

Where NP_x and NP_s are normal monthly precipitations at station x and surrounding s stations, P_x is the precipitation at surrounding stations and n is the number of surrounding stations under consideration.

2.2.2. Homogeneity tests

The stations having less than 10% rainfall missing data set sourced from Department of Hydrology and Meteorology were selected for homogeneity tests. The following four different types of homogeneity tests such as Pettitt test, Standard normal homogeneity test (SNHT), Buishand's range test and von Neumann ratio test were performed on the conducted in order to detect the inhomogeneity of the annual rainfall data (Che Ros *et al.*, 2016). All the tests are supposed the null hypothesis that the annual values of the testing variables are independent, whereas the alternative hypothesis assume there is break in the series. The Pettitt test, SNHT and Buishand's range test are capable of locating the year likely year of break, known as location specific tests whereas Von Neumann ratio test assumes under the alternative hypothesis that the series is not randomly distributed, referred as non-location specific (Wijngaard *et al.*, 2003).

Pettitt test

The Pettitt's test (Pettitt, 1979) test is a non- parametric rank test in which ranks r_i of Y_i series and ignores the normality of the series.

$$X_k = 2\sum_{i=1}^{k} r_i - k(n+1)\,, k = 1,2,\ldots\ldots,n \tag{III.2}$$

If a break occurs in year *k* then, $X_k = max|X_k|$

$$1 \le k \le n$$

Standard normal homogeneity test (SNHT)

It is used to identify the breaks at both the beginnings and ends of time series (Alexandersson, 1986; Alexandersson & Moberg, 1997) as

$$T(k) = k\bar{z_1}^2 + (n-k)\bar{z_2}^2, k = 1,2,\ldots\ldots\ldots n \tag{III.3}$$

Where, z_i are the mean value of during the first *k* years and (n-k) years respectively.

$$\bar{z}_1 = \frac{1}{k}\sum_{i=1}^{n}\frac{(Y_i-\bar{Y})}{s}, \bar{z}_2 = \frac{1}{n-k}\sum_{i=k+1}^{n}\frac{(Y_i-\bar{Y})}{s}, s = \frac{1}{n}\sum_{i=1}^{n}(Y_i-\bar{Y})^2$$

If a break occurs at the point *k*, then *T(k)* reaches a maximum near the year $k = k_i$. The indicator T_0 is defined as $T_0 = \max_{1 \le k \le n} T(k)$

Buishand's range test

It is a parametric test which assumes that the test values are independent and identically normally distributed (null hypothesis) and the alternative hypothesis assumes that the series contains a jump like shift or break (Buishand, 1982). The adjusted partial sum is defined as

$$s_0^* = 0 \tag{III.4}$$

$$s_k^* = \sum_{i=1}^{k} (Y_i - \bar{Y}), k = 1,2 \ldots . n \tag{III.5}$$

When the time series is homogenous, the values of s_k^* will rise and fall around zero.

The year *k* has break when s_k^* has reached a maximum (negative shift) or minimum (positive shift). Rescaled adjusted partial sums are obtained by dividing the values of $s_k^*$by the sample standard deviation. Buishand (1982) indicate that the values are not influenced by any linear transformation, therefore it is suitable to use the homogeneity test.

$$Q = \max_{0 \le k \le n} \left| {}^{s_k^*}/_{s} \right| \tag{III.6}$$

Another statistic test which could also be used is the range which computes the difference between the maximum and minimum value of the rescaled adjusted partial sums. The formula is given as follows:

The rescaled adjusted range, R is given by

$$R = \max_{0 \le k \le n} s_k^* - \min_{0 \le k \le n} s_k^* \tag{III.7}$$

Buishand (1982) gives critical values for both homogeneity tests ${}^{Q}/_{\sqrt{n}}$ and ${}^{R}/_{\sqrt{n}}$.

Von Neumann ratio test

It is a non- parametric test for which the null hypothesis is that the data are independent and identically distributed random values. The alternative hypothesis is that the values in the series are not randomly distributed. The von Neumann ratio (N) is defined as the ratio of mean square

successive (year to year) difference to the variance (Von Neumann, 1941).

$$N = \frac{\sum_{i=1}^{n-1}(Y_i - Y_{i+1})^2}{\sum_{i=1}^{n}(Y_i - \bar{Y})^2} \quad \text{(III.7)}$$

When the series is homogeneous, then the expected value E(N)=2. When the series has a break, then the value of N must be lower than 2. This imply that the sample has rapid variation in the mean (Wijngaard *et al.*, 2003; Kang & Yusof, 2012). On the other hand, the value greater than 2 implies that the series has rapid variations or oscillations in the mean (Bingham & Nelson, 1981).

2.2.3. Evaluation of homogeneity tests

The results of homogeneity tests are evaluated on the basis of classification assigned according to the number of tests rejecting the null hypothesis (Wijngaard *et al.*, 2003; Kang & Yusof, 2012).

Useful: In this class, the series that rejects one or none null hypothesis under the above four tests at 5% significance level are considered. This series is grouped as homogeneous and can be used for further analysis.

Doubtful: It considers that the series reject two null hypotheses of the four tests at 5% significance level is categorized as doubtful class. The series under this class have the inhomogeneous signal and should be critically inspected before further analysis.

Suspect: The series which contains three or all tests are rejecting the null hypothesis at 5% significance level, then the series is classified as suspect. The series can be deleted or ignored before further analysis.

The stations that are classified into 'suspect' should not be used in trend analysis so that they are excluded in the study.

2.2.3. Trend analysis

The Mann- Kendall trend test is based on the assumption of uncorrelated data. Before assessing MKT, lag1 autocorrelation for all the time series data were checked using autocorrelation

function (ACF) in Matlab R2016a software. The critical value at 5% significance level is calculated by using formula

$$ACF_{cr} = \pm \frac{1.96}{\sqrt{T-d}} \quad \text{(III.8)}$$

Where *T* is sample size and *d* represents the lag time. When autocorrelation is present, it is necessary to use the Modified Mann- Kendall test (Basistha *et al.*, 2009; Muthuwatta *et al.*, 2017). The non-parametric MKT test is commonly employed to detect monotonic trends in series of environmental data, climate data or hydrological data (Mann, 1945).

Mann – Kendall test (MK)

The Mann-Kendall statistics S is given by equation (Bari *et al.*, 2016; Gajbhiye *et al.*, 2016; Sonali & Kumar, 2013)

$$S = \sum_{k=1}^{n-1} \sum_{j=k+1}^{n} sgn(x_j - x_k) \quad \text{(III.9)}$$

where "*sgn*" is the sign function, and *n* is the number of observations in the data sets.

$$sgn(x) = \begin{cases} 1 \; if \; x > 0 \\ 0 \; if \; x = 0 \\ -1 \; if \; x < 0 \end{cases}$$

where x_j are the sequential data values, *n* is the length of the data set.

The mean of S is E(s)=0 and the variance σ^2 is

$$\sigma^2 = \left\{ n(n-1)(2n+5) - \sum_{j=1}^{p} t_j \left(t_j - 1\right)\left(2t_j + 5\right) \right\} / 18 \quad \text{(III.10)}$$

where *p* is the number of the tied groups in the data set and t_j is the number of data points in the j^{th} tied groups. The statistic S is approximately normal distributed provided that the following Z- transformation is employed.

$$Z = \begin{cases} \frac{S-1}{\sigma} \; if \; S > 0 \\ 0 \; if \; S = 0 \\ \frac{S+1}{\sigma} \; if \; S < 0 \end{cases} \quad \text{(III.11)}$$

The significance level of α =0.05 was used in this study. A positive value of Z indicates an increasing trend, whereas negative indicates decreasing trend. If the computed value of |Z|>Zα/2, the null hypothesis is rejected at the α level of significance in a two- sided test. Where *S* is sum of signs of the differences between any two observations for a series x_n. Also, where sign(z) is 0 when Z is zero and 1 when Z>-1 when Z<1.

If the series of values are in a random order, the expected value of *S* is zero and the variance σ^2 is given as:

$$\sigma^2 = n(n-1)(2n+5)/18 \quad \text{(III.12)}$$

Sen's Slope

The slope estimator (*S*) of the data *x* is expressed as below:

$$S = \text{median}\,(y) \quad \text{(III.13)}$$

Where $y = \frac{x_j - x_k}{j-k}$ where j=1, 2, 3,…., n and k < j.

Tau (Maurice G Kendall, 1938; Maurice George Kendall, 1948) measures the strength of the monotonic relationship between x and y . Kendall's tau correlation coefficient is given by

$$\tau = \frac{S}{n(n-1)/2} \quad \text{(III.14)}$$

Based on the Mann- Kendall test, the trends are significant at the 99.9%, 99%, 95% and 90% confidence levels. When autocorrelation presence in the series, it is necessary to use the Modified Man-Kendall test (Basistha *et al.*, 2009; Muthuwatta *et al.*, 2017)

Modified Mann- Kendall test (MMK)

The modified MK test has been used for trend detection of an autocorrelated series (Hamed &

Rao, 1998; Gajbhiye *et al.*, 2016; Mondal *et al.*, 2012).

A modified variance in the case of autocorrelated data is calculated by equation as follows (Bayley & Hammersley, 1946).

$$\sigma^{2*} = \sigma^2 . \frac{n}{n_s^*} = \frac{n(n-1)(2n+5) - \sum_{j=1}^{p} t_j \left(t_j - 1\right)\left(2t_j + 5\right)}{18} . \frac{n}{n_s^*} \quad \text{(III.15)}$$

where $\frac{n}{n_s^*}$ represents a correction due to the autocorrelation in the data, *n* is the actual number of observations and n_s* is an effective number of observations to account for correlation in the data. The best approximation to the theoretical values was obtained by using equation as follows (Hamed & Rao, 1998).

$$\frac{n}{n_s^*} = 1 + \frac{2}{n(n-1)(n-2)} \sum_{j=1}^{n-1} (n-i)(n-i-1)(n-i-2) r_i \quad \text{(III.16)}$$

Where n is actual number of observations and r_i is the autocorrelation function of the ranks of the observations.

Sequential Mann- Kendall test (SQMKT)

Abrupt change analysis is based on the sequential Mann- Kendall test which consists of progressive U(t) and retrograde U'(t) series in order to detect the change of the trend over time. U(t) is a standardized variable that has zero mean and unit standard deviation. U(t) is the same value as the Z values that are found from the first to last data point. The steps applied in sequence are as follows (Bari *et al.*, 2016).

The test statistic t is calculated by as

$$t_j = \sum_{1}^{j} n_j \quad \text{(III.17)}$$

The mean and variance of the test statistic are

$$E(t) = \frac{n(n-1)}{4} \quad \text{(III.18)}$$

$$E(t) = \frac{j(j-1)(2j+5)}{72} \quad \text{(III.19)}$$

The sequential values of the test statistic U(t) are:

$$U(t) = \frac{t_j - E_t}{\sigma} \quad \text{(III.20)}$$

Similarly, the retrograde U'(t) series are calculated backward, starting from the end of the time series.

CHAPTER 3.0 RESULTS AND DISCUSSION

3.1 Homogeneity tests results

Out of 27 rainfall measuring stations of whole catchment, stations Rangkhani[622], Kuhun[627], Darbang[621], Lete[607], Kushma[614], Sirkon[630] and Tribeni[620] showed inhomogeneity data so that these seven stations were excluded and only 20 homogeneous stations were used for MKT and SQMKT tests. The homogeneous and inhomogeneous stations resulted from different homogeneity tests are shown in Figure 37a,b and different homogeneity tests results were summarized in Table 15.

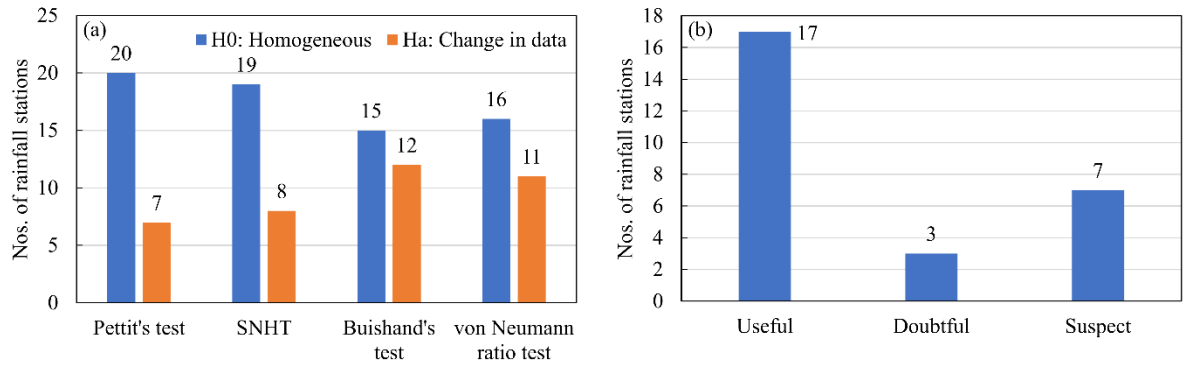

Figure 37. (a) Comparison of homogeneous and change in data stations (b) Classification of stations

The trend change rainfall stations by different location specific tests are presented in Figures 38a-i,39a-i and 40a-i. Because of trend changing point, each graph showed two mean values and corresponding year showed a trend change year in the time series.

Table 15. Homogeneity tests of meteorological stations in Kali Gandaki catchment.

Station name & ID No.	Data availability	Sample size (n)	Elevation (m)	Pettitt's test			SNHT			Buishand's test					Von Neumann		Remarks
				K value	Year	Trend	T0 value	Year	Trend	Q value	Year	Trend	R value	Trend	N value	Trend	
Baglung[605]	1970-2018	49	984	218	–	H0	9.36	–	H0	8.72	1979	Ha	9.58	H0	1.43	Ha	Doubtful
Bhobang[615]	1978-2018	42	2273	210	–	H0	7.32	–	H0	8.55	2001	Ha	8.55	H0	1.88	H0	Useful
Rangkhani[622]	1989-2018	31	1740	185	2003	Ha	15.08	2009	Ha	10.61	2003	Ha	10.62	Ha	1.08	Ha	Suspect
Bega[626]	1992-2018	28	1770	60	–	H0	3.34	–	H0	3.07	–	H0	6.14	H0	1.82	H0	Useful
Benibazar[609]	1957-2016	61	835	364	1980	Ha	8.17	–	H0	10.88	1992	Ha	11.89	Ha	1.82	H0	Doubtful
Bhagara[629]	1992-2018	28	2330	72	–	H0	8.45	–	H0	4.84	–	H0	6.04	H0	1.70	H0	Useful
Darbang[621]	1989-2018	31	1160	147	1997	Ha	11.04	1997	Ha	8.48	1997	Ha	8.84	Ha	1.15	Ha	Suspect
Ghorepaani[619]	1975-2018	45	2742	225	–	H0	8.15	–	H0	9.08	2003	Ha	12.14	Ha	1.20	Ha	Doubtful
Gurjakhani[616]	1979-2016	39	2530	94	–	H0	8.78	–	Ha	4.11	–	H0	6.69	H0	1.53	H0	Useful
Kuhun[627]	1992-2018	28	1550	148	2007	Ha	14.99	2008	Ha	9.90	2008	Ha	10.04	Ha	0.65	Ha	Suspect
Muna[628]	1992-2018	28	1970	46	–	H0	2.44	–	H0	3.77	–	H0	5.54	H0	1.99	H0	Useful
Tatopaani[606]	1970-2018	50	1243	264	–	H0	7.37	–	H0	9.60	1994	Ha	10.97	H0	1.98	H0	Useful
Jhomsom[601]	1958-2018	62	2744	236	–	H0	3.28	–	H0	6.97	–	H0	8.70	H0	1.67	H0	Useful
Lete[607]	1970-2018	50	2384	464	1984	Ha	27.48	1984	Ha	17.09	1984	Ha	17.09	Ha	0.77	Ha	Suspect
Thakmarpha[604]	1968-2018	52	2566	190	–	H0	4.60	–	H0	6.54	–	H0	7.96	H0	1.73	H0	Useful
Karkineta[613]	1977-2018	43	1720	100	–	H0	4.51	–	H0	5.19	–	H0	8.01	H0	1.49	Ha	Useful
Kushma[614]	1970-2018	50	891	268	–	H0	9.61	1980	Ha	9.15	1980	Ha	14.44	Ha	1.34	Ha	Suspect
Sirkon[630]	1992-2018	28	790	142	2003	Ha	10.86	2003	Ha	8.67	2003	Ha	8.67	Ha	1.29	Ha	Suspect
Tribeni[620]	1989-2018	31	700	135	1999	Ha	8.45	–	H0	7.80	1999	Ha	8.47	Ha	1.32	Ha	Suspect
Bhaudare[813]	1985-2018	35	1600	82	–	H0	4.43	–	H0	4.75	–	H0	7.13	H0	1.61	H0	Useful
Ghandruk[821]	1976-2018	44	1960	228	2007	Ha	8.47	2007	Ha	8.43	–	H0	8.43	H0	1.75	H0	Doubtful
Lumle[814]	1970-2018	50	1740	186	–	H0	3.89	–	H0	6.97	–	H0	11.33	Ha	1.54	H0	Useful
Pamdur[830]	1992-2018	28	1160	100	–	H0	4.63	–	H0	5.69	–	H0	7.48	H0	1.76	H0	Useful
Salyan[829]	1992-2018	28	1000	92	–	H0	5.30	–	H0	6.09	–	H0	7.81	Ha	1.58	H0	Useful
Dandaswarna[832]	2000-2018	20	1432	52	–	H0	5.82	–	H0	4.76	–	H0	4.76	H0	1.70	H0	Useful
Syangja[805]	1973-2018	47	868	149	–	H0	7.14	–	H0	5.28	–	H0	8.88	H0	1.45	Ha	Useful
Waling[826]	1989-2018	31	750	81	–	H0	4.11	–	H0	5.60	–	H0	6.80	H0	1.57	H0	Useful

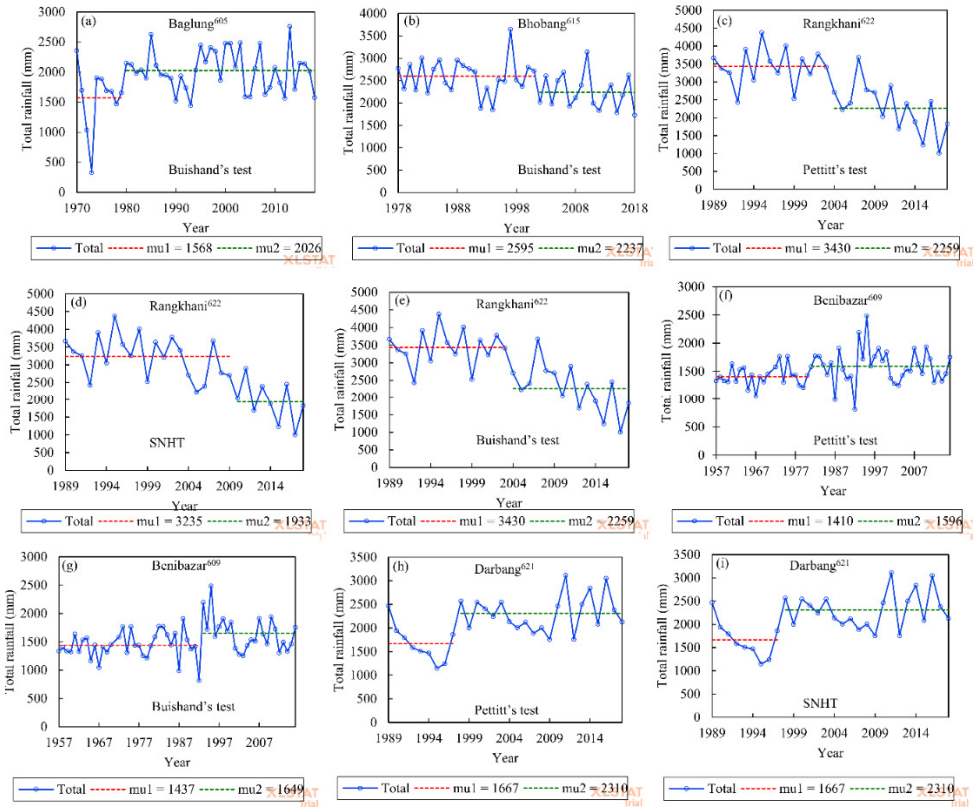

Figure 38. Change year in annual rainfall series for different stations

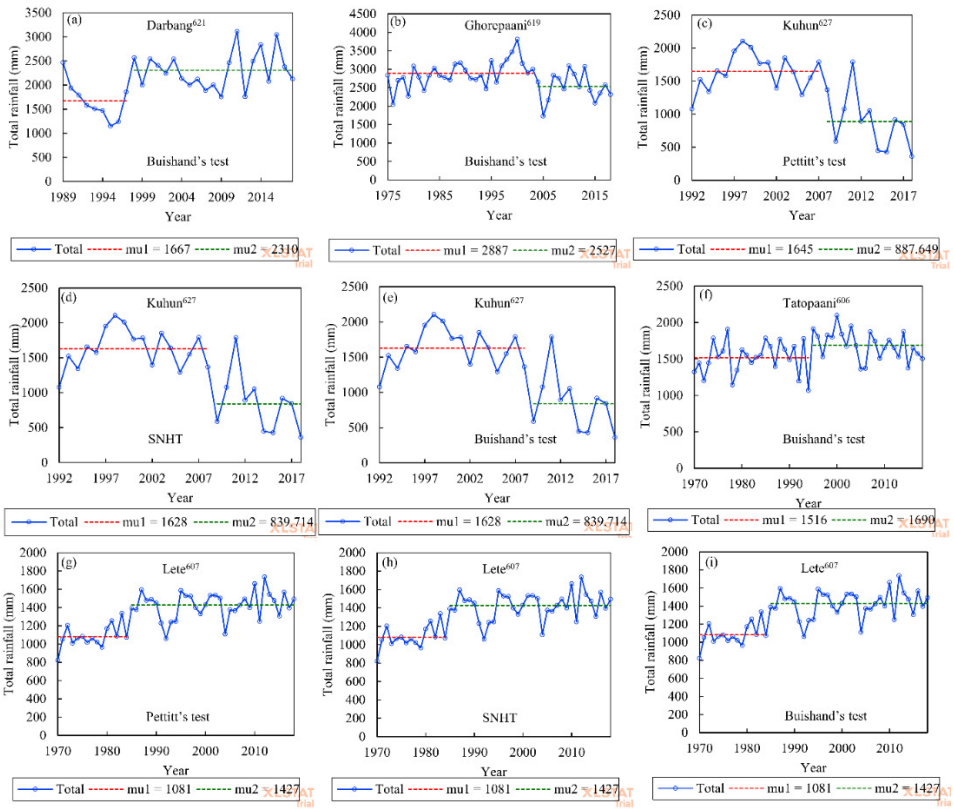

Figure 39. Change year in annual rainfall series for different stations

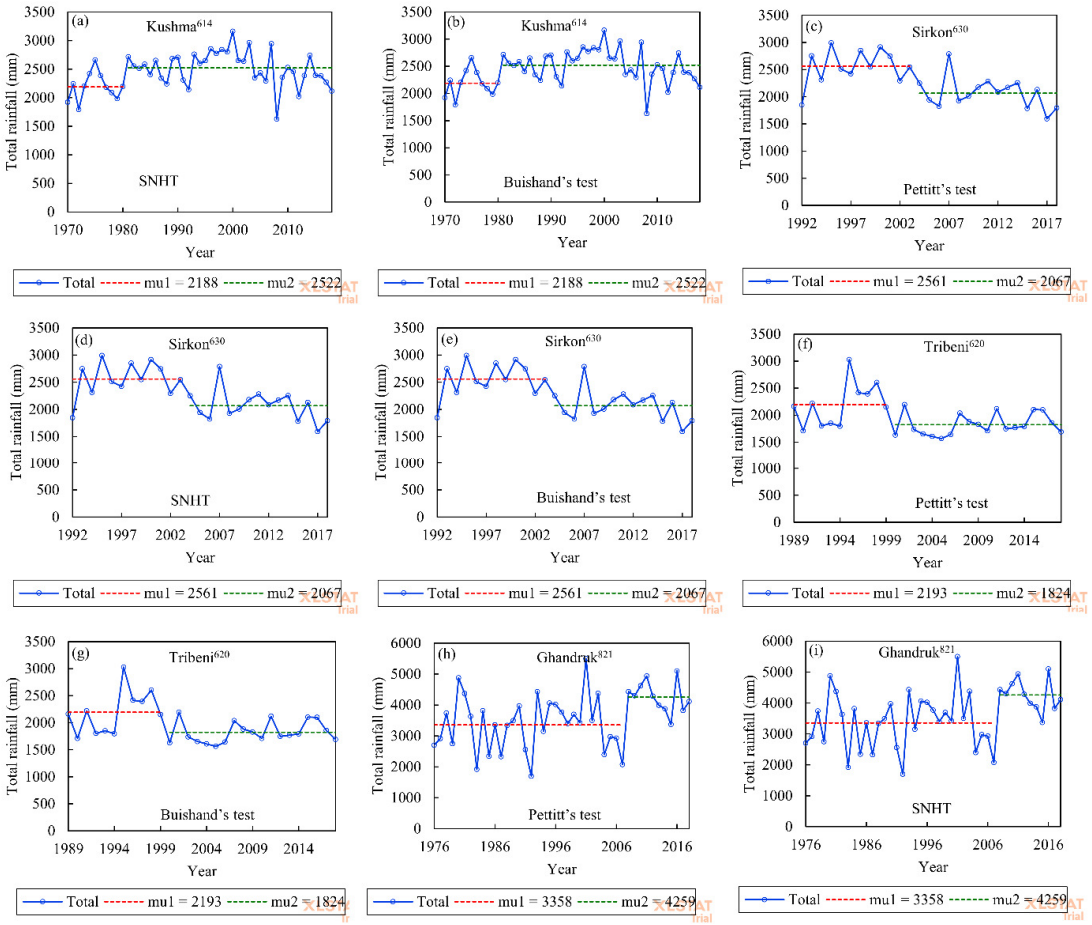

Figure 40. Change year in annual rainfall series for different stations

3.2 Monthly, seasonal and annual MKT test results

Lag 1 autocorrelation results showed that there were no time series data significantly correlated in 95% confidence limit so that MKT was applied for time series data. Figure 41a-b show the sample autocorrelation of meteorological stations of Jhomsom[601] and Lumle[814] respectively.

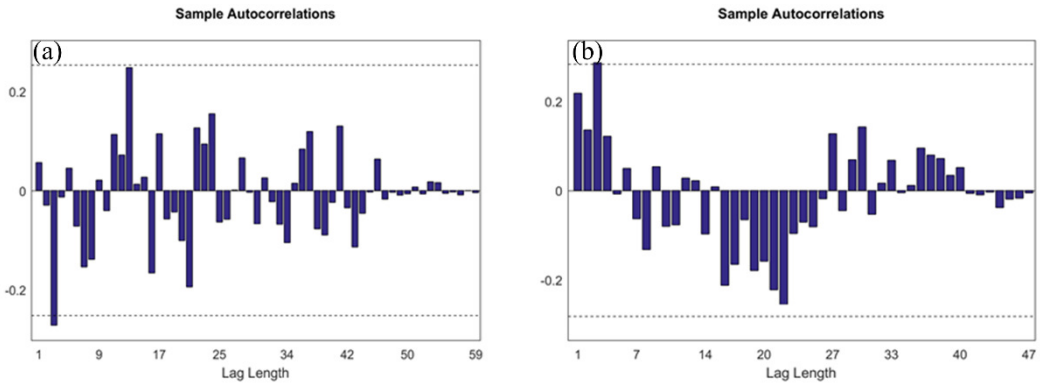

Figure 41. Sample autocorrelation of meteorological station (a) Jhomsom[601] and (b) Lumle[814].

Figure 42a shows MKT test of overall trends of rainfall measuring stations of KG catchment. Most of the months showed decreasing trend with some exceptions showing no trends at all. The rainfall increasing trend from March was decreased continuously up to June. The number of stations under increasing trends during pre-monsoon (March-May) and monsoon (June-September) rainfall of the catchment was higher. In contrast, the number of stations under decreasing trends during winter (December-February) and post-monsoon (October- November) were higher. Out of 20 stations, 80% stations showed decreasing trends during winter and 75% stations showed decreasing trends during post-monsoon. In contrast, 70% stations showed increasing trends during pre-monsoon and 55% stations showed increasing trends during monsoon. Only 2 stations of the catchment followed no trends during post-monsoon season. Subjected to annual total rainfall, 45% stations showed increasing and remaining 55% stations showed decreasing trends. This showed that the pre-monsoon and monsoon rainfall in KG basin was followed increasing trend.

Figure 42b showed the monthly and seasonal significant and non-significant number of rainfall stations of KG catchment. MKT trend test showed most of the stations showed non-significant increasing and decreasing trends. Only few stations from February to July showed increasing trend whereas from September to December showed significantly decreasing trend in 95% confidence limit.

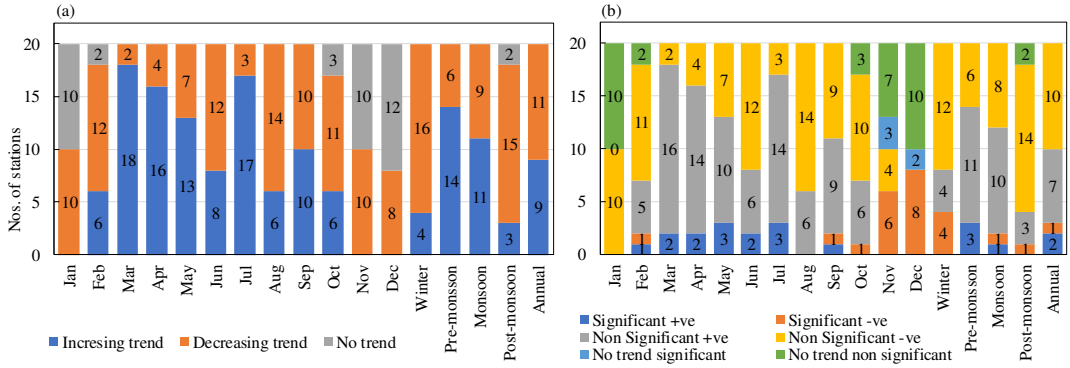

Figure 42. (a) Overall trends of rainfall stations (b) Significant and Non-significant number of rainfall stations

The details of MKT test statistics for different months of meteorological stations of KG catchment are shown in Table 16.

The MKT test statistics for seasonal rainfalls are shown in Table 17 that winter of station Bhobang[615], Karkineta[613], Bhaudare[813] and Syangja[805] have a significant negative trend in 95% confidence limit. Stations Beni[609], Ghorepaani[619] and Thakmarpha[604] showed the positive trend during pre-monsoon season in 95% confidence limit. Only stations Bhobang[615] showed negative trend and Ghandruk[821] showed positive trend during monsoon in 95% confidence limit and only one station Thakmarpha[604] showed negative trend during post-monsoon season in 95% confidence limit. In the case of MKT statistics for annual total rainfall, only Beni[609] and Ghandruk[821] showed positive trend having Sen's slope +3.63 mm/yr and +25.51 mm/yr respectively but Bhobang[615] showed negative trend having Sen's slope of -15.04 mm/yr in 95% confidence limit. An unchanging rainfall measures 0.0 mm/year was found for station Beni[609] during winter and Bhagara[629] and Waling[826] during post-monsoon season.

Table 16. Mann-Kendall trend test results for different months of meteorological stations of KG catchment

Station name & ID No.	Jan		Feb		Mar		Apr		May		Jun		Jul		Aug		Sept		Oct		Nov		Dec	
	Z-value	Sen's slope	Z-value	Sen's slope	Z-value	Sen's slope	Z-value	Sen's slope	Z-value	Sen's slope	Z-value	Sen's slope	Z-value	Sen's slope	Z-value	Sen's slope	Z-value	Sen's slope	Z-value	Sen's slope	Z-value	Sen's slope	Z-value	Sen's slope
Baglung[605]	0.22	0.00	0.96	0.19	**2.44**	0.68	0.77	0.36	-0.09	-0.06	1.39	1.31	1.34	2.57	0.97	1.69	-0.06	-0.20	-1.14	-0.65	**-2.33**	0.00	-1.91	0.00
Bhobang[615]	0.14	0.00	**-2.43**	-0.70	-0.96	-0.25	-1.05	-0.38	0.40	0.40	-1.13	-2.71	0.55	1.03	-1.42	-4.02	**-2.75**	-6.44	-1.17	-0.64	**-2.05**	0.00	**-3.06**	-0.33
Bega[626]	-0.25	-0.05	-0.33	-0.20	0.71	0.83	1.04	1.40	-1.54	-1.97	-1.21	-2.36	**2.17**	6.07	-1.88	-5.42	0.04	0.07	-1.06	-1.00	**-2.51**	-0.35	-0.32	0.00
Beni[609]	-0.36	0.00	1.81	0.21	0.68	0.08	1.37	0.33	**3.18**	1.08	1.50	1.08	1.50	1.23	-0.74	-0.68	0.81	0.49	-0.02	0.00	-0.15	0.00	**-2.19**	0.00
Bhagara[629]	-0.30	0.00	0.75	0.64	0.92	0.60	1.19	0.94	**2.69**	3.59	-0.58	-2.77	1.25	7.38	-0.33	-1.52	0.67	3.37	0.15	0.16	-0.74	0.00	0.72	0.00
Ghorepani[619]	-1.05	-0.14	-1.53	-0.36	1.93	0.96	**2.80**	2.25	0.98	1.23	0.20	0.25	-1.20	-2.54	-0.92	-2.01	-1.61	-2.97	-1.04	-0.77	-1.62	-0.04	**-2.88**	-0.15
Gurjakhani[616]	-0.20	0.00	-0.48	-0.11	0.63	0.28	0.47	0.17	0.45	0.3	-0.15	-0.25	-0.70	-1.85	0.63	1.58	-0.85	-1.78	0.60	0.20	-1.53	-0.07	**-2.24**	-0.14
Muna[628]	-0.61	-0.18	0.00	0.00	-0.58	-0.22	0.65	0.35	1.25	1.78	-0.75	-2.67	1.21	5.75	-0.13	-0.62	0.50	1.33	0.17	0.08	-1.20	0.00	-0.75	0.00
Tatopaani[606]	0.00	0.00	0.00	0.00	1.30	0.40	1.80	0.88	0.74	0.41	**2.60**	1.98	0.97	0.90	-0.06	-0.03	0.84	0.49	-1.22	-0.65	-0.96	0.00	-0.89	0.00
Jhomsom[601]	0.00	0.00	1.28	0.09	0.06	0.01	1.56	0.17	**2.60**	0.22	**2.65**	0.23	1.91	0.34	-0.55	-0.11	-0.12	-0.04	-0.14	0.00	-0.38	0.00	-0.36	0.00
Thakmarpha[604]	-0.30	0.00	**2.23**	0.24	0.69	0.15	1.88	0.35	0.67	0.13	0.39	0.09	**2.03**	0.61	-0.23	-0.05	-0.94	-0.29	**-2.14**	-0.36	**-2.09**	-0.01	**-2.03**	0.00
Karkineta[613]	-0.79	-0.15	-0.27	-0.05	1.21	0.40	-0.08	-0.03	0.67	0.68	1.30	2.91	1.21	2.81	0.08	0.3	-1.67	-3.86	1.84	1.01	**-2.39**	-0.08	**-3.53**	-0.35
Bhaudare[813]	-0.24	0.00	-1.77	-0.57	0.62	0.44	0.65	0.90	-1.01	-2.16	-1.22	-4.98	-0.09	-0.97	0.80	5.94	-0.03	-0.16	0.44	0.95	**-2.23**	-0.24	**-3.41**	-0.26
Ghandruk[821]	-0.79	-0.24	-1.13	-0.58	1.38	1.03	0.52	0.42	1.57	2.49	1.21	4.89	**2.01**	11.26	1.62	4.46	**2.13**	5.31	0.41	0.51	**-2.02**	-0.27	**-3.23**	-0.55
Lumle[814]	-0.71	-0.10	-0.30	-0.10	1.72	0.70	0.38	0.27	0.19	0.22	-0.59	-1.22	1.54	3.83	0.20	0.80	0.04	0.02	-0.15	-0.21	-1.79	-0.24	-0.94	0.00
Pamdur[830]	-0.54	-0.40	0.50	0.21	**2.11**	1.99	0.38	0.82	-1.46	-3.6	-1.42	-8.17	0.88	8.65	-0.88	-6.71	0.13	1.03	-0.96	-2.53	-1.82	-0.35	**-2.06**	-0.17
Salyan[829]	-0.75	-0.23	-0.81	-0.70	1.42	1.39	**2.00**	3.25	-1.38	-2.63	-1.54	-5.44	0.96	4.42	-1.67	-6.35	-0.04	-0.08	-0.50	-1.35	**-2.02**	-0.26	-1.09	0.00
Dandaswara[832]	-0.11	0.00	-0.67	-0.49	0.70	1.77	-1.12	-2.34	-1.40	-6.90	-0.98	-6.89	0.14	2.03	-0.98	-6.13	0.35	3.78	-0.67	-1.98	0.11	0.00	0.12	0.00
Syangja[805]	-1.49	-0.26	-1.06	-0.18	0.14	0.04	-0.25	-0.18	-0.45	-0.6	-0.95	-1.83	0.55	1.38	-0.66	-1.30	-0.06	-0.12	-0.64	-0.62	**-2.68**	0.00	**-2.54**	-0.07
Waling[826]	-0.78	-0.11	-0.56	-0.08	1.00	0.41	1.86	1.56	0.39	0.73	-1.46	-5.57	0.68	2.67	-1.61	-4.33	0.04	0.06	0.67	0.00	-1.18	0.00	-0.90	0.00

Table 17. Mann-Kendall trend test results for different seasons of meteorological stations of KG catchment

Station name & ID No.	Winter			Pre-monsoon			Monsoon			Post-monsoon			Annual		
	Tau	Z-value	Sen's slope	Tau	Z-value	Sen's slope	Tau	Z-value	Sen's slope	Tau	Z-value	Sen's slope	Tau	Z-value	Sen's slope
Baglung[605]	0.02	0.21	0.09	0.13	1.30	1.38	0.10	0.97	3.46	-0.14	-1.40	-0.92	0.13	1.32	4.89
Bhobang[615]	-0.29	**-2.67**	-1.57	-0.03	-0.24	-0.42	-0.28	**-2.57**	-12.35	-0.14	-1.31	-0.87	-0.30	**-2.71**	-15.04
Bega[626]	-0.10	-0.71	-1.07	-0.03	-0.21	-0.89	0.04	0.25	2.83	-0.24	-1.75	-1.78	-0.09	-0.63	-4.20
Beni[609]	-0.01	-0.05	-0.00	0.28	**3.11**	1.41	0.14	1.53	2.37	-0.02	-0.20	-0.08	0.19	**2.08**	3.63
Bhagara[629]	0.04	0.29	0.37	0.19	1.33	4.38	0.06	0.42	5.77	0.00	0.00	0.00	0.09	0.67	10.59
Ghorepani[619]	-0.20	-1.85	-1.08	0.38	**3.61**	4.22	-0.13	-1.18	-5.87	-0.13	-1.23	-0.85	-0.09	-0.84	-5.23
Gurjakhani[616]	-0.14	-1.21	-0.84	0.06	0.48	0.55	0.00	0.01	0.19	-0.03	-0.24	-0.16	-0.00	0.00	-0.19
Muna[628]	-0.16	-1.17	-1.50	0.08	0.54	1.10	0.09	0.67	6.56	0.01	0.06	0.08	0.08	0.54	6.88
Tatopaani[606]	-0.01	-0.10	-0.08	0.17	1.66	1.30	0.17	1.70	3.50	-0.15	-1.47	-0.75	0.18	1.78	4.16
Jhomsom[601]	0.11	1.26	0.17	0.13	1.43	0.43	0.15	1.64	0.59	-0.06	-0.62	-0.05	0.08	0.91	0.60
Thakmarpha[604]	0.10	1.05	0.18	0.27	**2.74**	0.78	0.04	0.43	0.26	-0.30	**-3.10**	-0.62	0.07	0.74	0.56
Karkineta[613]	-0.24	**-2.23**	-1.16	0.06	0.54	0.90	-0.01	-0.04	-0.56	0.13	1.17	0.76	-0.02	-0.13	-0.80
Bhaudare[813]	-0.27	**-2.22**	-2.00	-0.01	-0.09	-0.30	-0.01	-0.06	-0.89	-0.03	-0.21	-0.40	-0.02	-0.15	-3.69
Ghandruk[821]	-0.18	-1.72	-1.27	0.21	1.95	4.62	0.21	**2.00**	22.49	0.00	0.02	0.01	0.24	**2.24**	25.51
Lumle[814]	-0.02	-0.16	-0.20	0.08	0.82	1.26	0.04	0.35	2.44	-0.04	-0.41	-0.54	0.03	0.32	2.27
Pamdur[830]	-0.11	-0.79	-0.95	-0.07	-0.46	-1.94	-0.15	-1.08	-18.76	-0.19	-1.38	-4.28	-0.22	-1.58	-30.02
Salyan[829]	-0.14	-1.00	-1.23	0.06	0.42	1.33	-0.12	-0.88	-14.10	-0.15	-1.08	-2.85	-0.16	-1.13	-18.05
Dandaswara[832]	-0.11	-0.63	-1.01	-0.19	-1.12	-7.28	-0.25	-1.47	-16.74	-0.12	-0.70	-2.68	-0.28	-1.61	-27.40
Syangja[805]	-0.21	**-2.07**	-0.85	-0.08	-0.74	-1.21	-0.02	-0.23	-1.06	-0.11	-1.04	-0.92	-0.09	-0.89	-5.11
Waling[826]	-0.17	-1.28	-0.94	0.18	1.39	3.01	-0.16	-1.25	-7.32	0.08	0.60	0.00	-0.09	-0.64	-6.86

All seasonal and annual rainfall of remaining stations showed positive and negative trends statistically non-significant at 95% confidence limit. Additionally, the relationship of monotonic trend with time in terms of Kendall's tau value were found weak. Figure 43a,b show chronically Sen's slope magnitudes during winter and pre-monsoon whereas Figure 44a,b shows the Sen's slope magnitudes during monsoon and post-monsoon.

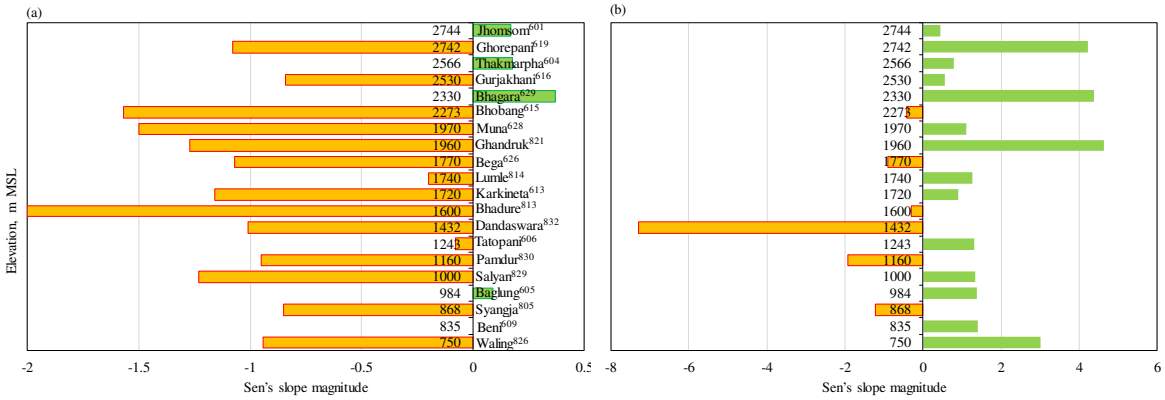

Figure 43. Sen's slope magnitude (a) for winter (b) for pre-monsoon

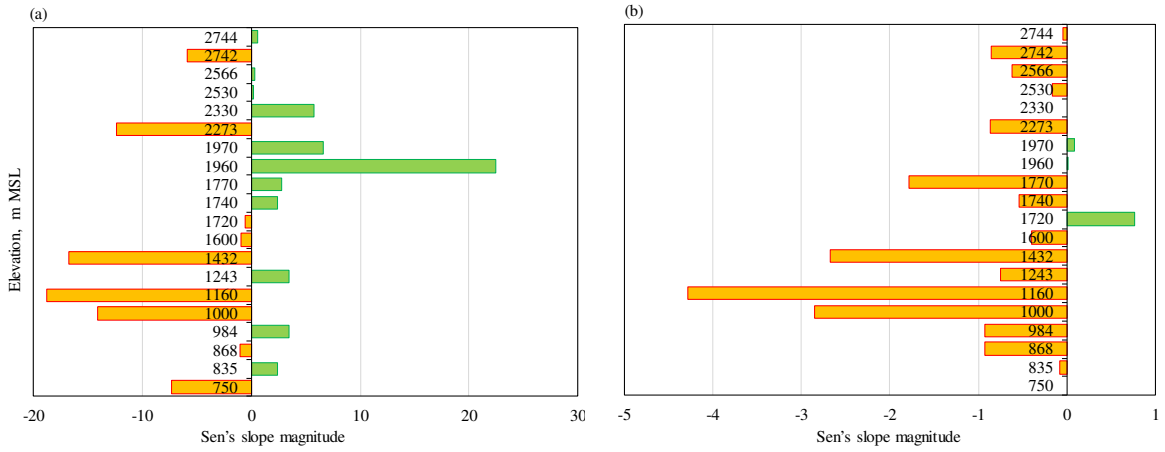

Figure 44. Sen's slope magnitude (a) for monsoon (b) for post-monsoon

Figure 45a shows elevation (Elv.) wise average total annual rainfall in different meteorological stations located inside the KG basin and Figure 45b shows annual Sen's slope magnitude of meteorological stations located inside the KG basin. Overall annual Sen's slope magnitude for elevations 1000 m to 1432 m showed highest magnitudes in decreasing trend, whereas stations having elevations 1960 m, 1970 m and 2330 m showed higher in increasing trend.

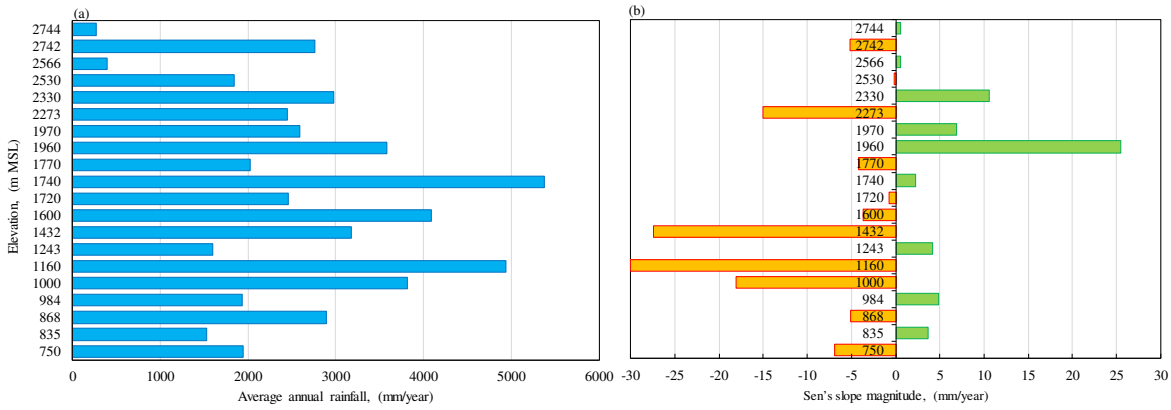

Figure 45. (a) Average annual rainfall (b) Annual Sen's slope magnitude

The highest rainfall station Lumle (Elv. 1740 m MSL avg. total rainfall 5377 mm/year) showed the increasing trend of magnitude +2.27 mm/year and the station Ghandruk (Elv. 1960 m MSL, avg. total rainfall 3589 mm/year) showed highest increasing trend of +25.51 mm/year. In contrast, the station Pamdur (Elv. 1160 m MSL, avg. total rainfall 4941 mm/year) showed overall highest decreasing trend of magnitude −30.02 mm/year. The distribution of the annual rainfall trend revealed that the stations of upper KG catchment have less rainfall events having rainfall increasing trend with less amount of Sens's slope whereas the middle part of KG catchment consists of hilly zone with high rainfall events followed the increasing trend and down part of KG catchment followed decreasing trends. No any significant trend in downstream of KG catchment.

3.3 Sequential Mann- Kendall trends analysis

The SQMKT was applied for rainfall for determining the approximate year of the beginning of the significant trends. The point where the progressive, U(t) and retrograde, U'(t) cross each other indicates the approximate year at which the trend begins, and a significant trend is detected when the curves exceeded the value ±1.96 at the 95% confidence limit on a time series graph.

3.3.1 Winter, pre-monsoon, monsoon and post-monsoon rainfall

Figure 46a,b show the plot of U(t) and U'(t) statistics of SQMKT z- values against time series

for winter and pre-monsoon rainfall of Bhaudare[813], Ghandruk[821], Lumle[814], Pamdur[830], Salyan[829], Dandaswarna[832], Syangja[805]and Waling[826] stations. SQMKT test results showed more than one change point for all stations except Bhaudare[813] station during winter and Dandaswarna[832] station during pre-monsoon. The u(t) statistics shows winter rainfall of the station Ghandruk[821], Lumle[814] after year 1998 and Syangja[805] after 1980 toward decreasing trend slowly whereas remaining all other stations show several change points which were statistically non-significant at 95% confidence limit.

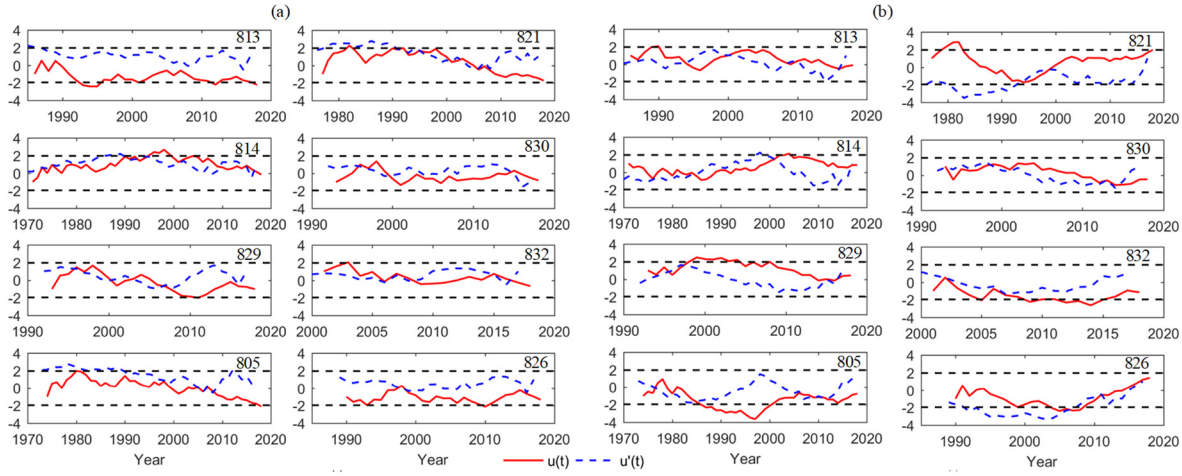

Figure 46. SQMKT z- values against time (a) for winter and (b) pre-monsoon for Bhaudare[813], Ghandruk[821], Lumle[814], Pamdur[830], Salyan[829], Dandaswarna[832], Syangja[805], Waling[826].

The SQMKT test results for monsoon and post-monsoon rainfall for these stations showed more than one change point for all stations except Syangja[805] and Waling[826] stations during post-monsoon (Figure 47a,b). The U(t) statistics shows monsoon rainfall of the station Ghandruk[821] after 1988 toward increasing and Lumle[814] after year 1980 showed increasing trend. In contrast, for monsoon, the station Pamdur[830] showed decreasing trend continuously after 1998. Remaining all other stations show statistically non-significant at 95% confidence limit.

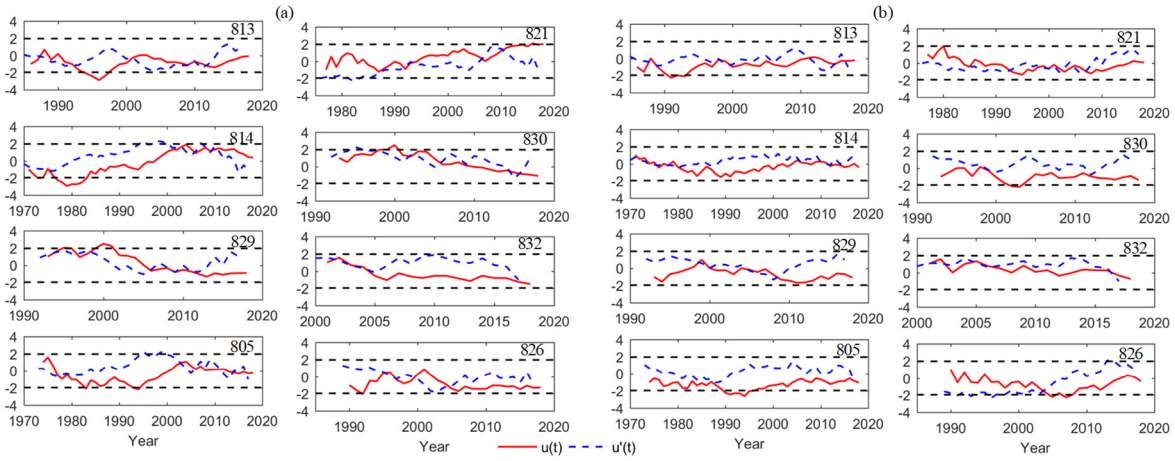

Figure 47. SQMKT z- values against time (a) for monsoon and (b) post-monsoon for Bhaudare[813], Ghandruk[821], Lumle[814], Pamdur[830], Salyan[829], Dandaswarna[832], Syangja[805], Waling[826].

Annual rainfall SQMKT test results for these stations showed more than one change point for all stations except Dandaswarna[832] station (Figure 48). The U(t) statistics shows annual rainfall of the station Lumle[814] after year 1980 toward significantly increasing trend and after 2005 slowly toward significantly decreasing trend whereas station Salyan[829] after 1998 year showed significantly decreasing trend. Remaining all other stations show several change points which were statistically non-significant at 95% confidence limit.

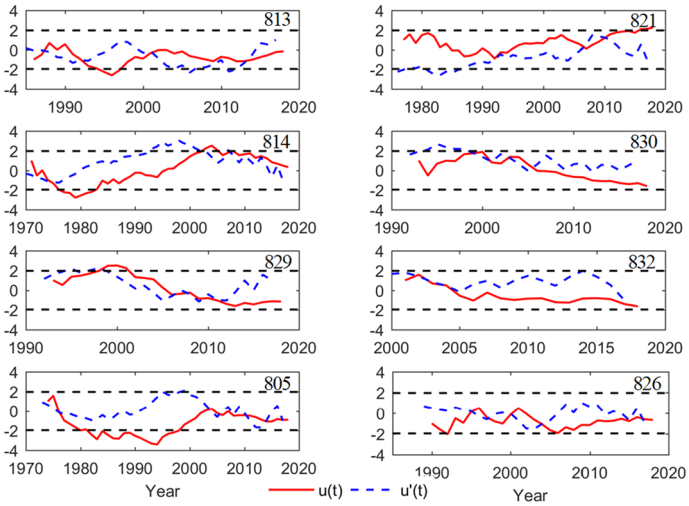

Figure 48. SQMKT z- values against time for annual total monsoon for Bhaudare[813], Ghandruk[821], Lumle[814], Pamdur[830], Salyan[829], Dandaswarna[832], Syangja[805], Waling[826].

Similarly, SQMKT test results for winter and pre-monsoon rainfall for Baglung[605], Benibazar[609], Bagara[629], Ghorepani[619], Gurjakhani[616], Muna[628], Karkineta[613]and Bhobang[615] stations showed more than one change point for all stations except Karkineta[613]and Bhobang[615] stations during winter have no change points (Figure 49a,b). Moreover, stations Baglung[605]and Beni[609] showed one change point whereas Bhagara[629], Ghorepani[619] showed no changing points during pre-monsoon. The U(t) statistics shows winter rainfall of the station Bhagara[629] showed significant positive trend began in the year 2000, whereas stations Ghorepani[619] after year 1992 and Gurjakhani[616] after 1995 toward decreasing trend. In contrast, the pre-monsoon rainfall of stations Beni[609], Ghorepani[619] and Karkineta[613] showed significantly positive trend began from the year 1970, 1985 and 1982 respectively. All other stations show several change points which were statistically non-significant at 95% confidence limit.

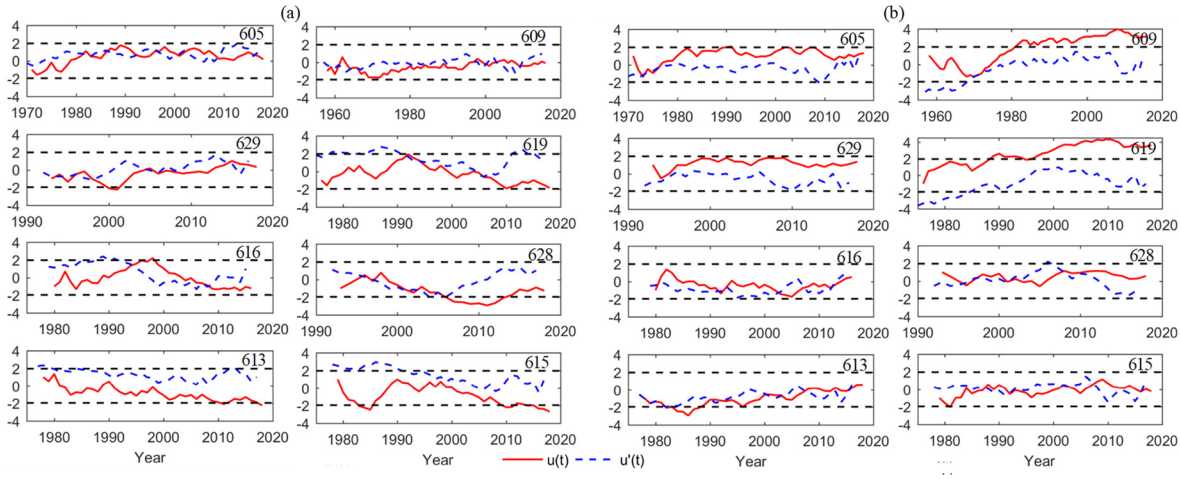

Figure 49. SQMKT z- values against time for (a) winter and (b) pre-monsoon for Baglung[605], Benibazar[609], Bhagara[629], Ghorepani[619], Gurjakhani[616], Muna[628], Karkineta[613], Bhobang[615].

Monsoon and post-monsoon rainfall SQMKT test results for same stations showed more than one change point for all stations except Baglung[605] and Bhobang[615] stations during post-monsoon (Figure 50a,b). The U(t) statistics shows monsoon rainfall of the station Baglung[605] after year 1972 toward increasing trend whereas from year 1998 began slowly decreasing trend at 95% confidence limit.

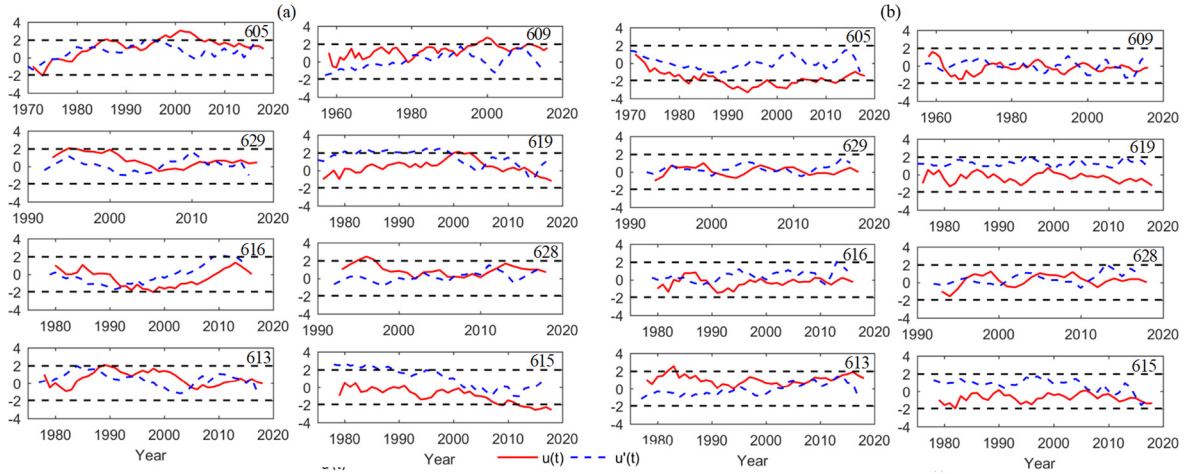

Figure 50. SQMKT z- values against time for (a) monsoon and (b) post-monsoon for Baglung[605], Benibazar[609], Bhagara[629], Ghorepani[619], Gurjakhani[616], Muna[628], Karkineta[613], Bhobang[615].

The annual total rainfall SQMKT test results for same stations show monsoon rainfall of the station Baglung[605] from year 1972 and Beni[609] from year 1960 toward increasing trend at 95% confidence limit (Figure 51).

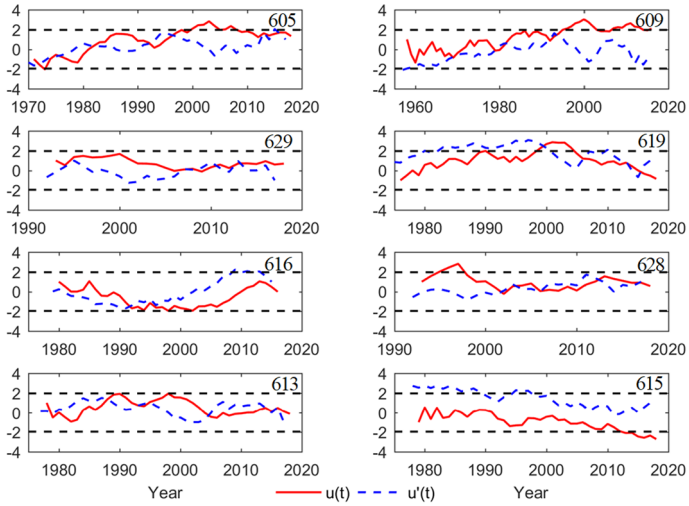

Figure 51. SQMKT z- values against time for annual total monsoon for Baglung605, Benibazar[609], Bhagara[629], Ghorepani[619], Gurjakhani[616], Muna[628], Karkineta[613], Bhobang[615].

In addition, the plot of U(t) and U'(t) statistics of SQMKT z- values against time series for winter and pre-monsoon rainfall for Jhomsom[601], Thakmarpha[604], Tatopani[606] and Bega[626] stations shown in Figure 52a,b. SQMKT test results showed that winter rainfall of Jhomsom[601] and Thakmarpha[604] began increasing trend from 1970 at 95% confidence limit.

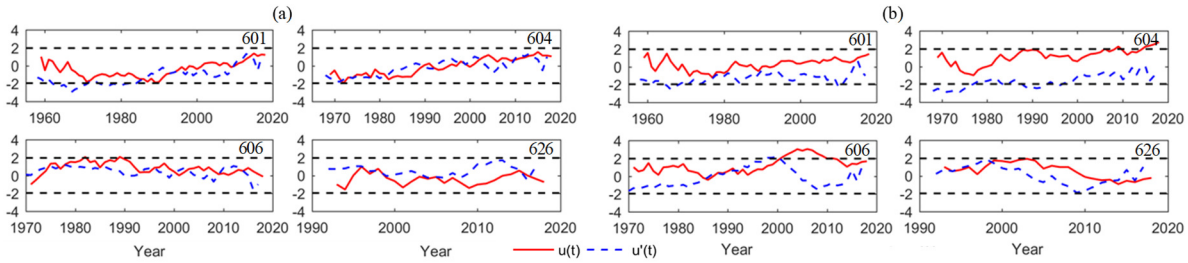

Figure 52. SQMKT z- values against time for (a) winter and (b) pre-monsoon for Jhomsom[601], Thakmarpha[604], Tatopaani[606], Bega[626].

The U(t) statistics shows monsoon rainfall of Bega[626] after year 2000 toward slow decreasing trend (Figure 53a,b).

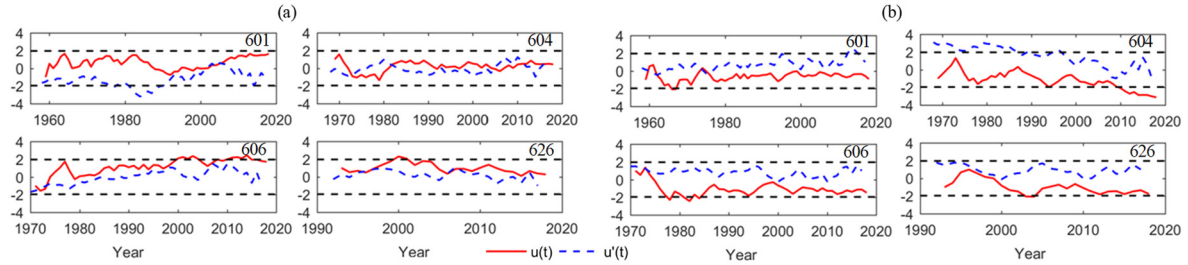

Figure 53. SQMKT z- values against time for (a) monsoon and (b) post-monsoon for Jhomsom[601], Thakmarpha[604], Tatopaani[606], Bega[626].

The annual rainfall U(t) statistics shows annual monsoon rainfall of Tatopani[606] and Bega[626] stations from year 1998 toward increasing and decreasing trend at 95% confidence limit respectively (Figure 54).

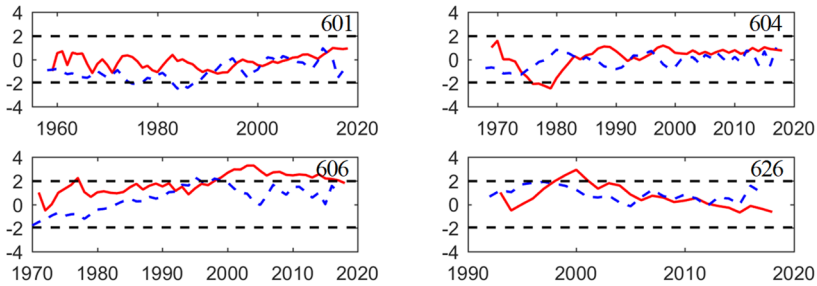

Figure 54. SQMKT z- values against time for annual total monsoon for Jhomsom[601], Thakmarpha[604], Tatopaani[606], Bega[626].

3.4 Rainfall and fluvial discharge comparison

The average daily and monthly rainfall inside KG basin and average daily and monthly fluvial

discharge of KG River are presented in Figure 55a,b. The increase in average daily/monthly fluvial discharge perfectly coincides with the average daily/monthly rainfall of KG basin. The fluvial discharge of KG River increases with the increases in rainfall during monsoonal months.

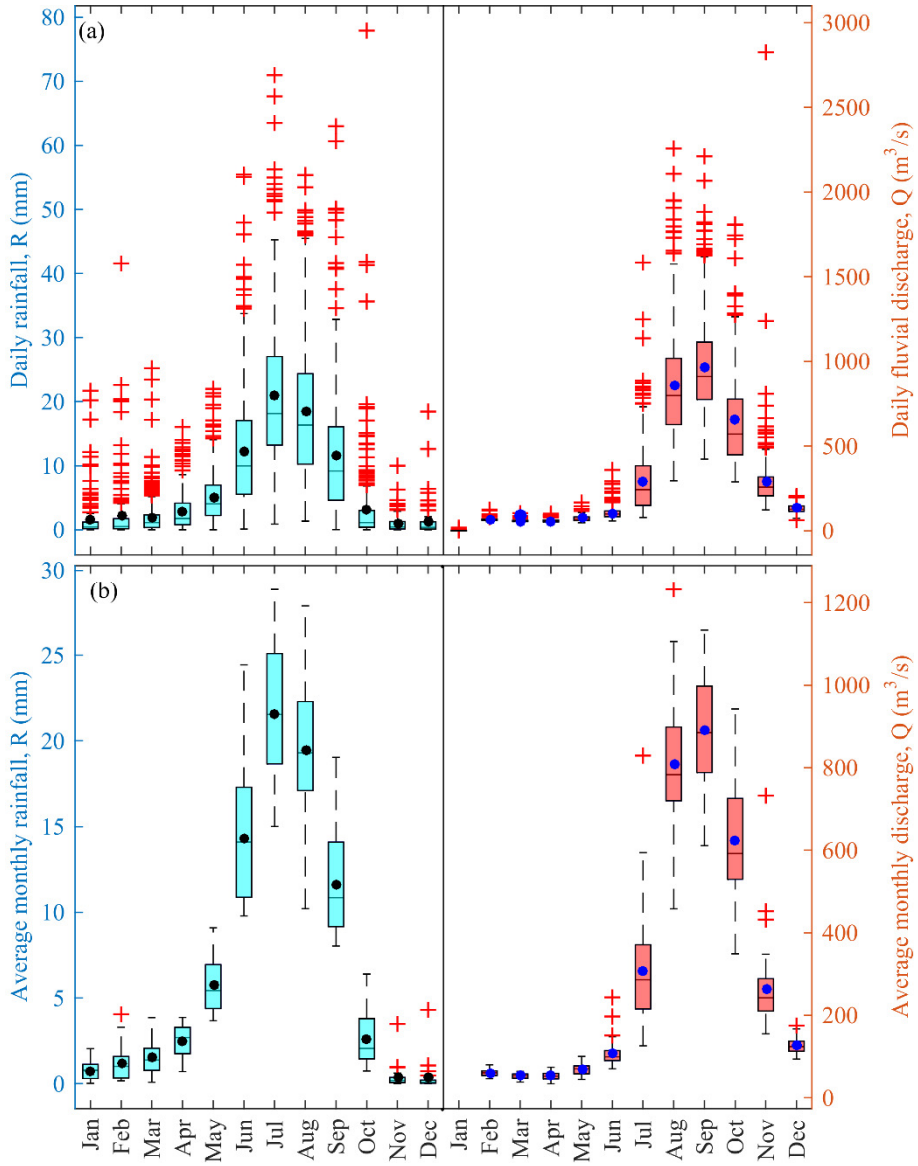

Figure 55. Average (a) daily rainfall and fluvial discharge (b) monthly rainfall and fluvial discharge in KG basin.

Central lines indicate the median and bottom and top edges of the box indicate the 25th and 75th percentiles respectively. The whiskers extend to the most extreme data points not considered outliers, the '+' sign represents outliers (1.5-fold interquartile range), and the circle shows the mean value.

The average monthly rainfalls of June (14.27±3.76 mm), July (21.55±3.64 mm), Aug

(19.47±3.72 mm) and September (11.59±2.82 mm) generated an average of 304.98±125.79, 806.29±162.37, 892.49±138.66 and 625.29±134.66 m^3/s fluvial discharge from the KG basin. A clear anticlockwise hysteresis loop was developed between fluvial discharge (Q) and rainfall (R) of KG River describe the situation where the rainfall variable increases during rising curve of the rainfall (Figure 56a). The higher river discharge during post-monsoon compared with the pre-monsoon for a given rainfall rate. These patterns illustrated that part of the last year's rainfall was temporarily reserved within the catchment. The entire rainfall received in catchment was not transferred directly to the river system during the pre-monsoon and the monsoon seasons, whereas the storage part was drained during the post-monsoon season (Andermann, Bonnet, *et al.*, 2012).

3.5 Rainfall and fluvial discharge hysteresis

The hysteresis effect is performed due to glacier and snow melt runoff in river system during the pre-monsoon and monsoon seasons (Andermann, Bonnet, *et al.*, 2012). In the Himalayas, higher rainfall during the monsoon is responsible for the recharge of basement aquifers, which are refilled during the monsoon and released in the post monsoon, leading to the observed annual hysteresis (Andermann, Bonnet, *et al.*, 2012). The minimum rainfall measured by DHM in rainfall stations is 1 mm. Out of 20 homogenized rainfall stations, number of rainy days events in KG basin during May to September showed 100% consistent in terms of rainfall events occurred inside the basin. The months January to April and October to December showed inconsistent showing number of rainy days were decreasing from January to February, whereas increasing trend in March to April. Similarly, the number of rainy days from October to December also showed in decreasing trend (Figure 56b).

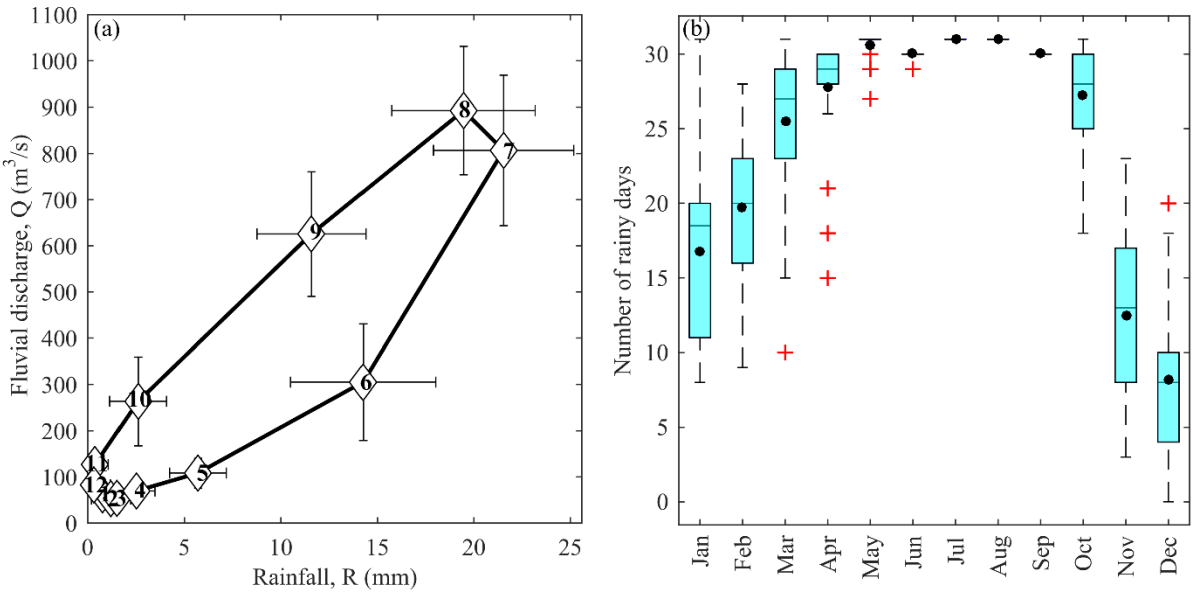

Figure 56. (a) Rainfall and fluvial discharge hysteresis. (b) Number of rainy days during different months.

The white filled diamonds with numbers (1 for January, …….and 12 for December) show the mean monthly values. The error bars represent standard deviation

CHAPTER4.0 GENERAL CONCLUSIONS AND RECOMMENDATIONS

4.1 Conclusion

In this study, the rainfall trends over KG basin, Himalayas from 1957-2018 were examined using Mann- Kendall trend test with Sen's slope estimator, showed that the station Ghandruk (Elv. 1960 m MSL) performed highest increasing trend (+25.5 mm/year) whereas station Pamdur (Elv.1160 m MSL) performed highest decreasing trend (−30.0 mm/year). In addition, sequential Mann- Kendall trend test detected the approximate year of the beginning of the significant trends inside the KG catchment. The fluvial discharge of KG River increases with the increases in rainfall during monsoonal months. A clear anticlockwise hysteresis loop was developed between fluvial discharge (Q) and rainfall (R) of KG River describe the situation where the rainfall variable increases during rising curve of the rainfall. The higher river discharge during post-monsoon compared with the pre-monsoon for a given rainfall rate illustrated that part of the last year's rainfall was temporarily reserved within the catchment. The entire rainfall received in catchment was not transferred directly to the river system during the pre-monsoon and the monsoon seasons, whereas the storage part was drained during the post-monsoon season. The hysteresis effect is performed due to glacier and snow melt runoff in river system during the pre-monsoon and monsoon seasons. In the Himalayas, higher rainfall during the monsoon is responsible for the recharge of basement aquifers, which are refilled during the monsoon and released in the post monsoon, leading to the observed annual hysteresis.

4.2 Application of study

This study will help to picturize the rainfall trends in Himalayas, which could be useful for hydropower reservoir management.

4.3 Recommendations

Rainfall variation within snow fall area is very low compared to rainfall

dominated hilly region. It is recommended to study the major local rainfall event responsible for sediment yield.

PART IV- MECHANISM OF RIPARIAN VEGETATION GROWTH AND SEDIMENT TRANSPORT INTERACTION IN FLOODPLAIN

ABSTRACT

The ecological dynamics of riparian area interact with sediment transport in river system, which plays an active role in riparian vegetation growth in the floodplain. The fluvial dynamics, hydraulics, hydro- meteorological and geomorphological characteristics of river are associated to sediment transport in river system and around the riparian area. The flood disturbance, sediment with nutrients and seeds transported by river, deposition and erosion phenomena which frequently occurred in the floodplain, changed the bare land area to vegetation area and vice versa. The difference in vegetation is caused by the difference in the sediment supply into the river channel and sediment particle size distribution with the sediment deposition along the river channel, which inhibits the recovery of vegetation afterwards in the river floodplain. Mathematical models describing vegetation growth in short period available in literature, but long-term modelling and validations are still lacking. In order to cover long-term vegetation growth modelling, a Dynamic Riparian Vegetation Model (DRIPVEM) was proposed. This paper highlights the existing modelling technique of DRIPVEM coupled with Dynamic Herbaceous Model used to establish the interactive relationship of sediment grain sizes and riparian vegetation in the floodplain.

CHAPTER 1. GENERAL INTRODUCTION AND LITERATURE REVIEW

1.1 Research background

Riparian vegetation plays a significant role in the ecological balance of a riparian area (Fu *et al.*, 2016). Riparian area is a transitional semiterrestrial area extended from the edges of water bodies to the edges of upland communities and regularly interacted with river water, flow alterations, sediment and nutrients (Camporeale & Ridolfi, 2006; Asaeda & Sanjaya, 2017; Zhao *et al.*, 2019). Flood disturbance is one of the major cause of vegetation mortality in the riparian zone either by inundation or bank erosion (Asaeda *et al.*, 2011; Asaeda *et al.*, 2019; Asaeda, Fujino, *et al.*, 2005). The morphological alterations in riparian area caused by a flood event either supports or suppresses the riparian vegetation, which depends also on the sediment grain sizes deposited on original sediment surface or exposed of previous underlying sediment surface (Asaeda & Rashid, 2014). The flood hydrology affects the hydrochory in the riparian area during flood time, recruit the seeds and begins colonization of trees (Asaeda *et al.*, 2015). Water is one of the major principal seed dispersal agent in the floodplain (Biology, 2019). The number of seeds floating during flood event, magnitude of flood, duration and frequency of flood occurrence determine the seeds recruitment phenomenon in the riparian area (Lytle & Poff, 2004; Boedeltje *et al.*, 2004; Vogt *et al.*, 2004). The area of vegetation coverage in the riparian zone is directly dependent on the availability of water, nutrients available in water and sediment before and after flood event and exchange of nutrients from atmosphere to the floodplain (Asaeda & Rashid, 2014).

Phragmites australis, *Typha spp.* and *Phragmites japonica* are perennial plants on riparian zone in Japanese River floodplains, have an extremely high ability to expand their territory by extending stolons (Asaeda *et al.*, 2008). The floods provide the habitat with nutrient rich water and sediment in the inundated bar. Sandy sediment sites are preferable for the growth of herbaceous plants, as moisture and nutrients in the coarse sediment layers are very limited

(Lippert *et al.*, 1999; Moriuchi & Winn, 2005; Asaeda *et al.*, 2009).

The flood controlling structures such as dam and weir control the natural flood dramatically (Asaeda *et al.*, 2011; Asaeda, Rashid, *et al.*, 2011) so that the bed shear stress, specific power and flow velocity of downstream reaches were reduced (Brandt, 2000). The low interacting flood events in the downstream area also curtail the sediment transport except wash load and make river channel more stable (Nallaperuma & Asaeda, 2019). This phenomenon gradually coarsens the downstream active riparian zone. From the sustainable reservoir management perspective, the intermittently artificial release of sediment with high nutrients deposited in reservoir through dams has been practiced in Japanese Rivers (Sumi & Kantoush, 2010), increased the depth of fine sediment in the floodplain, which also alters the inundation pattern and sediment grain sizes in the riparian zone (Asaeda & Rashid, 2012; Mueller *et al.*, 2017; Stähly *et al.*, 2019). The released fine sediments interlocked the coarsen sediment of the bar after sedimentation in the bar, supporting the vegetation encroachment.

The sediment yield from a catchment depends on numerous parameters including topography, gradient of river, rainfall in catchment, temperature and soil type of catchment area (Baniya *et al.*, 2019; Gudino-Elizondo *et al.*, 2019). Fluvial dynamics, hydraulics, hydro- meteorological and geomorphological conditions of river determine the transport of sediment from its origin (Mao *et al.*, 2009). The flood events with its magnitude, duration and frequency are associated with sediment transport (Soler *et al.*, 2007). The morphological characteristics of riparian zone was altered by flooding, which triggers erosion or deposition in the floodplain (Asaeda, Gomes, *et al.*, 2011). The floods have influenced on recruitment as well as vegetation colonization.

The interactive parameters for riparian vegetation growth in floodplain are illustrated Figure 57.

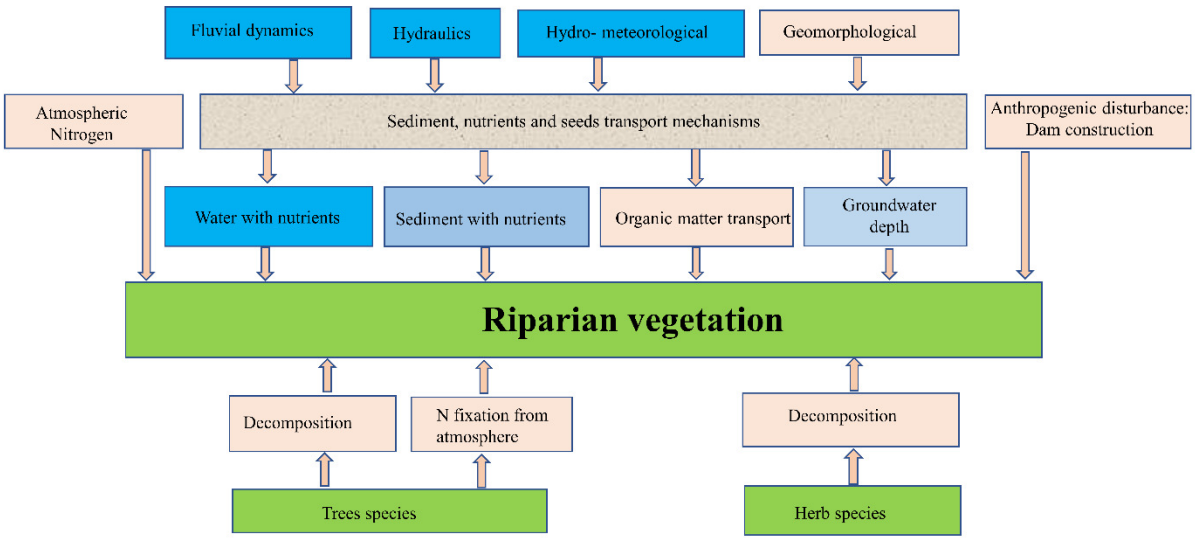

Figure 57. Interactive parameters for riparian vegetation growth in a floodplain

The intermittent floods encountered in floodplain alter morphology of riparian zone and the vegetation coverage change by erosion or deposition of sediment (Gurnell & Petts, 2006). The nutrients interchange from atmosphere, human disturbance, flooding play a role for riparian vegetation growth (Naiman *et al.*, 2000). Primarily, vegetation succession in floodplain starts from growth of herbaceous plants, which when senescence after completing their life cycle, decomposed in the form of nutrients to the floodplain. The supportive role of increasing nutrients by primary succession of herbaceous plants create favorable environment for tree recruitment in the floodplain. The decomposition of defoliated leaves of trees and above ground biomass (AGB) and below ground biomass (BGB) of herbaceous plants also increased the nutrients level of riparian zone. The absence of large floods due to artificial interventions such as dam, weir and spurs compelled vegetation colonization in the floodplain, which vanishes natural stony surface resulting a forest community.

The alterations of river hydrology and morphology after dam intervention, changes of sediment grain sizes with nutrients transport into riparian zone make the floodplain fertile. There are numerous interactive parameters responsible for changing bare land area to vegetation area. Numerical simulation describing riparian vegetation growth for long period and validations are

still limited in the literatures (Nones & Di Silvio, 2016; Perona *et al.*, 2009; Davies‐Colley *et al.*, 2009; Rivaes *et al.*, 2013; García‐Arias *et al.*, 2013). It is difficult to address all these interacting parameters within a single mathematical model. It is important to conduct this study in floodplain to know the excessive vegetation drivers and to predict the changes in long-term riparian vegetation coverage area. The objectives of this study are to link the interacting parameters relationships with vegetation growth in the mathematical model, to elucidate the mechanisms behind riparian vegetation growth dynamics in perspective of long-term vegetation growth modelling of riparian area. This study highlights the existing modelling technique of DRIPVEM (Asaeda & Rashid, 2014; Asaeda *et al.*, 2015; Sanjaya & Asaeda, 2017) coupled with Dynamic Herbaceous Model used to establish the interactive relationship of sediment grain size and riparian vegetation in the floodplain.

1.2 Research objectives

The following are the research objectives of this study (Part-IV).

1. To understand the excessive vegetation drivers and to predict the changes in long-term riparian vegetation coverage area.
2. To link up the interacting parameters relationships with vegetation growth in the mathematical model.
3. To elucidate effects of sediment particle size on the mechanisms behind riparian vegetation growth dynamics in perspective of long-term vegetation growth modelling of riparian area.

CHAPTER 2.0 MATERIALS AND METHODS

2.1 Study Site Description

(a) Case study I: Narayani River, Nepal

The downstream KG River from dam also passes through the deep canyon through Himalayas which meets with Trisuli River at about 185 km downstream from KG hydropower dam. After confluence point, the river named as Narayani River, opens to plain area having mild gradient. The degradation characteristics of river decreases, and transported sediment deposited on the floodplain. The floodplain about 1500 m× 570 m is located about 12 km downstream from the confluence point as shown in Figure 58.

Figure 58. Location map of floodplain located downstream of confluence of KG and Trisuli Rivers

(b) Case study II: Kuzuryu River, Japan

The Kuzuryu River flows through Fukui Prefecture, Japan and merges in to the sea of Japan (Figure 59a,b). The length of this river is about 116 Km. Several dams alter the river continuity. The floodplain is located about 24 km from the river mouth and 56 km downstream from the Kuzuryu River dam. The river basin has catchment area of 2930 km^2. The average annual discharge of the selected study reach is about 86 m^3/s and the average annual rainfall is about 2200 mm. The historical data sourced from Ministry of Land, Infrastructure, Transport and Tourism (MLIT), Japan recorded the maximum flood height was 7.54 m in October, 2004 and corresponding discharge was 3221 m^3/s (http://www1.river.go.jp/) in Kuzuryu River study reach. The floodplain (36°06'23" N, 136°16'06" E) is about 2370 m long and 542 m width

(Figure 59a-b). The gradient of the study reach is 0.3 %.

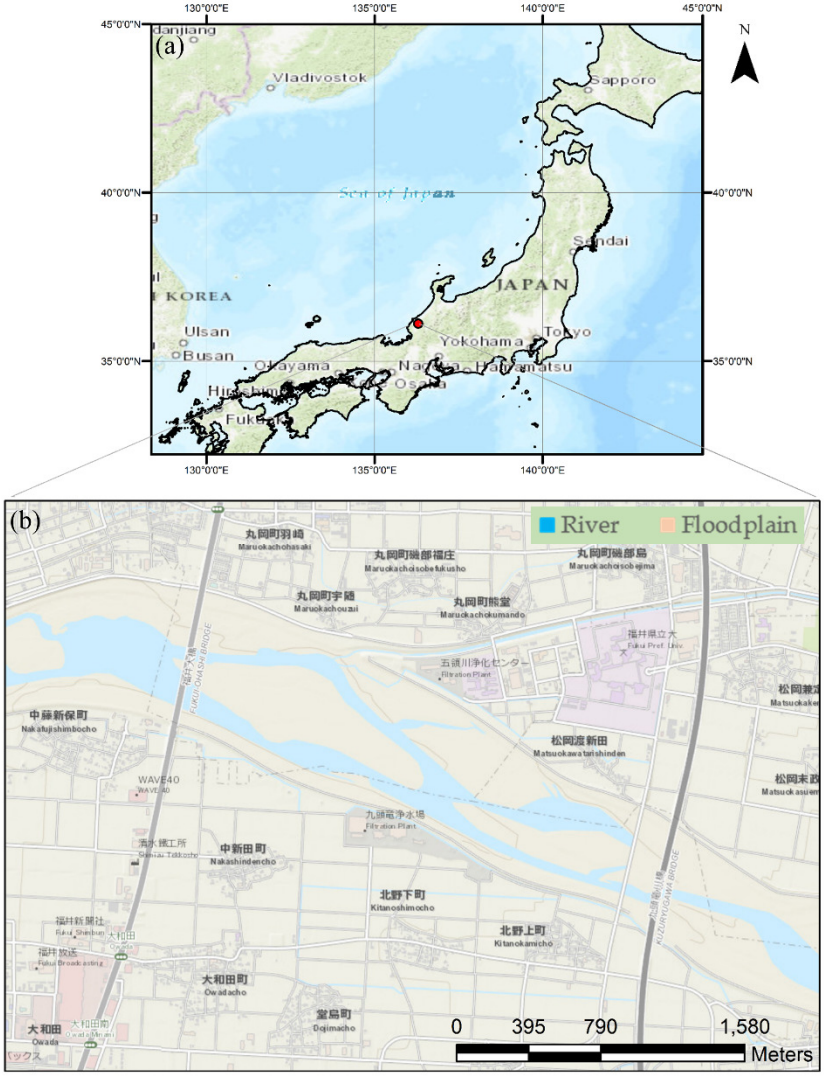

Figure 59. Location map of Kuzuryu River (a) Study reach (b) Magnified view of study reach

The main physiographic characteristics of the Kuzuryu River study reach is presented in Table 18.

Table 18. Main physiographic characteristics of study river reach.

Parameters	Descriptions
Floodplain size	2370 m × 542 m
Mean gradient of river	0.3%
Extreme Flood level from normal water level (0.000 m elevation)	7.54 m in Oct 2004; 6.24m in Oct 2002; 6.9 m and 6.82m in Sep 1998 and 1989
Extreme Flood Discharge	3221 m^3/s in Oct 2004; 2400 m^3/s in Oct 2002; 2517 m^3/s and 2144 m^3/s in Sep 1998 and 1989
Ground Elevation ranges from normal water level (0.000 m elevation)	0.102 m – 7.334 m
Precipitation	~ 2200 mm/yr

2.2 Model development

The modelling approach is a technique frequently adopted to predict the vegetation dynamics in the riparian area which is best tool for long term management perspective of riparian area. The alterations observed in riparian trees by hydro morphological alterations and climate changes provided researchers with evidence to be used for developing numerical models (Vargas‐Luna *et al.*, 2015; Nepf & Ghisalberti, 2008). Different mathematical and process-based approaches were used to express vegetative succession in riparian area (Sekine *et al.*, 2012; Benjankar *et al.*, 2011; García‐Arias & Francés, 2016) and for growth and yield simulator, planning, decision making and efficient forest management (Salminen *et al.*, 2005; Mendoza & Vanclay, 2008; Pretzsch *et al.*, 2002). However, coupling of all the interacting parameters with riparian vegetation growth once at a time within a single mathematical model is tedious task.

Most of the parameters associated in riparian vegetation growth mechanism were clearly compiled in mathematical models for spatial distribution of herbs and trees in DRIPVEM by Asaeda (Asaeda & Rashid, 2014; Asaeda *et al.*, 2015). The growth of herbaceous plants for monospecific stand in riparian zone was described in Dynamic Herbaceous Model (Asaeda & Karunaratne, 2000). The DRIPVEM coupled with a Dynamic Herbaceous Model was used to describe vegetation dynamics in the riparian zone.

2.2.1 Dynamic Herbaceous Model for monospecific stand

The herbaceous plants *P. australis*, *Typha* and *P. japonica* are some of the dominant herbaceous perennial plants in riverine wetlands. These plants can grow on sandy and stony habitats on the floodplains. Particle grain size of floodplain plays an important role in the growth of these plants. Dynamic Herbaceous Models were developed to simulate the growth dynamics of a monospecific stand of *P. australis*, *Typha spp.* and *P. japonica* in freshwater ecosystems. The mathematical models were formulated by Asaeda (Asaeda & Karunaratne, 2000) and the results

were validated in Czech Republic, Australia and Japan (Asaeda & Karunaratne, 2000), U.S.A. (Asaeda, Hai, *et al.*, 2005), Egypt (Eid *et al.*, 2012) and Japan (Asaeda *et al.*, 2011).

In this Dynamic Herbaceous Model, meteorological data such as daily temperature and daily solar radiation are the input parameters (Figure 60). In case of lacking meteorological data, latitude of the study site is considered as input for calculating the temperatures and solar radiation.

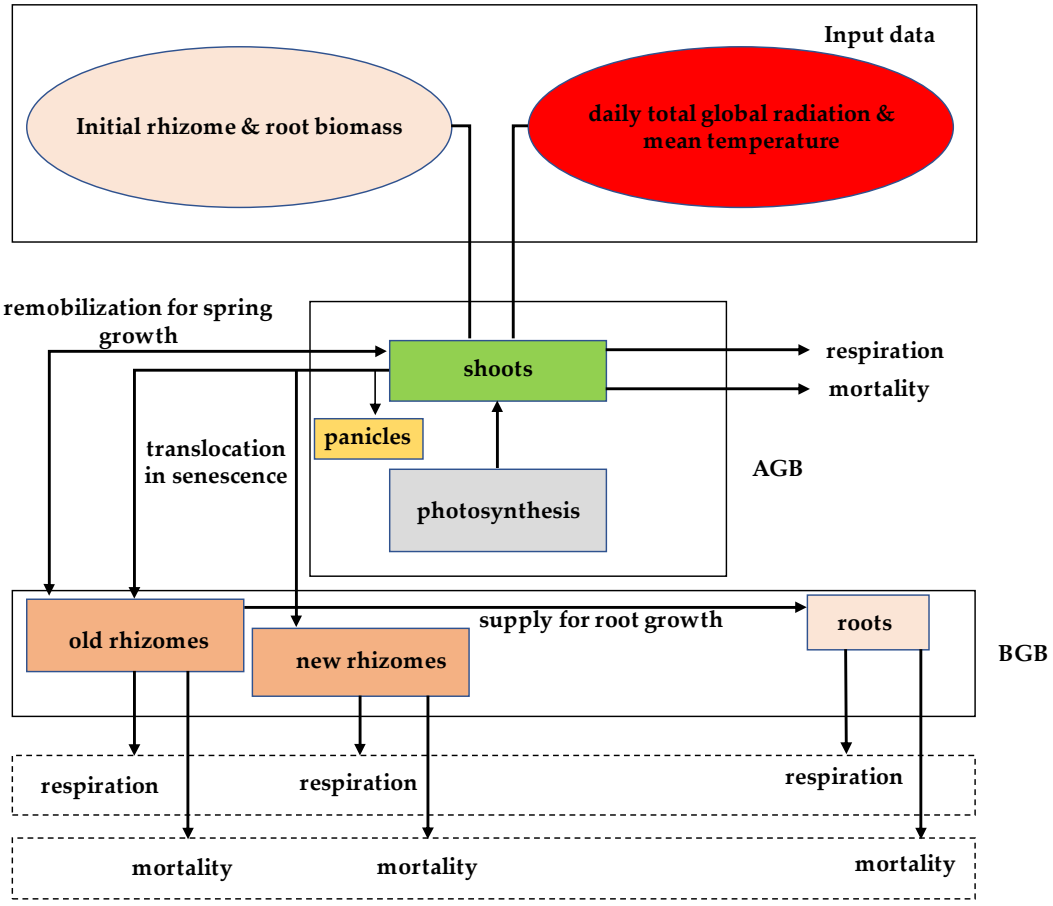

Figure 60. Schematic structure of Dynamic Herbaceous Model

The model consists of five different equations for shoots, inflorescence, roots, old rhizomes and new rhizomes (Asaeda *et al.*, 2011; Asaeda & Karunaratne, 2000). The initial rhizome and root biomass are also given as input variables for initiation of growth. The net growth of the whole plant is the combined effect of photosynthesis, respiration, mortality and transfer of assimilated materials.

The growth of *P. japonica* is based on the model developed by Asaeda and Karunaratne (2000) and Asaeda et al. (2005) for growth of *P. australis* and *Typha spp.*, respectively. The modal consists of five different equations of shoots, inflorescence, roots, old rhizomes and new rhizomes. The initial rhizome and root biomass, daily total global irradiance and daily mean air temperature are given as input data

The net growth of the whole plant is the combined effect of photosynthesis, respiration and mortality during life cycle of plant. Each organ of plant is associated to respiration and mortality, and the translocation from and to other organs. Shoots undertake photosynthesis, too. Then, five different material budget equations (IV.1) to (IV.5) were formulated for each plant organ following these processes. Shoot was stratified into 1 cm-thick horizontal layers, for which the photosynthesis rate was calculated separately corresponding to the light intensity at each height. Each growth equation was solved simultaneously for each layer using the Fourth order Runge–Kutta method with a daily time step.

The output of the modal are daily growth of total shoots, inflorescence, roots, old rhizomes and new rhizomes.

$$\frac{\partial B_{rhi}}{\partial t} = -R_{rhi} - D_{rhi} - Rhif \times f_{rhi} + y \sum_{i=1}^{i=i\max} \varepsilon_{sht} b_{sht}(i) f_{sht} + y \sum_{i=1}^{i=i\max} \varepsilon_{ph} Ph_{sht}(i) f_{ph} \quad \text{(IV.1)}$$

$$\frac{\partial B_{rt}}{\partial t} = G_{rt} f_{rt} - R_{rt} - D_{rt} + xRhif \times f_{rhi} \quad \text{(IV.2)}$$

$$\frac{\partial B_{n}}{\partial t} = -R_{n} - D_{n} + (1-y) \sum_{i=1}^{i=i\max} \varepsilon_{sht} b_{sht}(i) f_{sht} + (1-y) \sum_{i=1}^{i=i\max} \varepsilon_{ph} Ph_{sht}(i) f_{ph} \quad \text{(IV.3)}$$

$$\frac{\partial b_{sht}(i)}{\partial t} = Ph_{sht}(i) - R_{sht}(i) - D_{sht}(i) + (1-x) Rhif \times f_{rhi}\left(\frac{b_{sht}(i)}{B_{sht}}\right) - \varepsilon_{sht} b_{sht}(i) f_{sht} - \varepsilon_{ph} Ph_{sht}(i) f_{ph} - (b_{sht}(i)\varepsilon_{p} - Ph_{sht}(i)k)\, ff - G_{rt} f_{rt}\left(\frac{b_{sht}(i)}{B_{sht}}\right) \quad \text{(IV.4)}$$

$$\frac{\partial B_{p}}{\partial t} = -R_{p}(i) - D_{p}(i) + \sum_{i=1}^{i=i\max} Ph_{sht}(i)k \times ff + \sum_{i=1}^{i=i\max} \varepsilon_{p} b_{sht}(i)\, ff \quad \text{(IV.5)}$$

where B (g/m^2/day) and b (g/m^2/day/1 cm height) are the total and layer wise biomass, respectively and subscripts, *rhi, rt, n, sht,* and *p* indicates rhizomes, roots, newly-formed rhizomes during the year, shoots, and panicles, respectively; f_{rhi} =1when $t_b \le t \le t_e$, otherwise 0; f_{sht}=1 when t_s<t, otherwise 0; f_{ph}=1 when $t_p \le t \le t_e$, otherwise 0; ε_{sht} and ε_{ph} are the fractions reallocated from the shoots and current photosynthesis to the below ground plant organs, respectively, are the functions of habitat particle size and related as followed equations.

$$\varepsilon_{sht} = 0.002 \times (D_{50})^{0.2655} \quad (R^2=0.96) \tag{IV.6}$$

$$\varepsilon_{ph} = 0.2878 \times (D_{50})^{0.0738} \quad (R^2=0.97) \tag{IV.7}$$

The fraction y of ε_{sht} and ε_{ph} was allocated to the old rhizomes and the rest to the new rhizomes; f_{rt} = 1 when $t_r \le t \le t_p$otherwise 0; *(i)* represents the quantity in the i^{th} layer; *ff*=1 when $t_f \le t$ otherwise 0; t_b: the commencement of growth; t_r : the formation of new roots; t_e : the ending of mobilization from rhizomes to shoots and roots; t_p : the commencement of translocation of current photosynthesized material to below-ground plant organs; t_f : the appearance of panicles; t_s : commencement of shoot senescence; *imax* is the maximum number of layers in the plant stand; k and ε_p are the fractions of contribution of the current photosynthesis and accumulated shoot dry matter to the formation of panicles; R_{hif} is the mobilization of stored material from rhizome to roots and shoots during the initial stage of growth; x is the fraction of R_{hif} allocated for root growth and the rest for shoots. The amount of material mobilized from the rhizomes was taken to be proportional to its biomass and daily mean temperature.

The photosynthesis rate of shoots is given by

$$P_{sht}(i) = P_m K_{co} \theta^{(T-20)} \frac{I_{PAR}(i)}{K_{PAR}+I_{PAR}(i)} \times \frac{K_{age}}{(K_{age}+Age_{sht})} b_{sht}(i) \tag{IV.8}$$

where P_m , maximum photosynthesis rate is a decreasing function of particle size as

$$P_m = 0.2702 \times (D_{50})^{-0.0684} \quad (R^2=0.96) \tag{IV.9}$$

where K_{co} is the conversion constant of carbon dioxide to ash free dry weight, I_{PAR} is photosynthetically active radiation in the i^{th} layer, K_{PAR} and K_{age} are the half saturation coefficients of photosynthetically active radiation (PAR) and age, respectively.

$$Rhif = \alpha_{rhi}\theta^{(T-20)}B_{rhi} \quad \text{(IV.10)}$$

where α_{rhi} is a coefficient of translocation of rhizome and is given as $\alpha_{rhi}=\alpha_{soil}\times(\text{initial rhizome})^{-0.50}$ (Asaeda et al 2000) where α_{soil} is the soil coefficient and depends on the habitat particle size. This was related with sediment particle size as

$$\alpha_{soil}=0.4971\times(D_{50})^{-0.0789} \ (R^2=0.99) \quad \text{(IV.11)}$$

where R and D are the respiration and mortality (g/m^2 per day), respectively, which are proportional to their biomasses (Hootsmans, 1994) and the mean daily temperature, such as $R_a = \beta_a\theta^{(T-20)}B_a$, $D_a = \gamma_a\theta^{(T-20)}B_a$, where γ_a and β_a are the specific rates of mortality and respiration at 20°C; θ is the Arrhenius constant; T is the daily averaged temperature; subscript a represents old rhizome, new rhizome, root, panicle or shoot.

The supply of photosynthesized material for root growth (G_{rt}) is given by

$$G_{rt} = g_m\theta^{(T-20)}\frac{K_{rt}}{K_{rt}+Age_{rt}}B_{rt} \quad \text{(IV.12)}$$

where g_m shows the allocation to roots as a function of sediment particle size as

$$g_m= 0.0414\times(D_{50})^{0.4318} \ (R^2=0.82) \quad \text{(IV.13)}$$

where K_{rt} is the half saturation coefficient of root age as a function of sediment particle size as

$$K_{rt} =72.784\times(D_{50})^{0.0898} \ (R^2=0.98) \quad \text{(IV.14)}$$

Where Age_{rt} is the age of roots in days from the start of root growth. The total shoot biomass is given by the sum of the shoot biomass in each layer.

$$B_{sht} = \sum_{i=1}^{imax}(b_{sht}(i) \quad \text{(IV.15)}$$

The net production of herbaceous plant is calculated by using Equation (IV.16).

$$\text{Net production} = \frac{dB_T}{dt} = \sum_{\text{i=layer}} Ph(i) - \sum_{\text{organ}}(Respiration) - \sum_{\text{organ}}(Mortality) \pm \sum_{\text{organ}}(Translocation) \quad \text{(IV.16)}$$

Where $\sum_{\text{i=layer}} Ph(i)$ is sum of layer by layer photosynthesis performed by leaves of herbaceous plant, $\sum_{\text{organ}}(Respiration)$ is total loss of biomass due to respiration, $\sum_{\text{organ}}(Mortality)$ is total

loss of biomass due to dead of plants organ such as shoots, inflorescence, roots, old rhizomes and new rhizomes of herbaceous plants. $\sum_{organ}(Translocation)$ is transfer of assimilated materials. + sign indicates the upward transfer of assimilated materials from BGB to AGB and – sign indicates the downward transfer from AGB to BGB.

2.2.2 DRIPVEM coupled with Dynamic Herbaceous Model

For long-term modelling perspective and incorporation of numerous interacting parameters with riparian vegetation succession subjected to both herbaceous plants and trees, Asaeda (Asaeda & Rashid, 2014; Asaeda *et al.*, 2015) developed a dynamic model which can predict the vegetation succession and interaction with floods, riparian morphology, nutrients, sediment size etc.

Figure 61 shows the schematic diagram of DRIPVEM coupled with Dynamic Herbaceous Model. The DRIPVEM consists of HYDRO, TREE, HERB and NUTRIENTS modules with their interactive roles (Asaeda & Rashid, 2014; Asaeda *et al.*, 2015). The HYDRO module is used to link up flood hydrology to TREE and HERB modules which occurred in floodplain. The flushing effects of flood is also considered in the model. The TREE module calculates the spatial tree distribution in the floodplain by considering initial colonization after flooding. The sediment particle sizes are connected to determine the initial tree recruitment and also linked to determine the herbs biomass. The allometric relations with diameter at breast height (DBH) and age were also included in the model to predict the biomass growth of tree species such as *Salix gilgiana*, *Robinia pseudoacacia* and *Albizia julibrissin* (Asaeda & Rashid, 2014; Asaeda *et al.*, 2015; Asaeda *et al.*, 2010). The HERB module calculates the herbaceous plants biomass with its spatial distribution in the floodplain in which particle size, shading effects of tree canopy as well as the nutrient interactions and effects of floods are incorporated in the model. The NUTRIENTS module depicts the soil nutrients budget by interacting atmospheric nitrogen, flood nitrogen, nitrogen release after decomposition of litter biomass and N- fixation process

of rhizobium bacteria with soil in floodplain. Important equations employed in the herb biomass are summarized in the Table 19. The outputs of DRIPVEM were validated for Japanese steep rivers (Sanjaya & Asaeda, 2017).

Table 19. Some important equations employed in the herb biomass calculation

Factor	**Herbs**
TN effect (gDW/m^2)	AGB_G=AGB_{max}×($TN^{2.5}$/(0.04$^{2.5}$+$TN^{2.5}$))
Particle size D_{50} (gDW/m^2)	AGB_G=AGB_{max}×(2.5^3/(2.5^3+(2+log(D_{50}))^3)
Sky view factor	SVF= 1-2×C_d
Shading effect	AGB_G= AGB_G × ($SVF^{0.6}$)

The allometric relationship used to calculate biomass of trees are summarized in the Table 20.

Table 20. Allometric relationships and conditions employed for trees

	Salix spp.	*Robinia* sp.
Initial sprout density (Nos./m^2)	30	0.3
Effective floods	May	August-September
Canopy coverage, *Canopy D*	*Canopy D* = Trees $_{isp}$ ×(*Leaf* /π (*Cap*/2)^2)	
Self-thinning rate	Trees $_{sal}$ = Trees $_{age=0}$ / AGE^2	Trees$_{rob}$ = Trees $_{age=0}$× (8^4/ 8^4+AGE^4)
Diameter of breadth height, *DBH* (cm), Tree age *AGE* (year)	DBH = 0.278$AGE^{1.96}$	DBH = 0.169$AGE^{2.04}$
Tree height, *H* (cm)	H = 22.9 $AGE^{1.99}$	H = 118.7 $AGE^{0.701}$
Canopy diameter, *Cap* (cm)	Cap = 122$DBH^{0.416}$	Cap = 94.6 $DBH^{0.638}$
Aboveground biomass, *AGB* (except leaves) (kgDw)	AGB = 0.08$DBH^{2.27}$	AGB = 0.08$DBH^{2.27}$
Belowground biomass, *BGB* (kgDw)	BGB = 0.11$DBH^{1.79}$	BGB = 0.11$DBH^{1.79}$
Leaf biomass, *Leaf* (kgDW)	$Leaf$ = 0.0147$DBH^{2.13}$	$Leaf$ = 0.0147$DBH^{2.13}$

In HERB module of DRIPVEM, the maximum herb biomass is one of the input parameters. In the absence of observed data of maximum herb biomass in floodplain, Dynamic Herbaceous Model is used to calculate the maximum herbs biomass in the floodplain. The output value of maximum biomass simulated by Dynamic Herbaceous Model transfers to HERB MODULE which is one input parameter of DRIPVEM. This is a new technique to couple DRIPVEM model with Dynamic Herbaceous Model to describe the vegetation growth in riparian zone (Figure 61).

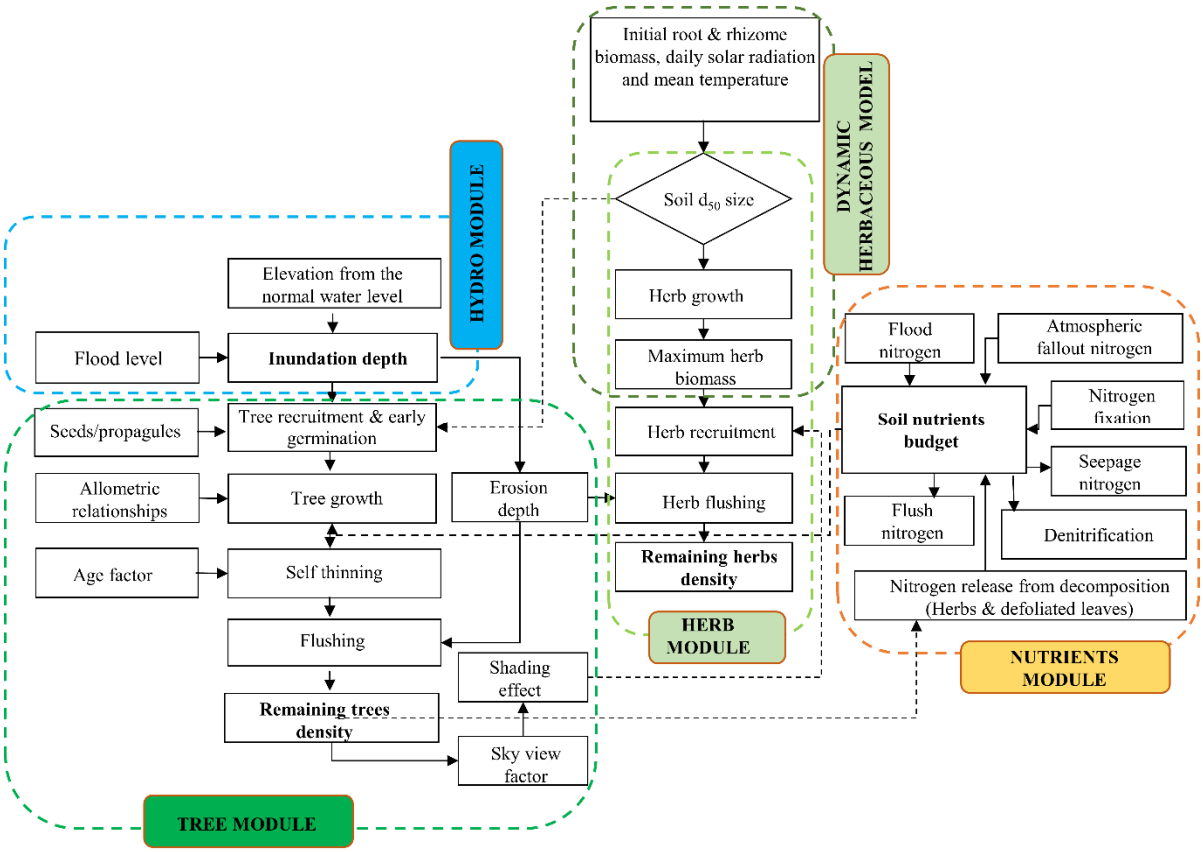

Figure 61. Schematic structure of Dynamic Riparian Vegetation Model (DRIPVEM) coupled with Dynamic Herbaceous Model.

P. japonica, a pioneering perennial species on floodplains in East Asia, has an extremely high ability to expand its territory by extending stolons for more than 10 m in a year with its high plasticity. Although floods provide the habitat with nutrient rich water, the soil of flood plain is still unsuitable for *P. japonica*, as moisture and nutrients in the coarse sediment layer are very limited. Little moisture retained in the coarse sediment apparently restricts the growth of *P. japonica*, as the uptake of the same and nutrients is highly limited. Moisture content in fine sediment is higher than in coarse sediment as water vapour transfer is far smaller for fine beds compared with coarse beds. Therefore, sandy sediment sites are preferable for the growth of *P. japonica*, compared with stony sites. Total biomass difference was more than twice between fine and coarse sediment sites.

As indicated by the dynamic model of plants, the net growth of the plant stand is the integral

effect of photosynthesis, respiration, mortality and translocation of assimilated materials between shoots and belowground organs. Therefore, the change in biomass is highly affected by the balance of the biomass partitioning, in addition to photosynthesis and respiration and mortality losses. In the case of perennial plants, the translocation between the aboveground and belowground biomass differentiates their morphology depending on their plasticity. The shortage of moisture and nutrients restricts at coarse sediment sites the growth of plants, while the belowground organs grow more for higher access to water and nutrients. The allocation of biomass to the belowground organs, however, does not contribute to the photosynthesis production, thus the total biomass becomes lower than the case of fine sediment sites. In the model, effects of plasticity were successfully described by changing values of translocation coefficients.

CHAPTER 3.0 RESULTS

3.1 Case study (Nepal)

3.1.1 Historical evidence of growth of herbs and trees in floodplain

Figure 62a-d show the historical aerial images in chronological sequence of development of vegetation growth in Narayani River floodplain from 2004 to 2020. The sediment deposition area decreased and riparian vegetation area increased year by year. The noticeable riparian vegetation coverage established after 16 years interaction of flood and sediment in riparian area.

Figure 62. Historical aerial images in chronological sequence illustrating vegetation growth in Narayani River, Nepal (a) 2004 (b) 2010 (c) 2014 (d) 2020

The annual flood and sediment interaction depict the floodplain area, herb area and tree area, which are extracted from the historical aerial images (Figure 63a-d). The red boundary shows the floodplain area. The faint green boundary shows the herb area whereas the dark green boundary shows the tree coverage area in the Narayani, River floodplain.

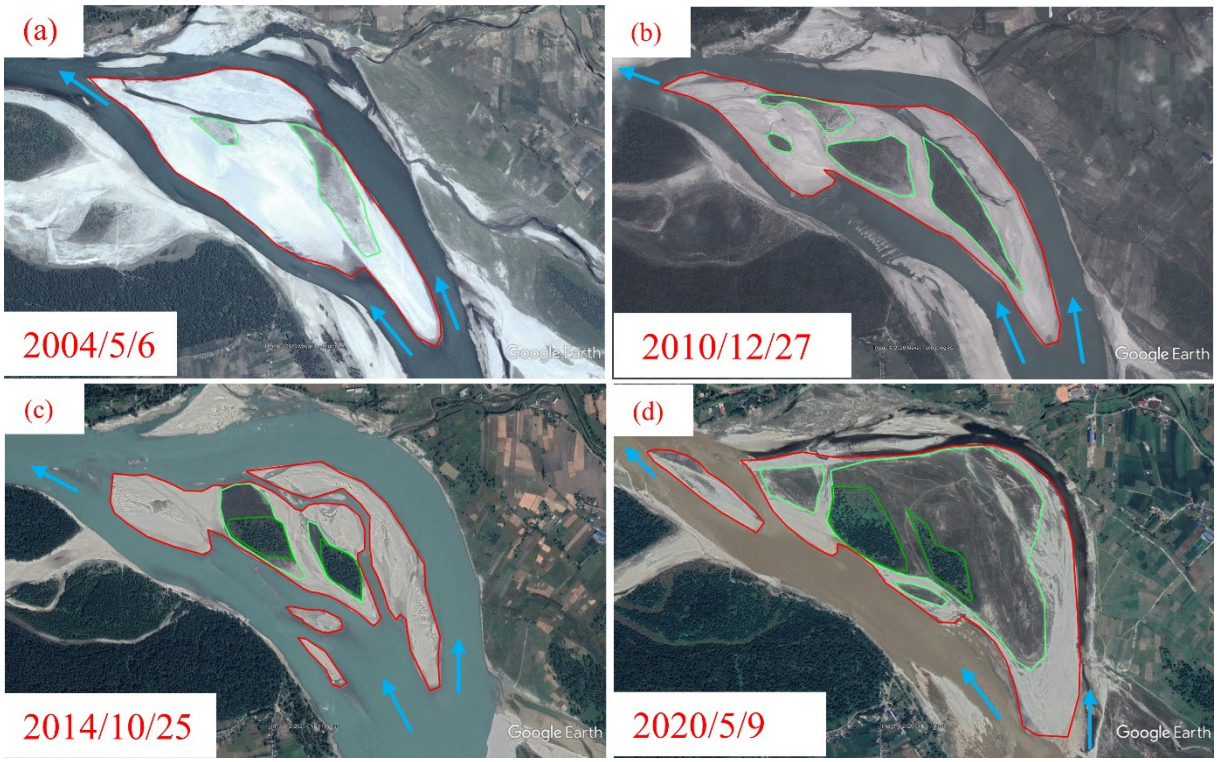

Figure 63. Riparian area calculation from historical aerial images in chronological sequence in Narayani River, Nepal (a) 2004 (b) 2010 (c) 2014 (d) 2020

The riparian area shows increasing function with sediment deposition area shown in Figure 64a. The herb area was existed during 10 years since 2004, and tree species were introduced after 10 years period. The riparian area was interacted with floods and sediment continuously up to 10 years so that a forest area was permanently established after 16 years in the floodplain (Figure 63 and 64b).

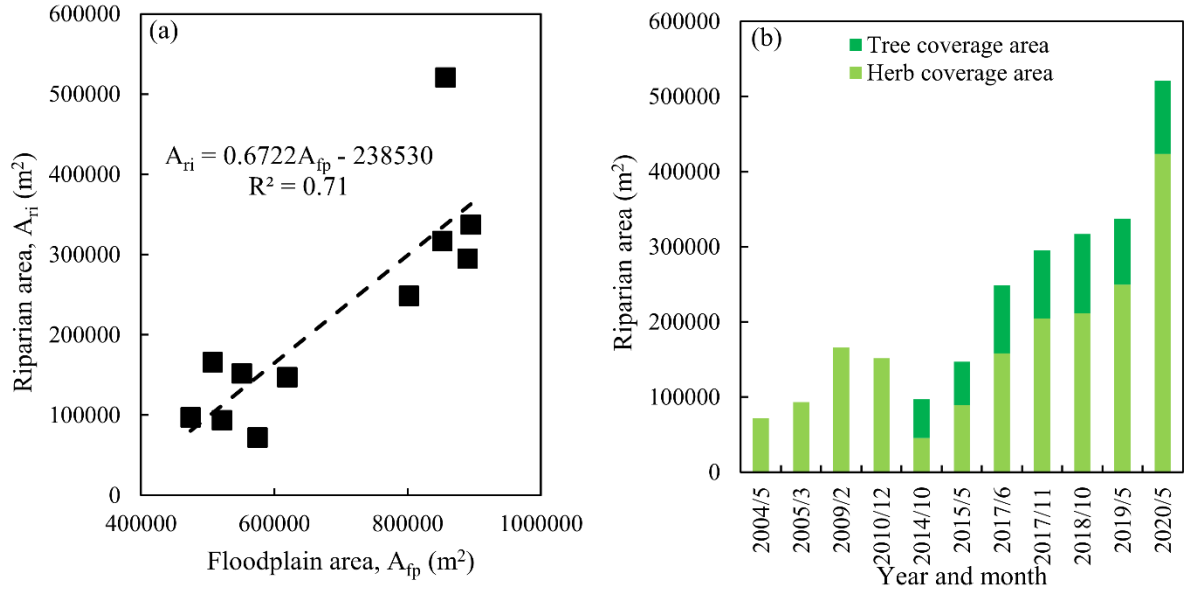

Figure 64. (a) Relationship between riparian area and floodplain area (b) Tree and herb coverage area

3.1.2 Prediction of vegetation growth by using DRIPVEM coupled with dynamic herbaceous plants model

The vicinity area is dominated with riverine grassland species *Saccharum*, *Narenga* and *Themeda* and riverine forest *Shorea rubusta* occupy old and new floodplain terraces with a variety of soil moisture conditions (Lehmkuhl, 1994).

In case of prediction of riparian vegetation growth in Narayani River floodplain, the DRIPVEM should be calibrated in the context of Narayani River floodplain (Nepal) which requires field observations of riparian vegetation in the floodplain. This broad research area is now an emerging field in developing countries like Nepal and prospect an immense research scope in future. For calibration of coupled DRIPVEM model, species wise biomass of herbs and trees such as above ground and below ground biomass growth in the floodplain are needed with the sediment particle size deposited in the floodplain. The nutrients available in the sediment is also major governing factor during calibration of the model. The field observation of riparian vegetation and application of this coupled DRIPVEM for this river floodplain at this moment would be future perspective of the study.

3.2 Case study (Japan)

The historical monthly maximum flood levels (1969-2014) in Kuzuryu River study reach is shown in Figure 65a (http://www1.river.go.jp/). The riparian area is divided in to 10 m ×10 m meshes having elevations ranges from 0 (normal water level) to 7.33 m. The upstream riparian zone consists of highest elevations and more than 50% riparian area composed of low elevations from 0.1 m to 3 m (Figure 65b).

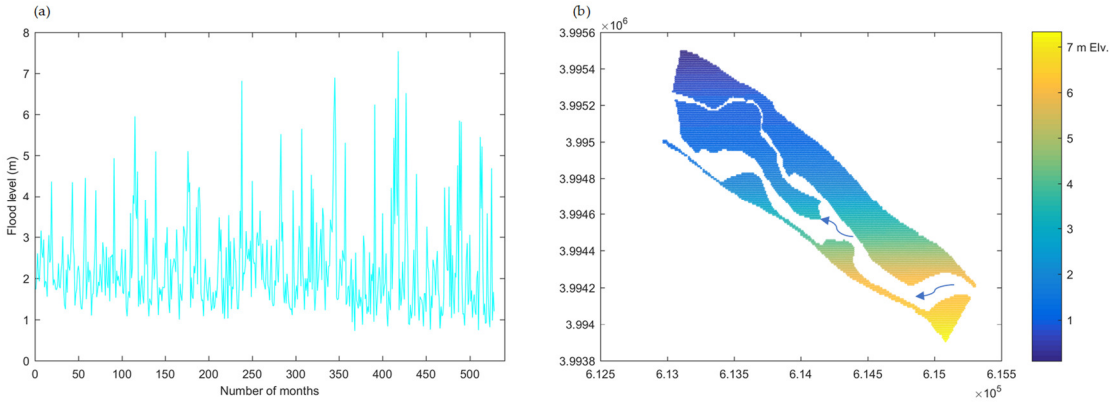

Figure 65. Kuzuryu River (a) Historical flood level (b) Floodplain elevation

3.2.1 Seasonal growth of herbaceous plants

The monthly mean observed AGB and BGB of *P. japonica* on the floodplain in sandy habitat is higher than gravelly habitat (Figure 66a,b). The morphology of this plant such as plant density and height of plant are higher in sandy soil compared to gravelly soil. Flood disturbance and sediment interaction in the riparian zone alter the morphological conditions of riparian zone such that the vegetation growth changes in the floodplain. The monthly mean observed AGB was significantly higher than at gravelly site (two sample t-test, $p < 0.05$). Similarly, the monthly mean observed BGB at sandy sites was significantly higher than at gravelly site (two sample t-test, $p < 0.05$). The observed maximum AGB was 1406 g/m^2 at 0.13 mm sediment grain size (sandy site) whereas its value was 400 g/m^2 at 15.2 mm sediment grain size (gravelly site). Similarly, the observed BGB was 1147 g/m^2 in sandy site and 808 g/m^2 in gravelly site

respectively. The AGB is easily removed subjected to floods and thereafter the photosynthesis is curtailed throughout the rest growth periods of the year, although the secondary shoots grow if the flood occurs early in the growing season (Asaeda *et al.*, 2006; Asaeda & Rajapakse, 2008). The Dynamic Herbaceous Model predicted that the maximum AGBs were 1347 g/m^2 at sandy site and 462 g/m^2 at gravelly site. Similarly, the model predicted the maximum BGBs were 853 g/m^2 at sandy site and 541 g/m^2 at gravelly site. The comparison of observed and simulated AGB (R^2 = 0.92) and BGB (R^2 = 0.85) at sandy soil and AGB (R^2 = 0.51) and BGB (R^2 = 0.66) at gravelly soil (Kumagaye, Japan) are shown in Figure 66a,b.

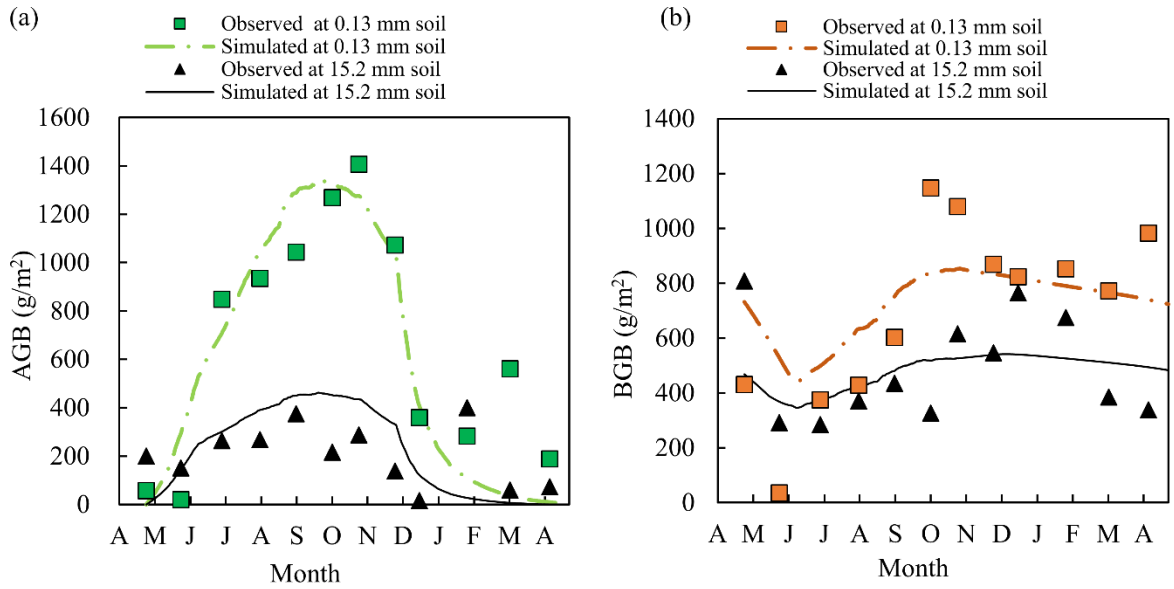

Figure 66. Observed and simulated biomass *P. japonica* at different habitants (a) Above ground biomass (AGB) (b) Below ground biomass (BGB).

3.2.2 Historical evidence of growth of herbs and trees in floodplain

Figure 67a-d show the historical aerial images in chronological sequence of development of vegetation growth in Kuzuryu River study reach from 1982 to 2018. From the historical imagery observations, one can notice that the sediment deposition area decreased and riparian vegetation area increased year by year. A major flood of 2144 m^3/s with flood level 6.82 m occurred in September 1989. This major flood changed the morphology of river and increased the riparian zone coverage rapidly. After 9 years, another major flood of discharge 2517 m^3/s

with flood level 6.9 m occurred in September 1998. Similarly, a high flood of discharge 2400 m^3/s with 6.24 m flood level encountered in the study reach in October 2002 and a highest flood of discharge 3221 m^3/s with inundation level 7.54 was encountered in October 2004 (Figure 65a). These major floods changed the morphology of the floodplain.

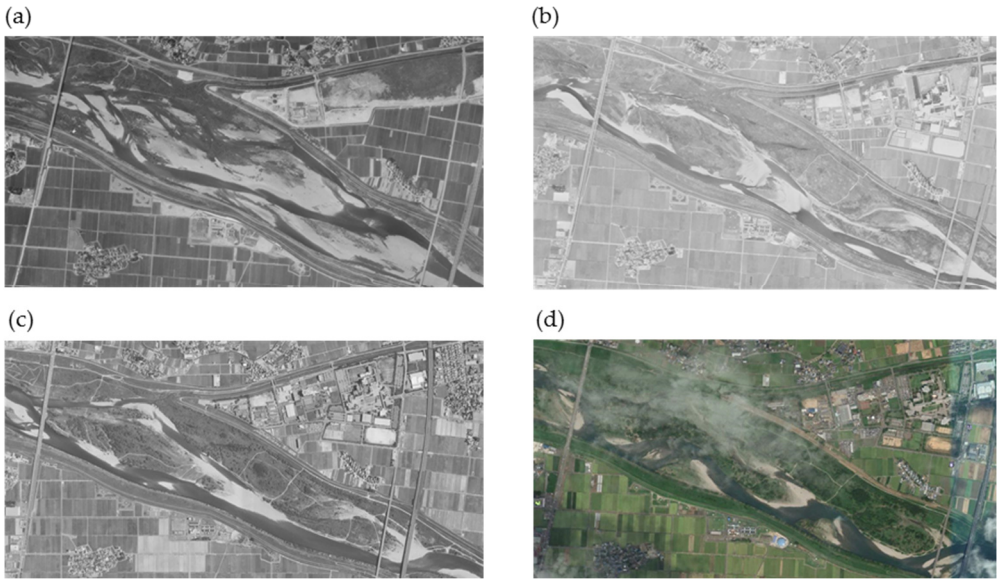

Figure 67. Historical aerial images in chronological sequence illustrating vegetation growth in Kuzuryu River, Japan (a) 1982 (b) 1994 (c) 2004 (d) 2018

(Source: Geographical Information Authority of Japan https://mapps.gsi.go.jp/maplibSearch.do#1 and Google Earth 2018).

3.2.3 Prediction of vegetation growth by using DRIPVEM coupled with dynamic herbaceous plants model

Figure 68a,b show the simulated spatial distribution of herb biomass on the floodplain after 49 years of simulation in sandy (D_{50} = 1 mm) and stony (D_{50} = 50 mm) site. After large flood, nearly all area of riparian zone was inundated except for few high elevated areas whereby they retain the herbs biomass as well as the soil TN concentrations on each meshes. Herbs were easily washed away and soil TN concentration also decreases in flood affected areas (Asaeda & Rashid, 2014). After completing life cycle of herbaceous plants, the AGB parts senescence and decomposed so that nutrients were released into the floodplain. The retained nutrients were used for the next growing seasons for herbaceous plants and creates favorable condition for

tree growth. The DRIPVEM results after 49 years of simulation, showed that spatial distribution in sandy site performed minimum 700 g/m^2 and maximum 1100 g/m^2 of herbaceous biomass whereas in stony site ranges from 220 g/m^2 to 400 g/m^2. Out of 8639 number of meshes, 7661 number of meshes are covered with herbs in 2018 and the DRIPVEM generated 4224 meshes were covered with herb biomass (R^2 = 0.55).

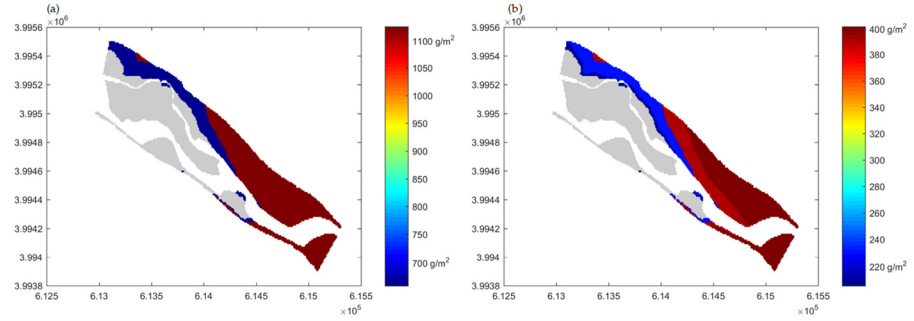

Figure 68. Simulated spatial distribution of herbs in floodplain (a) D_{50}= 1 mm size (b) D_{50}= 50 mm size.

Figure 69a shows the simulated density wise spatial distribution of trees on the floodplain after 49 years of simulation in sandy site. The density wise distribution of trees varied from 0.05 Nos/m^2 to 0.5 Nos/m^2 consisting of different ages of trees varied from 2 to 18 years old (Figure 68b). Out of 8639 number of meshes, 7217 number of meshes are covered with trees in 2018 and the coupled DRIPVEM calculated 4224 meshes were covered with trees (R^2=0.65). The discrepancies were expected due to the external factors for example: hydraulic factors, temperature, human disturbance at higher elevations and environmental factors change after flood events.

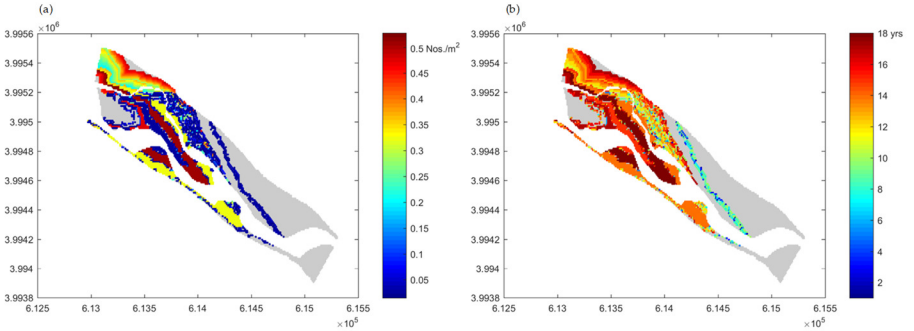

Figure 69. Simulated spatial distribution of trees in sandy floodplain (a) Density wise distribution (b) Age wise distribution.

CHAPTER 4.0 DISCUSSION

4.1 Growth of herbaceous plants in the riparian zone

The dynamic herbaceous plants model performed that the net growth of the plant stand is the integral effect of photosynthesis, respiration, mortality and translocation of assimilated materials between shoots and belowground organs (Asaeda *et al.*, 2011; Asaeda & Karunaratne, 2000; Hootsmans, 1994; Soetaert *et al.*, 2004). The transfer between the aboveground and belowground biomass in the case of perennial plants differentiates their morphology depending on their plasticity (Asaeda *et al.*, 2006; McConnaughay & Coleman, 1999; Funk, 2008). The limiting of moisture and nutrients in coarse sediment sites decreases the growth of plants whereas the available moisture and nutrients in sandy sites increases the growth of herbaceous plants so that the total biomass in fine sediment was more than coarse sediment.

The aboveground part of herbaceous plants begin in the mid spring with the expense of reserve rhizomes by the upward translocation (Tursun *et al.*, 2011). This upward translocation continues up to early summer and rhizome biomass decreases so that above ground biomass continuously increases. When upward translocation at near stopping stage, photosynthesized material starts download translocation to rhizomes reserving for next growing season. Also, biomass of shoot continues grow and maximum AGB occurs at autumn (Votrubov *et al.*, 2008). The aboveground parts die or are removed by the flood flow. The photosynthesis production is highly curtailed during the flooding period in the year, although secondary shoots grow if the flood occurs early in the growing season (Asaeda & Rajapakse, 2008). The sediment trapping behavior of herbaceous plants deposited sediments in the upstream of herbaceous plants and scour formed behind the vegetation with changing flow velocity profile (Li *et al.*, 2018). The sediment trapped zone around the herbaceous plants (Gomes & Asaeda, 2009) supports the floodplain enrich with nutrients. Herbaceous plants subjected to annual floods, therefore, gradually shrinks

year after year, particularly if floods occur when the plants are in active growth stage.

The flushing of suspended sediments through dams also transported high nutrients in to the downstream area (Kantoush32 *et al.*, 2010). These interactive relationships between flooded water, erosion or deposition area, sediment and nutrients contributed in creating riparian zones more fertile (Gurnell & Petts, 2006), which created the favorable condition for rapid growth of riparian vegetation.

4.2 Growth of trees in the riparian zone

The substrate texture of floodplain changes after flood flows. Thus, in case of low flow disturbance and shallow inundation, the substrate texture changes from coarse to fine, as fine sediment deposits on the top surface of floodplain (Steiger *et al.*, 2001) such that the growth of herbaceous plants are enhanced. Subjected to high flow disturbance and deep inundation, existing fine sediments of top surface of floodplain wash away exposing the underlying coarse textures on the floodplain, suppresses the growth of herbaceous plants. Atmospheric nitrogen, nutrients release after decomposition of AGB and BGB parts of herbaceous plants (Standish *et al.*, 2004) also supports to increase nutrients in the riparian zone, creates the favorable conditions for trees growth. The vegetation was colonized after the large floods, therefore gradually covered with trees year after year resulting nearly whole sediment deposited area was covered with herbs and mature trees.

The coupled DRIPVEM considered most of the physical, chemical and biological interactive parameters for examples: flood disturbance, riparian morphology, median sediment sizes (D_{50}), erosion depth, deposition areas, allometric relationships of trees growth, shading effects of trees canopy, self-thinning phenomenon, availability of nutrients in water and sediment with riparian zone etc. The simulated results of spatial distribution of herbs ($R^2 = 0.55$) and trees ($R^2=0.65$) by using coupled DRIPVEM tool have an acceptable agreement.

CHAPTER 5 GENERAL CONCLUSIONS AND RECOMMENDATIONS

5.1 Conclusion

The interactive parameters associated in fluvial flow, erosion and deposition area of floodplain, nutrients availability support riparian vegetation growth in the floodplain. The long-term riparian vegetation growth in the floodplain is quantified by using mathematical models. Dynamic Herbaceous Model can predict the maximum biomass of herbs in the floodplain, which links to DRIPVEM as an input part. The DRIPVEM coupled with Dynamic Herbaceous Model can simulate the spatial distribution of herbs and trees in respect of biomass as well as age-wise distribution of trees in the floodplain.

5.2 Application of the model

The potential use of this study is to predict the long-term riparian vegetation changes in floodplain. The model could be used in mixed forests in different scenarios and locations by incorporating allometric observations of different species wise growth of trees and availability of water and sediment with nutrients on floodplain with elevation wise sediment grain sizes (D50) and morphology of riparian zones. This model could be very useful tool for long-term forest planning, decision making and forest management perspective.

5.3 Recommendations

The model is tested in context of Japanese River. It is recommended to link the quantity of deposited or eroded suspended sediment during flood events and alteration of riparian topography. For calibration of coupled DRIPVEM in context of Nepalese River, observations of herbs and trees (above and below ground) biomass are needed. The flood hydrology, sediment particle sizes with the nutrients availability are also needed for calibration of the model. The riparian biomass observation and calibration of coupled DRIPVEM for Nepalese River recommended as future perspective.

Overall conclusion and recommendation

The water budget within the catchment are dependent on the temperature, evaporation, rainfall, amount of snow fall and melt inside the catchment. It is concluded that the hydraulic parameters such as bed shear stress (τ_b), specific stream power (ω), and flow velocity (v) are associated with maximum boulder size transport and quantity of sediment transport in the river system. Sediment yield from a catchment is a complex phenomenon of weathering, land sliding, glacial and fluvial erosion which depends on catchment area, topography, the slope of the catchment terrain, rainfall, temperature and soil characteristics. As rainfall during pre-monsoon (March-May) and monsoon (June-September) increases, fluvial discharge in tributaries and main river increases so that high amount of suspended sediment transport in the fluvial system. Clockwise hysteresis loops were generated between suspended sediment concentration and fluvial discharge in a catchment due to increasing sediment concentration more rapidly in rising limb with increasing fluvial discharge which indicated that a source of sediment close to the monitoring point. However, anticlockwise hysteresis loops were generated between specific discharge and rainfall which illustrated that part of the last year's rainfall was temporarily reserved within the catchment and the storage part was drained during the post-monsoon season. The flood events and cross section topography of riverbed are associated to magnitude of the hydraulic parameters. The erosion of sediment from a catchment transported by fluvial flow and deposited the sediment into another location changes the topography of the riparian area. The spatial distribution of riparian vegetation in river floodplain is highly dependent on the parameters such as sediment particle size (D_{50}), fluvial flow disturbance, erosion and deposition area of floodplain, nutrients availability in the floodplain. Higher the finer mean sediment particle size (D_{50}) of the riparian zone, higher the vegetation coverage in the floodplain compared with vegetation growth in coarse sized sediment. The long-term riparian vegetation growth in respect of herbs biomass, trees biomass as well as density-wise and age-wise spatial

tree distribution in the floodplain are predicted by DRIPVEM coupled with Dynamic Herbaceous Model.

The coupled DRIPVEM is tested by the available vegetation data in Japanese River floodplain. It is highly recommended a specific riparian vegetation observation and calibration of this model in Nepalese River floodplain as future perspective.

References

Abdulkareem, J. H. & Sulaiman, W. N. A. (2016) Trend analysis of precipation data in flood source area of Kelantan River basin. *J. Teknol.* **78**(9–4).

Adhikari, B. R. & Wagreich, M. (2011) Provenance evolution of collapse graben fill in the Himalaya—The Miocene to Quaternary Thakkhola-Mustang graben (Nepal). *Sediment. Geol.* **233**(1–4), 1–14. Elsevier.

Alexandersson, H. (1986) A homogeneity test applied to precipitation data. *J. Climatol.* **6**(6), 661–675. Wiley Online Library.

Alexandersson, H. & Moberg, A. (1997) Homogenization of Swedish temperature data. Part I: Homogeneity test for linear trends. *Int. J. Climatol. A J. R. Meteorol. Soc.* **17**(1), 25–34. Wiley Online Library.

Ali, M., Sterk, G., Seeger, M., Boersema, M. & Peters, P. (2012) Effect of hydraulic parameters on sediment transport capacity in overland flow over erodible beds. *Hydrol. Earth Syst. Sci.* **16**(2), 591–601. doi:10.5194/hess-16-591-2012

Andermann, C., Bonnet, S., Crave, A., Davy, P., Longuevergne, L. & Gloaguen, R. (2012) Sediment transfer and the hydrological cycle of Himalayan rivers in Nepal. *Comptes Rendus Geosci.* **344**(11–12), 627–635. Elsevier.

Andermann, C., Longuevergne, L., Bonnet, S., Crave, A., Davy, P. & Gloaguen, R. (2012) Impact of transient groundwater storage on the discharge of Himalayan rivers. *Nat. Geosci.* **5**(2), 127–132. Nature Publishing Group.

Annandale, G. W. (2006) Reservoir sedimentation. *Encycl. Hydrol. Sci.* Wiley Online Library.

Araujo, J. C. De, Güntner, A. & Bronstert, A. (2006) Loss of reservoir volume by sediment deposition and its impact on water availability in semiarid Brazil. *Hydrol. Sci. J.* **51**(1), 157–170. Taylor & Francis.

Asaeda, T., Baniya, M. B. & Rashid, M. H. (2011) Effect of floods on the growth of *Phragmites*

japonica on the sediment bar of regulated rivers: A modelling approach. *Int. J. River Basin Manag.* **9**(3–4). doi:10.1080/15715124.2011.613837

Asaeda, T, Rashid, M. H. & Abu Bakar, R. (2015) Dynamic modelling of soil nitrogen budget and vegetation colonization in sediment bars of a regulated river. *River Res. Appl.* **31**(4), 470–484. Wiley Online Library.

Asaeda, T & Sanjaya, K. (2017) The effect of the shortage of gravel sediment in midstream river channels on riparian vegetation cover. *River Res. Appl.* **33**(7), 1107–1118. Wiley Online Library.

Asaeda, T, Fujino, T. & Manatunge, J. (2005) Morphological adaptations of emergent plants to water flow: a case study with *Typha angustifolia*, *Zizania latifolia* and *Phragmites australis*. *Freshw. Biol.* **50**(12), 1991–2001. Wiley Online Library.

Asaeda, T, Gomes, P. I. A., Sakamoto, K. & Rashid, M. H. (2011) Tree colonization trends on a sediment bar after a major flood. *River Res. Appl.* **27**(8), 976–984. Wiley Online Library.

Asaeda, T, Gomes, P. I. A. & Takeda, E. (2010) Spatial and temporal tree colonization in a midstream sediment bar and the mechanisms governing tree mortality during a flood event. *River Res. Appl.* **26**(8), 960–976. Wiley Online Library.

Asaeda, T, Hai, D. N., Manatunge, J., Williams, D. & Roberts, J. (2005) Latitudinal characteristics of below-and above-ground biomass of *Typha*: a modelling approach. *Ann. Bot.* **96**(2), 299–312. Oxford University Press.

Asaeda, T & Karunaratne, S. (2000) Dynamic modeling of the growth of *Phragmites australis*: model description. *Aquat. Bot.* **67**(4), 301–318. Elsevier.

Asaeda, T, Manatunge, J., Roberts, J. & Hai, D. N. (2006) Seasonal dynamics of resource translocation between the aboveground organs and age-specific rhizome segments of *Phragmites australis*. *Environ. Exp. Bot.* **57**(1–2), 9–18. Elsevier.

Asaeda, T, Nallaperuma, B., Baniya, M. B. & Mdh, S. (2019) Riparian vegetation classification

using the dynamic riparian vegetation model. In Proceedings of the E-proceedings 38th IAHR World Congress, Panama City, Panama, 1-6 September 2019. doi:10.3850/38WC092019-0989

Asaeda, T & Rajapakse, L. (2008) Effects of spates of different magnitudes on a *Phragmites japonica* population on a sandbar of a frequently disturbed river. *River Res. Appl.* **24**(9), 1310–1324. Wiley Online Library.

Asaeda, T & Rashid, M. D. H. (2014) Modelling of nutrient dynamics and vegetation succession in midstream sediment bars of a regulated river. *Int. J. river basin Manag.* **12**(2), 123–133. Taylor & Francis.

Asaeda, T & Rashid, M. H. (2012) The impacts of sediment released from dams on downstream sediment bar vegetation. *J. Hydrol.* **430**, 25–38. Elsevier.

Asaeda, T, Rashid, M. H., Kotagiri, S. & Uchida, T. (2011) The role of soil characteristics in the succession of two herbaceous lianas in a modified river floodplain. *River Res. Appl.* **27**(5), 591–601. Wiley Online Library.

Asaeda, T, Sharma, P. & Rajapakse, L. (2008) Seasonal patterns of carbohydrate translocation and synthesis of structural carbon components in *Typha angustifolia*. *Hydrobiologia* **607**(1), 87–101. Springer.

Asaeda, T, Siong, K., Kawashima, T. & Sakamoto, K. (2009) Growth of *Phragmites japonica* on a sandbar of regulated river: morphological adaptation of the plant to low water and nutrient availability in the substrate. *River Res. Appl.* **25**(7), 874–891. Wiley Online Library.

Ayadi, I., Abida, H., Djebbar, Y. & Raouf Mahjoub, M. (2010) Sediment yield variability in central Tunisia: a quantitative analysis of its controlling factors. *Hydrol. Sci. Journal–Journal des Sci. Hydrol.* **55**(3), 446–458. Taylor & Francis.

Bača, P. (2008) Hysteresis effect in suspended sediment concentration in the Rybárik basin, Slovakia/Effet d'hystérèse dans la concentration des sédiments en suspension dans le bassin versant de Rybárik (Slovaquie). *Hydrol. Sci. J.* **53**(1), 224–235. Taylor & Francis.

Bajracharya, A. R., Bajracharya, S. R., Shrestha, A. B. & Maharjan, S. B. (2018) Climate change impact assessment on the hydrological regime of the Kaligandaki Basin, Nepal. *Sci. Total Environ.* **625**, 837–848. Elsevier.

Baker, V. R. & Ritter, D. F. (1975) Competence of rivers to transport coarse bedload material. *Geol. Soc. Am. Bull.* **86**(7), 975–978. Geological Society of America.

Banasik, K. & Hejduk, L. (2013) Flow duration curves for two small catchments with various records in lowland part of poland. *Rocz Ochr Środow.(Annu Set Env. Prot.)* **15**(1), 287–300.

Baniya, M. B., Asaeda, T., KC, S. & Jayashanka, S. M. D. H. (2019) Hydraulic Parameters for Sediment Transport and Prediction of Suspended Sediment for Kali Gandaki River Basin, Himalaya, Nepal. *Water* **11**(6), 1229. Multidisciplinary Digital Publishing Institute.

Bari, S. H., Rahman, M. T. U., Hoque, M. A. & Hussain, M. M. (2016) Analysis of seasonal and annual rainfall trends in the northern region of Bangladesh. *Atmos. Res.* **176**, 148–158. Elsevier.

Basistha, A., Arya, D. S. & Goel, N. K. (2009) Analysis of historical changes in rainfall in the Indian Himalayas. *Int. J. Climatol. A J. R. Meteorol. Soc.* **29**(4), 555–572. Wiley Online Library.

Bayley, G. V & Hammersley, J. M. (1946) The" effective" number of independent observations in an autocorrelated time series. *Suppl. to J. R. Stat. Soc.* **8**(2), 184–197. JSTOR.

Benjankar, R., Egger, G., Jorde, K., Goodwin, P. & Glenn, N. F. (2011) Dynamic floodplain vegetation model development for the Kootenai River, USA. *J. Environ. Manage.* **92**(12), 3058–3070. Elsevier.

Bhusal, J. K. & Subedi, B. P. (2015) Effect of climate change on suspended sediment load in the Himalayan basin: A case study of Upper Kaligandaki River. *J. Hydrol. (New Zealand)* **54**(1), 1–10. doi:10.2307/43945067

Bingham, C. & Nelson, L. S. (1981) An approximation for the distribution of the von Neumann ratio. *Technometrics* **23**(3), 285–288. Taylor & Francis Group.

Biology, T. (2019) Seed Dispersal in Flood Plain Forests of Amazonia Author (s): Klaus Kubitzki and Albrecht Ziburski Published by : Association for Tropical Biology and Conservation Stable URL : https://www.jstor.org/stable/2389108 preserve and extend access to Biotropic **26**(1), 30–43.

Boedeltje, G. E. R., Bakker, J. P., Brinke, A. Ten, Groenendael, J. M. Van & Soesbergen, M. (2004) Dispersal phenology of hydrochorous plants in relation to discharge, seed release time and buoyancy of seeds: the flood pulse concept supported. *J. Ecol.* **92**(5), 786–796. Wiley Online Library.

Bookhagen, B. & Burbank, D. W. (2010) Toward a complete Himalayan hydrological budget: Spatiotemporal distribution of snowmelt and rainfall and their impact on river discharge. *J. Geophys. Res. Earth Surf.* **115**(F3). Wiley Online Library.

Bookhagen, B., Thiede, R. C. & Strecker, M. R. (2005) Abnormal monsoon years and their control on erosion and sediment flux in the high, arid northwest Himalaya. *Earth Planet. Sci. Lett.* **231**(1–2), 131–146. Elsevier.

Bradley, W. C. & Mears, A. I. (1980) Calculations of flows needed to transport coarse fraction of Boulder Creek alluvium at Boulder, Colorado. *Geol. Soc. Am. Bull.* **91**(3_Part_II), 1057–1090. The Geological Society of America, Inc.

Brandt, S. A. (2000) Prediction of downstream geomorphological changes after dam construction: a stream power approach. *Int. J. Water Resour. Dev.* **16**(3), 343–367. Taylor & Francis.

Bricker, J. D., Schwanghart, W., Adhikari, B. R., Moriguchi, S., Roeber, V. & Giri, S. (2017) Performance of Models for Flash Flood Warning and Hazard Assessment: The 2015 Kali Gandaki Landslide Dam Breach in Nepal. *Mt. Res. Dev.* **37**(1), 5–15. doi:10.1659/mrd-journal-d-16-00043.1

Buishand, T. A. (1982) Some methods for testing the homogeneity of rainfall records. *J. Hydrol.* **58**(1–2), 11–27. Elsevier.

Burbank, D. W., Bookhagen, B., Gabet, E. J. & Putkonen, J. (2012) Modern climate and erosion in the Himalaya. *Comptes Rendus Geosci.* **344**(11–12), 610–626. Elsevier.

Bussi, G., Francés, F., Montoya, J. J. & Julien, P. Y. (2014) Distributed sediment yield modelling: Importance of initial sediment conditions. *Environ. Model. Softw.* **58**, 58–70. Elsevier.

Camporeale, C. & Ridolfi, L. (2006) Riparian vegetation distribution induced by river flow variability: A stochastic approach. *Water Resour. Res.* **42**(10). Wiley Online Library.

Carver, M. (1997) Diagnosis of headwater sediment dynamics in Nepal's middle mountains: implications for land management. University of British Columbia, Vancouver, BC, CA.

Chakrapani, G. J. & Saini, R. K. (2009) Temporal and spatial variations in water discharge and sediment load in the Alaknanda and Bhagirathi Rivers in Himalaya, India. *J. Asian Earth Sci.* **35**(6), 545–553. Elsevier.

Che Ros, F., Tosaka, H., Sidek, L. M. & Basri, H. (2016) Homogeneity and trends in long-term rainfall data, Kelantan River Basin, Malaysia. *Int. J. river basin Manag.* **14**(2), 151–163. Taylor & Francis.

Chhetry, B. & Rana, K. (2015) Effect of Sand Erosion on Turbine Components: A Case Study of Kali Gandaki "A" Hydroelectric Project (144 MW), Nepal. *Hydro Nepal J. Water, Energy Environ.* **17**, 24–33.

Costa, J. E. (1983) Paleohydraulic reconstruction of flash-flood peaks from boulder deposits in the Colorado Front Range. *Geol. Soc. Am. Bull.* **94**(8), 986–1004. Geological Society of America.

Costa, J. E. & Schuster, R. L. (1988) The formation and failure of natural dams. *Geol. Soc. Am. Bull.* **100**(7), 1054–1068. Geological Society of America.

Dahal, R. K. & Hasegawa, S. (2008) Representative rainfall thresholds for landslides in the Nepal Himalaya. *Geomorphology* **100**(3–4), 429–443. Elsevier.

Dandekhya, S., England, M., Ghate, R., Goodrich, C. G., Nepal, S., Prakash, A., Shrestha, A., et al. (2017) The Gandaki basin: Maintaining livelihoods in the face of landslides, floods, and

drought. *HI-AWARE Work. Pap.* **9**.

Davies-Colley, R. J., Meleason, M. A., Hall, R. M. J. & Rutherford, J. C. (2009) Modelling the time course of shade, temperature, and wood recovery in streams with riparian forest restoration. *New Zeal. J. Mar. Freshw. Res.* **43**(3), 673–688. Taylor & Francis.

Duncan, J. M. A., Biggs, E. M., Dash, J. & Atkinson, P. M. (2013) Spatio-temporal trends in precipitation and their implications for water resources management in climate-sensitive Nepal. *Appl. Geogr.* **43**, 138–146. Elsevier.

Eckhardt, K. (2005) How to construct recursive digital filters for baseflow separation. *Hydrol. Process. An Int. J.* **19**(2), 507–515. Wiley Online Library.

Eid, E. M., Shaltout, K. H. & Asaeda, T. (2012) Modeling growth dynamics of Typha domingensis (Pers.) Poir. ex Steud. in Lake Burullus, Egypt. *Ecol. Modell.* **243**, 63–72. Elsevier.

Fort, M., Cossart, E. & Arnaud-Fassetta, G. (2010) Hillslope-channel coupling in the Nepal Himalayas and threat to man-made structures: The middle Kali Gandaki valley. *Geomorphology* **124**(3–4), 178–199. doi:10.1016/j.geomorph.2010.09.010

Fort, MONIOUE. (1987) Sporadic morphogenesis in a continental subduction setting: an example from the Annapurna Range, Nepal Himalaya. *Zeitschrift für Geomorphol.* **63**(9), 36.

Fort, Monique. (2016) Sedimentary fluxes in Himalaya. In: *Source-to-Sink Fluxes in Undisturbed Cold Environments* (A. A. Beylich, J. C. Dixon & Z. Zwolinski, eds.), 326–350. Cambridge: Cambridge University Press. doi:10.1017/CBO9781107705791.024

Fort, Monique & Cossart, E. (2013) Erosion assessment in the middle Kali Gandaki (Nepal): A sediment budget approach. *J. Nepal Geol. Soc.* **46**, 25–40.

Fort, Monique, Cossart, E. & Arnaud-Fassetta, G. (2010) Hillslope-channel coupling in the Nepal Himalayas and threat to man-made structures: The middle Kali Gandaki valley. *Geomorphology* **124**(3–4), 178–199. Elsevier.

Fu, B., Li, Y., Wang, Y., Zhang, B., Yin, S., Zhu, H. & Xing, Z. (2016) Evaluation of ecosystem service

value of riparian zone using land use data from 1986 to 2012. *Ecol. Indic.* **69**, 873–881. Elsevier.

Funk, J. L. (2008) Differences in plasticity between invasive and native plants from a low resource environment 1162–1173. doi:10.1111/j.1365-2745.2008.01435.x

Gabet, E. J., Burbank, D. W., Putkonen, J. K., Pratt-Sitaula, B. A. & Ojha, T. (2004) Rainfall thresholds for landsliding in the Himalayas of Nepal. *Geomorphology* **63**(3–4), 131–143. Elsevier.

Gajbhiye, S., Meshram, C., Mirabbasi, R. & Sharma, S. K. (2016) Trend analysis of rainfall time series for Sindh river basin in India. *Theor. Appl. Climatol.* **125**(3–4), 593–608. Springer.

García-Arias, A. & Francés, F. (2016) The RVDM: modelling impacts, evolution and competition processes to determine riparian vegetation dynamics. *Ecohydrology* **9**(3), 438–459. Wiley Online Library.

García-Arias, A., Francés, F., Ferreira, T., Egger, G., Martínez-Capel, F., Garófano-Gómez, V., Andrés-Doménech, I., et al. (2013) Implementing a dynamic riparian vegetation model in three European river systems. *Ecohydrology* **6**(4), 635–651. Wiley Online Library.

Gautam, M. R. & Acharya, K. (2012) Streamflow trends in Nepal. *Hydrol. Sci. J.* **57**(2), 344–357. Taylor & Francis.

Glysson, G. D. (1987) Sediment- transport curves. *U.S.Geological Surv. Open-File Rep. 87–218*.

Gomes, P. I. A. & Asaeda, T. (2009) Spatial and temporal heterogeneity of Eragrostis curvula in the downstream flood meadow of a regulated river. *Ann. Limnol. J. Limnol.*, Vol. 45, 181–193. EDP Sciences.

Granet, M., Chabaux, F., Stille, P., France-Lanord, C. & Pelt, E. (2007) Time-scales of sedimentary transfer and weathering processes from U-series nuclides: clues from the Himalayan rivers. *Earth Planet. Sci. Lett.* **261**(3–4), 389–406. Elsevier.

Grant, G. E., Swanson, F. J. & Wolman, M. G. (1990) Pattern and origin of stepped-bed morphology

in high-gradient streams, Western Cascades, Oregon. *Bull. Geol. Soc. Am.* **102**(3), 340–352. doi:10.1130/0016-7606(1990)102<0340:PAOOSB>2.3.CO;2

Griffiths, G. A. (1977) Origin and transport of large boulders in mountain streams. *J. Hydrol. (New Zealand)* 1–6. JSTOR.

Gudino-Elizondo, N., Biggs, T. W., Bingner, R. L., Langendoen, E. J., Kretzschmar, T., Taguas, E. V., Taniguchi-Quan, K. T., et al. (2019) Modelling Runoff and Sediment Loads in a Developing Coastal Watershed of the US-Mexico Border. *Water* **11**, 1024, 1–23.

Guillén-Ludeña, S., Manso, P. A. & Schleiss, A. J. (2018) Multidecadal sediment balance modelling of a cascade of alpine reservoirs and perspectives based on climate warming. *Water (Switzerland)* **10**(12), 10–13. doi:10.3390/w10121759

Gurnell, A. & Petts, G. (2006) Trees as riparian engineers : The Tagliamento River , Italy **1574**(May), 1558–1574. doi:10.1002/esp

Hamed, K. H. & Rao, A. R. (1998) A modified Mann-Kendall trend test for autocorrelated data. *J. Hydrol.* **204**(1–4), 182–196. Elsevier.

Haun, S. & Olsen, N. R. B. (2012) Three-dimensional numerical modelling of the flushing process of the Kali Gandaki hydropower reservoir. *Lakes Reserv. Res. Manag.* **17**(1), 25–33. Wiley Online Library.

Helley, E. J. (1969) Field measurement of the initiation of large bed particle motion in Blue Creek near Klamath, California. *US Gov. Print. Off.*

Hootsmans, M. J. M. (1994) A growth analysis model for Potamogeton pectinatus L. In: *Lake Veluwe, a macrophyte-dominated system under eutrophication stress*, 250–286. Springer.

Jarrett, R. D. (1984) Hydraulics of high-gradient streams. *J. Hydraul. Eng.* **110**(11), 1519–1539. American Society of Civil Engineers.

Kale, V. S. & Hire, P. S. (2004) Effectiveness of monsoon floods on the Tapi River, India: Role of channel geometry and hydrologic regime. *Geomorphology* **57**(3–4), 275–291.

doi:10.1016/S0169-555X(03)00107-7

Kang, H. M. & Yusof, F. (2012) Homogeneity tests on daily rainfall series. *Int. J. Contemp. Math. Sci.* **7**(1), 9–22.

Kantoush32, S. A., Sumi, T., Kubota34, A. & Suzuki, T. (2010) Impacts of sediment replenishment below dams on flow and bed morphology of river.

Karki, M., Mool, P. & Shrestha, A. (2009) Climate change and its increasing impacts in Nepal. *Initiat.* **3**, 30–37.

Karki, R., Schickhoff, U., Scholten, T. & Böhner, J. (2017) Rising precipitation extremes across Nepal. *Climate* **5**(1), 4. Multidisciplinary Digital Publishing Institute.

Kendall, Maurice G. (1938) A new measure of rank correlation. *Biometrika* **30**(1/2), 81–93. JSTOR.

Kendall, Maurice George. (1948) Rank correlation methods. Griffin.

Koirala, R., Thapa, B., Neopane, H. P., Zhu, B. & Chhetry, B. (2016) Sediment erosion in guide vanes of Francis turbine: A case study of Kaligandaki Hydropower Plant, Nepal. *Wear* **362**, 53–60. Elsevier.

Komar, P. D.; Carling, P. A. (1991) Grain sorting in gravel-bed streams and the choice of particle sizes for flow-competence evaluations. *Sedimentology* **38**, 489–502.

Komar P. D. (1987) Selective Gravel Entrainment and the Empirical Evaluation of Flow Competence. *Sedimentology* **34**, 1165–1176.

Kummu, M. & Varis, O. (2007) Sediment-related impacts due to upstream reservoir trapping, the Lower Mekong River. *Geomorphology* **85**(3–4), 275–293. Elsevier.

Lana-Renault, N. & Regüés, D. (2009) Seasonal patterns of suspended sediment transport in an abandoned farmland catchment in the Central Spanish Pyrenees. *Earth Surf. Process. Landforms* **34**(9), 1291–1301. Wiley Online Library.

Langat, P., Kumar, L. & Koech, R. (2017) Temporal variability and trends of rainfall and streamflow in tana river basin, kenya. *Sustainability* **9**(11), 1963. Multidisciplinary Digital Publishing

Institute.

Lawler, D. M., Petts, G. E., Foster, I. D. L. & Harper, S. (2006) Turbidity dynamics during spring storm events in an urban headwater river system: The Upper Tame, West Midlands, UK. *Sci. Total Environ.* **360**(1–3), 109–126. Elsevier.

Lehmkuhl, J. F. (1994) A classification of subtropical riverine grassland and forest in Chitwan National Park, Nepal. *Vegetatio* **111**(1), 29–43. Springer.

Lenzi, Mario A, D'Agostino, V. & Billi, P. (1999) Bedload transport in the instrumented catchment of the Rio Cordon: Part I: Analysis of bedload records, conditions and threshold of bedload entrainment. *Catena* **36**(3), 171–190. Elsevier.

Lenzi, Mario Aristide, Mao, L. & Comiti, F. (2006) When does bedload transport begin in steep boulder-bed streams? *Hydrol. Process.* **20**(16), 3517–3533. doi:10.1002/hyp.6168

Li, J.-F., Tfwala, S. & Chen, S.-C. (2018) Effects of Vegetation Density and Arrangement on Sediment Budget in a Sediment-Laden Flow. *Water* **10**(10), 1412. Multidisciplinary Digital Publishing Institute.

Lim, K. J., Park, Y. S., Kim, J., Shin, Y.-C., Kim, N. W., Kim, S. J., Jeon, J.-H., et al. (2010) Development of genetic algorithm-based optimization module in WHAT system for hydrograph analysis and model application. *Comput. Geosci.* **36**(7), 936–944. Elsevier.

Lippert, I., Rolletschek, H., Kühl, H. & Kohl, J.-G. (1999) Internal and external nutrient cycles in stands of Phragmites australis—a model for two ecotypes. In: *Shallow Lakes' 98*, 343–348. Springer.

Lloyd, C. E. M., Freer, J. E., Johnes, P. J. & Collins, A. L. (2016) Using hysteresis analysis of high-resolution water quality monitoring data, including uncertainty, to infer controls on nutrient and sediment transfer in catchments. *Sci. Total Environ.* **543**, 388–404. Elsevier.

Lotsari, E., Wang, Y., Kaartinen, H., Jaakkola, A., Kukko, A., Vaaja, M., Hyyppä, H., et al. (2015) Geomorphology Gravel transport by ice in a subarctic river from accurate laser scanning.

Geomorphology **246**, 113–122. Elsevier B.V. doi:10.1016/j.geomorph.2015.06.009

Lytle, D. A. & Poff, N. L. (2004) Adaptation to natural flow regimes. *Trends Ecol. Evol.* **19**(2), 94–100. Elsevier.

Mao, L, Cavalli, M., Comiti, F., Marchi, L., Lenzi, M. A. & Arattano, M. (2009) Sediment transfer processes in two Alpine catchments of contrasting morphological settings. *J. Hydrol.* **364**(1–2), 88–98. Elsevier.

Mao, Luca, Uyttendaele, G. P., Iroumé, A. & Lenzi, M. A. (2008) Field based analysis of sediment entrainment in two high gradient streams located in Alpine and Andine environments. *Geomorphology* **93**(3–4), 368–383. doi:10.1016/j.geomorph.2007.03.008

Marahatta, S. (2015) Earthquake and.

Martin, S. E., Conklin, M. H. & Bales, R. C. (2014) Seasonal accumulation and depletion of local sediment stores of four headwater catchments. *Water* **6**(7), 2144–2163. Multidisciplinary Digital Publishing Institute.

McConnaughay, K. D. M. & Coleman, J. S. (1999) Biomass allocation in plants: ontogeny or optimality? A test along three resource gradients. *Ecology* **80**(8), 2581–2593. Wiley Online Library.

Megnounif, A., Terfous, A. & Ouillon, S. (2013) A graphical method to study suspended sediment dynamics during flood events in the Wadi Sebdou, NW Algeria (1973-2004). *J. Hydrol.* **497**, 24–36. doi:10.1016/j.jhydrol.2013.05.029

Mendoza, G. A. & Vanclay, J. K. (2008) Trends in forestry modelling. *CAB Rev. Perspect. Agric. Vet. Sci. Nutr. Nat. Resour.* **3**(010).

Merz, J., Dangol, P. M., Dhakal, M. P., Dongol, B. S., Nakarmi, G. & Weingartner, R. (2006) Rainfall-runoff events in a middle mountain catchment of Nepal. *J. Hydrol.* **331**(3–4), 446–458. Elsevier.

Min, S.-K., Zhang, X., Zwiers, F. W., Friederichs, P. & Hense, A. (2009) Signal detectability in

extreme precipitation changes assessed from twentieth century climate simulations. *Clim. Dyn.* **32**(1), 95–111. Springer.

Mishra, B., Babel, M. S. & Tripathi, N. K. (2014) Analysis of climatic variability and snow cover in the Kaligandaki River Basin, Himalaya, Nepal. *Theor. Appl. Climatol.* **116**(3–4), 681–694. doi:10.1007/s00704-013-0966-1

Mondal, A., Kundu, S. & Mukhopadhyay, A. (2012) Rainfall trend analysis by Mann-Kendall test: A case study of north-eastern part of Cuttack district, Orissa. *Int. J. Geol. Earth Environ. Sci.* **2**(1), 70–78.

Montgomery, D. R. & Buffington, J. M. (1997) Channel-reach morphology in mountain drainage basins. *Bull. Geol. Soc. Am.* **109**(5), 596–611. doi:10.1130/0016-7606(1997)109<0596:CRMIMD>2.3.CO;2

Moriasi, D. N., Arnold, J. G., Liew, M. W. Van, Bingner, R. L., Harmel, R. D. & Veith, T. L. (2007) Model Evaluation guidelines **50**(3), 885–900. doi:10.13031/2013.23153

Morin, G. P., Lavé, J., France-Lanord, C., Rigaudier, T., Gajurel, A. P. & Sinha, R. (2018) Annual sediment transport dynamics in the Narayani basin, Central Nepal: Assessing the impacts of erosion processes in the annual sediment budget. *J. Geophys. Res. Earth Surf.* **123**(10), 2341–2376. Wiley Online Library.

Moriuchi, K. S. & Winn, A. A. (2005) Relationships among growth, development and plastic response to environment quality in a perennial plant. *New Phytol.* **166**(1), 149–158. Wiley Online Library.

Mueller, E. R., Schmidt, J. C., Topping, D. J., Shafroth, P. B., Rodríguez-Burgueño, J. E., Ramírez-Hernández, J. & Grams, P. E. (2017) Geomorphic change and sediment transport during a small artificial flood in a transformed post-dam delta: The Colorado River delta, United States and Mexico. *Ecol. Eng.* **106**, 757–775. Elsevier.

Muthuwatta, L., Perera, H., Eriyagama, N., Upamali Surangika, K. B. N. & Premachandra, W. W.

(2017) Trend and variability of rainfall in two river basins in Sri Lanka: an analysis of meteorological data and farmers' perceptions. *Water Int.* **42**(8), 981–999. Taylor & Francis.

Naiman, R. J., Bilby, R. E. & Bisson, P. A. (2000) Riparian ecology and management in the Pacific coastal rain forest. *Bioscience* **50**(11), 996–1011. American Institute of Biological Sciences.

Nallaperuma, B. & Asaeda, T. (2019) Long-term changes in riparian forest cover under a dam-induced flow scheme: the accompanying a numerical modelling perspective. *J. Ecohydraulics* 1–7. Taylor & Francis.

Nepf, H. & Ghisalberti, M. (2008) Flow and transport in channels with submerged vegetation. *Acta Geophys.* **56**(3), 753–777. Springer.

Neumann, J. Von. (1941) Distribution of the ratio of the mean square successive difference to the variance. *Ann. Math. Stat.* **12**(4), 367–395. JSTOR.

Nones, M. & Silvio, G. Di. (2016) Modeling of river width variations based on hydrological, morphological, and biological dynamics. *J. Hydraul. Eng.* **142**(7), 4016012. American Society of Civil Engineers.

O'Connor, J. E. (1993) *Hydrology, hydraulics, and geomorphology of the Bonneville flood*, Vol. 274. Geological Society of America.

O'Connor, J. E. & Costa, J. E. (1993) Geologic and hydrologic hazards in glacierized basins in North America resulting from 19th and 20th century global warming. *Nat. Hazards* **8**(2), 121–140. doi:10.1007/BF00605437

Onen, F. & Bagatur, T. (2017) Prediction of Flood Frequency Factor for Gumbel Distribution Using Regression and GEP Model. *Arab. J. Sci. Eng.* **42**(9), 3895–3906. doi:10.1007/s13369-017-2507-1

Pagano, S. G., Rainato, R., García-Rama, A., Gentile, F. & Lenzi, M. A. (2019) Analysis of suspended sediment dynamics at event scale: comparison between a Mediterranean and an Alpine basin. *Hydrol. Sci. J.* **64**(8), 948–961. Taylor & Francis.

Pandey, M., Zakwan, M., Sharma, P. K. & Ahmad, Z. (2018) Multiple linear regression and genetic algorithm approaches to predict temporal scour depth near circular pier in non-cohesive sediment. *ISH J. Hydraul. Eng.* 1–8. Taylor & Francis.

Perona, P., Camporeale, C., Perucca, E., Savina, M., Molnar, P., Burlando, P. & Ridolfi, L. (2009) Modelling river and riparian vegetation interactions and related importance for sustainable ecosystem management. *Aquat. Sci.* **71**(3), 266. Springer.

Pettitt, A. N. (1979) A non-parametric approach to the change-point problem. *J. R. Stat. Soc. Ser. C (Applied Stat.* **28**(2), 126–135. Wiley Online Library.

Pretzsch, H., Biber, P. & Ďurský, J. (2002) The single tree-based stand simulator SILVA: construction, application and evaluation. *For. Ecol. Manage.* **162**(1), 3–21. Elsevier.

Reimann, T., Menges, J., Hovius, N., Andermann, C., Dietze, M., Swoboda, C., Cook, K., et al. (2019) High sediment export from a trans-Himalayan semi-desert driven by late Holocene climate change and human impact. *EGU Gen. Assem. 2019*.

Rivaes, R., Rodríguez-González, P. M., Albuquerque, A., Pinheiro, A. N., Egger, G. & Ferreira, M. T. (2013) Riparian vegetation responses to altered flow regimes driven by climate change in Mediterranean rivers. *Ecohydrology* **6**(3), 413–424. Wiley Online Library.

Robinson, D. M., DeCelles, P. G., Patchett, P. J. & Garzione, C. N. (2001) The kinematic evolution of the Nepalese Himalaya interpreted from Nd isotopes. *Earth Planet. Sci. Lett.* **192**(4), 507–521. Elsevier.

Salminen, H., Lehtonen, M. & Hynynen, J. (2005) Reusing legacy FORTRAN in the MOTTI growth and yield simulator. *Comput. Electron. Agric.* **49**(1), 103–113. Elsevier.

Sanjaya, K. & Asaeda, T. (2017) Assessing the performance of a riparian vegetation model in a river with a low slope and fine sediment. *Environ. Technol.* **38**(5), 517–528. Taylor & Francis.

Sekine, H., Sakamoto, K., Nishimura, T. & Asaeda, T. (2012) Development of a simulation model considering vegetation growth and flushing in Arakawa River. *KSCE J. Civ. Eng.* **16**(2), 239–

246. Springer.

Shrestha, A. B., Bajracharya, S. R., Sharma, A. R., Duo, C. & Kulkarni, A. (2017) Observed trends and changes in daily temperature and precipitation extremes over the Koshi river basin 1975–2010. *Int. J. Climatol.* **37**(2), 1066–1083. Wiley Online Library.

Shrestha, U. B., Gautam, S. & Bawa, K. S. (2012) Widespread climate change in the Himalayas and associated changes in local ecosystems. *PLoS One* **7**(5). Public Library of Science.

Shrestha, U. B., Shrestha, A. M. & Aryal, S. (2019) Climate change in Nepal：a comprehensive analysis of instrumental data and people ' s perceptions 315–334. Climatic Change.

Singh, P. & Kumar, N. (1997) Impact assessment of climate change on the hydrological response of a snow and glacier melt runoff dominated Himalayan river. *J. Hydrol.* **193**(1–4), 316–350. Elsevier.

Smith, H. G. & Dragovich, D. (2009) Interpreting sediment delivery processes using suspended sediment-discharge hysteresis patterns from nested upland catchments, south-eastern Australia. *Hydrol. Process. An Int. J.* **23**(17), 2415–2426. Wiley Online Library.

Soetaert, K., Hoffmann, M., Meire, P., Starink, M., Oevelen, D. van, Regenmortel, S. Van & Cox, T. (2004) Modeling growth and carbon allocation in two reed beds (Phragmites australis) in the Scheldt estuary. *Aquat. Bot.* **79**(3), 211–234. Elsevier.

Soler, M., Regüés, D., Latron, J. & Gallart, F. (2007) Frequency–magnitude relationships for precipitation, stream flow and sediment load events in a small Mediterranean basin (Vallcebre basin, Eastern Pyrenees). *Catena* **71**(1), 164–171. Elsevier.

Sonali, P. & Kumar, D. N. (2013) Review of trend detection methods and their application to detect temperature changes in India. *J. Hydrol.* **476**, 212–227. Elsevier.

Stähly, S., Franca, M. J., Robinson, C. T. & Schleiss, A. J. (2019) Sediment replenishment combined with an artificial flood improves river habitats downstream of a dam. *Sci. Rep.* **9**(1), 1–8. Nature Publishing Group.

Standish, R. J., Williams, P. A., Robertson, A. W., Scott, N. A. & Hedderley, D. I. (2004) Invasion by a perennial herb increases decomposition rate and alters nutrient availability in warm temperate lowland forest remnants. *Biol. Invasions* **6**(1), 71–81. Springer.

Steiger, J., Gurnell, A. M. & Petts, G. E. (2001) Sediment deposition along the channel margins of a reach of the middle River Severn, UK. *Regul. Rivers Res. Manag. An Int. J. Devoted to River Res. Manag.* **17**(4-5), 443–460. Wiley Online Library.

Struck, M., Andermann, C., Bista, R. & Korup, O. (2013) Towards a complete contemporary sediment budget of a major Himalayan river: Kali Gandaki, Nepal. *EGU Gen. Assem. Conf. Abstr.*, Vol. 15.

Struck, M., Andermann, C., Hovius, N., Korup, O., Turowski, J. M., Bista, R., Pandit, H. P., et al. (2015) Monsoonal hillslope processes determine grain size-specific suspended sediment fluxes in a trans-Himalayan river. *Geophys. Res. Lett.* **42**(7), 2302–2308. Wiley Online Library.

Sumi, T. & Kantoush, S. A. (2010) Integrated management of reservoir sediment routing by flushing, replenishing, and bypassing sediments in Japanese river basins. *Proc. 8th Int. Symp. Ecohydraulics, Seoul, Korea*, 12–16.

Talchabhadel, R. & Karki, R. (2019) Assessing climate boundary shifting under climate change scenarios across Nepal. *Environ. Monit. Assess.* **191**(8), 520. Springer.

Talchabhadel, R., Karki, R., Thapa, B. R., Maharjan, M. & Parajuli, B. (2018) Spatio-temporal variability of extreme precipitation in Nepal. *Int. J. Climatol.* **38**(11), 4296–4313. Wiley Online Library.

Temple, P. H. & Sundborg, Å. (1972) The Rufiji River, Tanzania hydrology and sediment transport. *Geogr. Ann. Ser. A, Phys. Geogr.* **54**(3–4), 345–368. Taylor & Francis.

Thapa, B., Shrestha, R., Dhakal, P. & Thapa, B. S. (2005) Problems of Nepalese hydropower projects due to suspended sediments. *Aquat. Ecosyst. Health Manag.* **8**(3), 251–257. Taylor & Francis.

Tursun, N., Seyithanoglu, M., Nezihi, F., Ozer, I. & Arzu, E. (2011) Seasonal dynamics of soluble

carbohydrates in rhizomes of Phragmites australis and Typha latifolia. *Flora* **206**(8), 731–735. Elsevier GmbH. doi:10.1016/j.flora.2011.01.011

Uca, Toriman, E., Jaafar, O., Maru, R., Arfan, A. & Ahmar, A. S. (2018) Daily Suspended Sediment Discharge Prediction Using Multiple Linear Regression and Artificial Neural Network. *J. Phys. Conf. Ser.* **954**(1). doi:10.1088/1742-6596/954/1/012030

Ulke, A., Tayfur, G. & Ozkul, S. (2009) Predicting suspended sediment loads and missing data for Gediz River, Turkey. *J. Hydrol. Eng.* **14**(9), 954–965. American Society of Civil Engineers.

Vargas-Luna, A., Crosato, A. & Uijttewaal, W. S. J. (2015) Effects of vegetation on flow and sediment transport: comparative analyses and validation of predicting models. *Earth Surf. Process. Landforms* **40**(2), 157–176. Wiley Online Library.

Vogt, K., Rasran, L. & Jensen, K. (2004) Water-borne seed transport and seed deposition during flooding in a small river-valley in Northern Germany. *Flora-Morphology, Distrib. Funct. Ecol. Plants* **199**(5), 377–388. Elsevier.

Votrubov, O., Tylov, E. & Steinbachov, L. (2008) Phenology and autumnal accumulation of N reserves in belowground organs of wetland helophytes Phragmites australis and Glyceria maxima affected by nutrient surplus **63**, 28–38. doi:10.1016/j.envexpbot.2007.10.011

Westra, S., Alexander, L. V & Zwiers, F. W. (2013) Global increasing trends in annual maximum daily precipitation. *J. Clim.* **26**(11), 3904–3918.

Wicher-Dysarz, J. (2019) Analysis of Shear Stress and Stream Power Spatial Distributions for Detection of Operational Problems in the Stare Miasto Reservoir. *Water* **11**(4), 691. doi:10.3390/w11040691

Wijngaard, J. B., Klein Tank, A. M. G. & Können, G. P. (2003) Homogeneity of 20th century European daily temperature and precipitation series. *Int. J. Climatol. A J. R. Meteorol. Soc.* **23**(6), 679–692. Wiley Online Library.

Williams, G. P. (1989) Sediment concentration versus water discharge during single hydrologic

events in rivers. *J. Hydrol.* **111**(1–4), 89–106. doi:10.1016/0022-1694(89)90254-0

Williams, Garnett P. (1983) Paleohydrological methods and some examples from Swedish fluvial environments: I cobble and boulder deposits. *Geogr. Ann. Ser. A, Phys. Geogr.* **65**(3–4), 227–243. Taylor & Francis.

Yang, C.-C. & Lee, K. T. (2018) Analysis of flow-sediment rating curve hysteresis based on flow and sediment travel time estimations. *Int. J. Sediment Res.* **33**(2), 171–182. Elsevier.

Yonggui, Y., Xuefa, S., Houjie, W., Chengkun, Y., Shenliang, C., Yanguang, L., Limin, H., et al. (2013) Effects of dams on water and sediment delivery to the sea by the Huanghe (Yellow River): The special role of Water-Sediment Modulation. *Anthropocene* **3**, 72–82. Elsevier.

Yoshida, T., Suganuma, Y. & Sakai, T. (2015) Distribution and its sedimentary process of river terrace deposits along the middle Kali-gandaki, central Nepal.

Zhang, G., Liu, Y., Han, Y. & Zhang, X. C. (2009) Sediment Transport and Soil Detachment on Steep Slopes: I. Transport Capacity Estimation. *Soil Sci. Soc. Am. J.* **73**(4), 1291. doi:10.2136/sssaj2008.0145

Zhang, L. & Zhou, T. (2011) An assessment of monsoon precipitation changes during 1901–2001. *Clim. Dyn.* **37**(1–2), 279–296. Springer.

Zhang, Q., Xu, C.-Y., Zhang, Z., Chen, Y. D., Liu, C. & Lin, H. (2008) Spatial and temporal variability of precipitation maxima during 1960–2005 in the Yangtze River basin and possible association with large-scale circulation. *J. Hydrol.* **353**(3–4), 215–227. Elsevier.

Zhao, H., Yan, J., Yuan, S., Liu, J. & Zheng, J. (2019) Effects of Submerged Vegetation Density on Turbulent Flow Characteristics in an Open Channel. *Water* **11**(10), 2154. Multidisciplinary Digital Publishing Institute.